Fall 12-20-2019

State-Dependent Mapping of GlyR-Cholesterol Interactions by Coupling Crosslinking with Mass Spectrometry

Nicholas Ferraro

STATE-DEPENDENT MAPPING OF GLYR-CHOLESTEROL INTERACTIONS BY COUPLING CROSSLINKING WITH MASS SPECTROMETRY

A Dissertation

Submitted to the Bayer School of Natural and Environmental Science

Duquesne University

In partial fulfillment of the requirements for

the degree of Doctor of Philosophy

By

Nicholas Ferraro

December 2019

STATE-DEPENDENT MAPPING OF GLYR-CHOLESTEROL INTERACTIONS BY

COUPLING CROSSLINKING WITH MASS SPECTROMETRY

By

Nicholas Ferraro

Approved November 1, 2019

Michael Cascio Associate Professor of Chemistry (Committee Chair)	Stephanie Wetzel Assistant Professor of Chemistry (Committee Member)
Jana Patton-Vogt Professor of Biology (Committee Member)	H.M.S. Kingston Professor of Chemistry (Committee Member)
Philip Reeder Dean, Natural and Environmental Sciences Professor of Chemistry	Ellen Gawalt Chair, Chemistry and Biochemistry Professor of Chemistry

ABSTRACT

STATE-DEPENDENT MAPPING OF GLYR-CHOLESTEROL INTERACTIONS BY COUPLING CROSSLINKING WITH MASS SPECTROMETRY

By

Nicholas Ferraro

December 2019

Dissertation supervised by Michael Cascio

The glycine receptor (GlyR) belongs to a superfamily of pentameric ligand-gated ion channels (pLGICs) that mediate fast neurotransmission. GlyR typically modulates inhibitory transmission by antagonizing membrane depolarization through anion influx. Allosteric interactions between the receptor and its lipid surroundings affect receptor function, and cholesterol is essential for pLGIC activity. Human α1 GlyR was purified from baculovirus infected insect cells and reconstituted in unilamellar vesicles at cholesterol: lipid ratios below and above the cholesterol activity threshold with aliquots of azi-cholesterol. State-dependent crosslinking studies of receptors primarily in its resting (no glycine), desensitized (10mM glycine) and open (F207A/A288G, 30nM ivermectin) states were then performed at elevated cholesterol levels necessary for activity. After photoactivation, covalently crosslinked cholesterol-GlyR were trypsinized, mass fingerprinted by tandem mass spectrometry (MS-MS), and sites of cholesterol

crosslinks in peptides were refined by targeted MS-MS. Within the GlyR apo state, cholesterol interactions differed as a function of membrane cholesterol concentration correlating to the chemical activity of cholesterol, suggesting two distinct conformations. Differential cholesterol crosslinking patterns between resting, desensitized, and open states were observed, highlighting state-dependent differences in GlyR lipid accessibility. Distinct state-dependent crosslinking patterns indicative of alterations in either the lipid environment and/or channel structure were observed throughout GlyR, most prominently observed in the M4 transmembrane helix, extracellular domain loops and regions nearing the bilayer interface, and the large intracellular M3-M4 loop. The changes in M4 accessibility (transition from surface-mapped crosslinking to regions of the helix less exposed when mapped) suggest an outward twisting motion and translocation towards the bilayer/lipids as GlyR allosterically transitions. Strikingly, crosslinking patterns within the M3-M4 loop offer insight into the generalized structure of this unresolved region in all current pLGIC structural models, by suggesting the crosslinked regions of this intracellular loop are intimately associated or buried within the lipid bilayer. Taken together, crosslinking coupled with MS-MS has the capability to accurately probe and define physiological protein frameworks which can aid in the refinement of allosteric modulation and current structural models.

TABLE OF CONTENTS

Page

LIST OF FIGURES

Page

LIST OF ABBREVIATIONS

$5HT_3$-R	serotonin receptor
ATPase	adenosine triphosphatase
CARC	inverted cholesterol recognition amino acid consensus
CID	collision-induced dissociation
CNS	central nervous system
CRAC	cholesterol recognition amino acid consensus
CX-MS	photocrosslinking coupled with tandem mass spectrometry
DAG	diacylglycerol
DTT	dithiothreitol
ECD	extracellular domain
EDTA	ethylenediaminetetraacetic acid
EGTA	ethylene glycol tetraacetic acid
ELIC	*Erwinia chrysanthemi* ligand-gated ion channel
ESI	electrospray ionization
GABAR	γ-aminobutyric acid receptor
GLIC	*Gloeobacter* ligand-gated ion channel
GluCl	glutamate-gated chloride channel
GlyR	glycine receptor
GPCR	G-protein coupled receptor
HPLC	high performance liquid chromatography

ICD	intracellular domain
M1-M4	1^{st}- 4^{th} transmembrane alpha helices
MS	mass spectrometry
MS-MS	tandem mass spectrometry
nAChR	nicotinic acetylcholine receptor
PA	phosphatidic acid
PBR	peripheral-type benzodiazepine receptor
PBS	phosphate buffered saline
PC	phosphatidylcholine
PE	phosphatidylethanolamine
pLGIC	pentameric ligand-gated ion channel
PMSF	phenylmethanesulfonyl fluoride
PS	phosphatidylserine
SERT	serotonin transporter
TMD	transmembrane domain
WT	wild-type

CHAPTER 1: INTRODUCTION

In order to provide a context for the experimental crosslinking mass spectrometry (CX-MS) studies examining the effect of cholesterol concentration on the structure of the resting state of the glycine receptor (GlyR)(Chapter 2), and using CX-MS to examine cholesterol-GlyR interactions in a state-dependent manner (Chapter 3), the dynamics of membranes as a function of composition, GlyR structure and CX-MS methodology are reviewed in this introductory chapter.

1.1 Membrane Dynamics

1.1.1 Lipid Bilayer Properties

Lipids are vital bioactive compounds that are a major energy reservoir,[1] function as chemical messengers in signal transduction[2] as well as protein regulation,[3] and are critical for proper physiological processes.[4] Lipids form the structural component of cellular membranes and their diversity leads to varying microenvironments of a membrane to accomplish a multitude of functions.[5] Bilayers spontaneously come together due to the amphiphilic nature of lipids, segregating internal cellular components from the outside environment, as the propensity of hydrophobic moieties within a lipid to self-associate coupled with the tendency of the hydrophilic head groups to interact with other hydrophilic moieties and the aqueous environment.[6]

In considering phospholipids (Figure 1), there is great diversity in head groups, tail lengths, and degrees of saturation resulting in over 100 compounds, and when coupled with the multiplicity of other membrane lipids (Figure 1), leads to a wide range of dynamic physical properties of cellular membranes.[7,8] The lipid's headgroup (size) and acyl chain (length and saturation) composition establish its intrinsic properties (shape, occupational space, interactions) which in turn determines side-by-side packing and the shape of each monolayer creating a net spontaneous membrane curvature of both inner and outer monolayers.[9] Cylindrical lipids such as phosphatidylcholine (PC) and phosphatidylserine (PS) promote flat monolayer formation compared to the conical shape of phosphatidylethanolamine (PE), phosphatidic acid (PA),

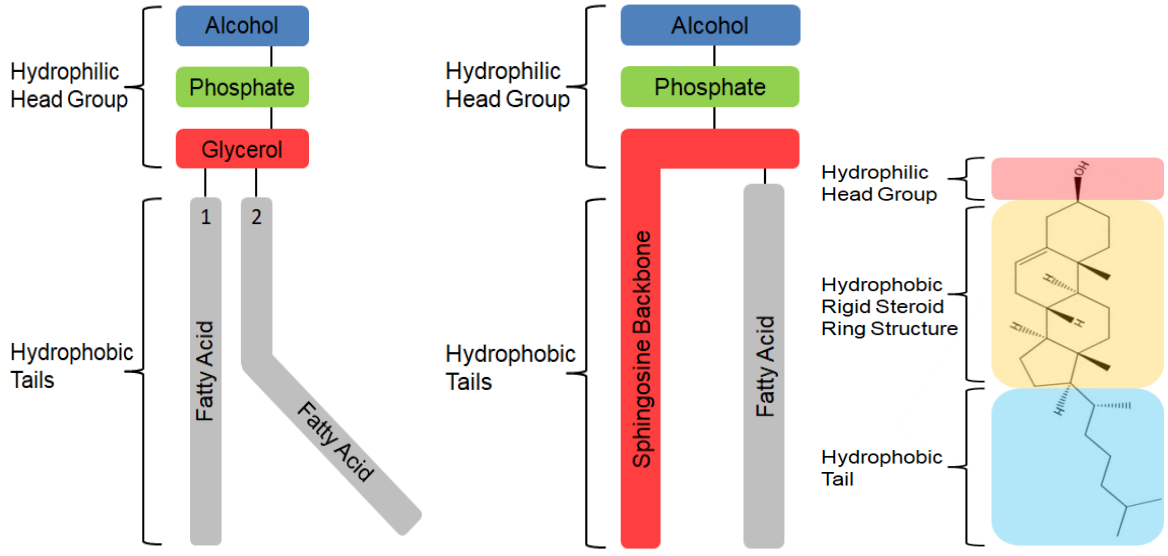

Figure 1. Diagram of general lipids. (Left) A general schematic of a phospholipid, with the hydrophilic region is depicted as consisting of the choline head group, the phosphate linkage, and the glycerol backbone. The hydrophobic region is depicted with fatty acid chains of saturation (1) and unsaturation (2). (Middle) A general schematic of a sphingolipid, with the hydrophilic region depicted as consisting of an amino alcohol linked to a phosphate linked to the sphingosine backbone. The sphingosine backbone is linked to a fatty acid creating the

diacylglycerol (DAG), and cardiolipin (headgroups smaller than PC) impose negative curvature of head groups being closer together compared to lipids such as lysophosphatidylcholine and phosphatidylinositol (larger head group to acyl chain ratio) that promote positive membrane curvature bending away from headgroups.[10–12] Acyl chain unsaturation (incorporation of double bonds) induces kinks in the acyl chain disrupting chain packing which causes each individual lipid to occupy more space than saturated acyl chains, thereby making acyl chain saturation along with head groups a major factor in the geometry of the membrane, affecting fluidity and melting temperatures.[9] The incorporation of *cis*-unsaturation reduces close ordering and side-by-side packing which increases membrane permeability.[13] Phospholipid head groups play a significant role in membrane fluidity and permeability where the strength and relative amount of head group intermolecular interactions with the hydrophilic environment can influence relative permeability.[14] Membrane lateral pressure is modulated through head group attraction/repulsion, incorporation of sterols or interfacially active solutes, and by acyl chain length and degree and position of chain unsaturation.[15] Lipid's influence on cellular function are complex and vary from cell to cell, making it difficult to generalize lipid modifications on a given system.[8]

1.1.2 Cholesterol Characteristics

1.1.2.1 Structural Properties

Cholesterol is a major component of nearly all mammalian membranes where its heterogeneous distribution among organelles, membranes, and leaflets creates diversity in membrane physiochemical properties and function.[16] Derived from a sterane backbone, cholesterol is a polycyclic amphipathic molecule with a relatively small polar region of a single hydroxyl

group linked to a larger apolar section consisting of a four-member ring structure and isooctyl chain tail (Figure 1, right).[17] The polar hydroxyl "head group" is oriented with the aqueous phase and polar head groups of membrane phospholipids and participates as both a hydrogen bond acceptor and donor with proximal lipid or protein. This is juxtaposed with the predominant van der Waal hydrophobic interactions of the aliphatic groups and aromatic π stacking with lipid acyl chains in the hydrophobic region.[17,18] The apolar region of cholesterol is asymmetric with two distinct faces (α and β), a planar α face and the rough β face defined by the aliphatic methyl groups and the isooctyl tail allowing for distinct and preferential interactions with each face.[19] These properties enable cholesterol interactions with membrane lipids to exhibit bidirectional modulation of membrane fluidity, decreasing fluidity of acyl tails above and decreasing fluidity below the gel to liquid-crystalline phase transition temperature, respectively.[20] Cholesterol reduces the rate of motion of phospholipid acyl chains while increasing the degree of orientation order that leads to laterally more condensed membranes with increased phospholipid packing density and decreased membrane permeability.[20–22] These unique properties of cholesterol allow for the tight regulation of a variety of critical cellular functions.[23]

1.1.2.2 Cholesterol and Microdomains in the Bilayer

Cellular bilayers are laterally heterogeneous with distinct sub-populations present in leaflets of biological membranes whose distinct interactions drive the association of other lipids and proteins.[24] Cholesterol is essential for lipid raft formation, a localized highly ordered microdomain within a membrane leaflet of higher cholesterol/sphingolipid/saturated phospholipid concentration eliciting distinctly less membrane fluidity than the surrounding membrane, where cholesterol exhibits a higher affinity to partition in the raft phase than non-raft phase.[25,26] These

dynamic cholesterol-enriched nanoscale domains are essential for key processes such as membrane trafficking, signal transduction, and protein function where the membrane's heterogeneity is critical for specific modulation.[27] Proteins partition with lipid rafts at differing degrees and kinetics where oligimerization, ligand binding, and modifications such as palmitoylation alter a protein's affinity to partition within the rafts, allowing for precise regulation of raft composition.[26] Lipid rafts can modulate and respond to protein activation through clustering that concentrates proteins and/or provides a protected microenvironment for activation/modification to occur, commonly observed in signal transduction pathways.[28] Membrane microdomains modulate dopamine transporter function where cholesterol-rich membrane fractions promote specific structural conformations influencing drug binding.[29] The partitioning of the serotonin transporter (SERT) in lipid raft microdomains is critical for serotonin uptake activity and dependent on cholesterol concentrations.[30] Microdomains rich in cholesterol and sphingomyelin modulate several G-protein coupled receptor (GPCR) functions including signaling, trafficking, and localization.[31] Lipid rafts are essential for nicotinic acetylcholine receptor (nAChR) membrane trafficking whereby raft disruption alters cell surface exposure and also stabilizes channels in uncoupled conformations.[32] Taken together, microdomains within lipid bilayers and their dynamic compositions are critical for the modulation, recruitment, and regulation of membrane proteins.[33]

1.1.2.3 Activity of Cholesterol

A given lipid within a bilayer leaflet exhibits diffusion and partitions into different lateral phases according to relative affinity for the phase with the potential to flip leaflets and redistribute aqueous region interactions within phases. Therefore, every lipid within the membrane will have individual "fugacity" or tendency to partition laterally, distribute transversely, and transfer

outwardly between condensed lipid phases of varying order.[34] Sterols within lipid complexes can exceed the threshold complexing capacity and become dispersed in the bilayer characterized by increased escape tendency.[35] Cholesterol in molar excess of the capacity of these complexes has high fugacity, or termed "active cholesterol",[36] as seen by a abrupt increase in sterol availability to cholesterol oxidase,[37] perfringolysin,[38] and methyl-β-cyclodextrin,[39] emerging at concentrations above 25-35 mol percent (typical physiological concentrations).[40,41] Excess cholesterol exhibits high chemical activity in a chemical phase distinct from that observed under negligible chemical activity.[42] Thus, slight variations in cholesterol concentrations about its typical physiological levels has the potential to drive regulatory processes within or on the plasma membrane surface,[43] either indirectly by modulating plasma membrane physical properties or directly as a protein regulator.[20] Phospholipid acyl tail configuration (*cis* vs. *trans* unsaturation) alters cholesterol-phospholipid affinity in which *trans* unsaturation exhibited lower cholesterol activity than *cis* counterparts.[44] The presence of active cholesterol elicits a variety of feedback response mechanisms including cholesterol esterification, side-chain oxysterol synthesis, and down-regulation of synthesis through exportation.[35]Taken together, cholesterol's unique structure allows for essential physiological modulation of lipid bilayers altering physiochemical properties and subsequent components within the membrane environment.

1.2 Role of Lipids on Protein Activity

The lipid membrane historically has been considered a passive protein-anchoring environment enabling proteins to mediate cellular functions. More recently, the membrane has been redefined as a medium that engages directly and specifically with an array of proteins including channels, transporters, and enzymes.[45] Proteins embedded within or contiguous with the

lipid bilayer interact intimately with lipids and these interactions modulate their structure and function.[46,47] Minor structural changes to lipids (head group, tail length, and saturation) can alter the structure and properties of the bilayer, as well as affect protein function via direct binding interactions, increasing the difficulty to distinguish each specific lipid influence from a diverse network of membrane lipids.[48]

It is difficult to accurately differentiate specific protein-lipid interactions (including hydrogen bonding, hydrophobic effects, and charge interactions) from global membrane alterations (including fluidity and tension) that influence protein function.[47,49,50] In addition to bulk lipids which have stable dynamic properties, a population of lipids have motional constraints through interactions either of low affinity hydrophobic surfaces (annular) or high affinity sites in clefts of protein surfaces or subunit interfaces (non-annular).[51] Acyl tail length and head group variation drastically alters hydrophobic bilayer size and intermolecular interactions critical for the stabilization of proteins.[50] These dynamic interactions of the protein-lipid interface can be within microdomains of the membrane and are dependent on lipid compositions that modulate either direct lipid binding/interaction with protein or the physiochemical properties of the bilayer.[52–54] Protein activities may be modulated by bilayer properties (thickness and curvature) conversely to lipid fluctuations (membrane deformation and lipid sorting mechanisms) induced by hydrophobic mismatch of protein hydrophobic region.[55,56] An example of bilayer-induced protein modulation is bacterial mechanosensitive channels where bilayer tension alters the open state probability of channels.[57] Similarly, the monomer-dimer equilibrium of the amyloid precursor protein is altered by differential membrane thickness due to varying membrane compositions.[58] A comprehensive understanding of the influence lipids have at the protein-lipid interface is essential to completely discern peripheral and integral membrane protein function.[45]

1.2.1 Membrane Proteins

Lipid membrane composition and structure can be targeted to alter localization and activity of proteins within signaling cascades implicated in diseases like cancer and diabetes.[59] An example of this "membrane lipid therapy" is seen by the modulation of specific interactions of DAG, PS, and PE with protein kinase C isozymes favoring recruitment into microdomains.[60,61] Thus, distinguishing complex protein-lipid interactions can offer therapeutic benefits.

The structure and function of membrane proteins can also be affected by specific lipid-protein interactions. For example, the β2-adrenergic receptor dimer interface is stabilized by cholesterol occupancy.[62] Delipidation of interfacial lipids, including cardiolipin, alters oligomeric stability of Na+/H+ antiporters and bacterial leucine transporter diminishing dimer formation.[63] GPCRs localization, activation, and signal propagation are regulated by specific lipid interactions and membrane composition.[61] Similarly, activity of SERT is cholesterol dependent as cholesterol depletion caused loss of substrate affinity, ligand binding, and transport rate reduction and recovery of activity required incubation with cholesterol as opposed to other sterols tested (ergosterol, 5-cholestene, pregnenolone), suggesting essential specific cholesterol interactions.[64]

Lipids are frequently observed tightly bound to proteins with over 100 unique lipid binding sites identified in x-ray diffraction, nuclear magnetic resonance spectroscopy, and electron crystallographic studies, further underlining the importance of specific protein-lipid interactions.[65] Annular phospholipid interactions observed in x-ray crystallographic studies of bacteriorhodopsin show over a dozen tightly bound lipids depicting bilayers exposing protein surface interactions.[66] Non-annular lipid interactions are observed in K^+ channels and cytochrome bc_1 complexes in more buried regions between adjacent monomers of oligomeric complexes and subunits of multisubunit

complexes, respectively.[67] Cholesterol interactions are maintained in structures including the glutamate receptor,[68] Na^+,K^+ adenosine triphosphatase (ATPase),[69] β_2-adrenergic receptor,[70] and dopamine transporter,[71] highlighting cholesterol specific interactions of membrane proteins. Taken together, the presence of a variety of lipids maintained in current structures demonstrates how essential these molecules are in the stabilization of membrane proteins.

1.2.2 Lipids and Ion Channels

The lipid bilayer and its dynamic composition creates a modulatory environment for ion channels (including pentameric ligand-gated ion channels (pLGICs)).[72–74] Current ion channel structures including glutamate-gated chloride channel (GluCl),[75] K^+ channels,[76] and *Gloeobacter* ligand-gated ion channel (GLIC)[77] reveal lipids bound at both the periphery annulus of the channel[77] and non-annularly.[75,76] Agonist binding of GluCl is modulated by select lipids through binding of membrane-spanning intersubunit crevices potentiating the receptor in an expanded, open-like conformation.[75] Phosphatidylinositol 4,5-bisphosphate regulates inward rectifying potassium channels, acting as a coupling agent inducing large conformation changes of the transmembrane domain (TMD)-C-terminal domain association.[78]

Cholesterol is an essential component of eukaryote membranes, and this specific lipid has been shown to affect ion channel structure and activity. Cholesterol reversibly affects γ-aminobutyric acid receptor (GABAR) activity as cholesterol depletion reduces activity and this can be restored through cholesterol enrichment of cholesterol-depleted neurons.[79] A variety of additional ion channels (inwardly-rectifying K^+, Ca^{2+}-sensitive K^+, voltage-regulated anion, vanilloid transient receptor potential channel, voltage-gated K^+, voltage-gated Na^+, and voltage-gated Ca^{2+} channels) similarly display cholesterol sensitivity, as reduction in cholesterol content

in membranes suppresses activity by decreasing open state probability, unitary conductance, or the number of active channels in the membrane.[80] Although decreasing cholesterol concentration typically down regulates channel activity, a few cases such as G protein inwardly rectifying channel display up regulation of channel activity during cholesterol depletion.[81] Cholesterol and anionic phospholipids modulate nAChR function where membrane cholesterol enrichment up to a given threshold (~35 mol%) enhanced receptor-mediated ion flux.[82–86] This profound regulatory effect of cholesterol on nAChR is due to distinct asymmetric cholesterol-dependent conformations, where the allosteric coupling between neurotransmitter binding sites and the transmembrane pore is lost, termed the "uncoupled state", in the absence of cholesterol or anionic phospholipids.[87,88] Altogether, lipids play a critical yet unresolved role in ion channel function due to the complexity of lipid molecules and effects produced to each specific protein.

1.3 pLGIC Channel Allostery

1.3.1 3.1 pLGIC Superfamily Structure

The pLGIC superfamily is essential for rapid neuronal communication through conversion of a chemical signal to an electrical impulse.[89] pLGICs are found in a variety of organisms from single archaea to several bacteria species and complex vertebrates like humans.[89] pLGICs evolved from a single ancestral gene to share an overall common architecture which provides an array of structural models to one another for probing receptor topology.[90,91] Mammalian pLGIC orthologs are abundant in neuronal networks with regions including neuromuscular junctions as well as neuronal synapses in the peripheral and central nervous systems.[89] pLGICs are comprised pseudo-symmetric arrangement of five subunits forming a central ion-conducting pore.[92] The activity of these channels is generally correlated with the selectivity of this pore as cationic channels such as

the nAChR and serotonin receptor ($5HT_3$-R) are excitatory and anionic such as GABAR, GluCl, and GlyR are inhibitory.[93] pLGICs are known as "Cys-loop" receptors due to a typically conserved 13 amino acid loop enclosed by a pair of disulfide-bonded cysteine residues within the extracellular domain (ECD).[92,94]

All pLGIC subunits share a common global domain organization and common transmembrane topology,[89] with each subunit consisting of a large N-terminal β-sandwich immunoglobulin-like structure ECD harboring the agonist binding site at the interface of adjacent subunits, a transmembrane domain containing four membrane-spanning α helices, and an intracellular domain (ICD) consisting of largely heterogenic transmembrane helix connecting loops (Figure 2).[93,95,96]

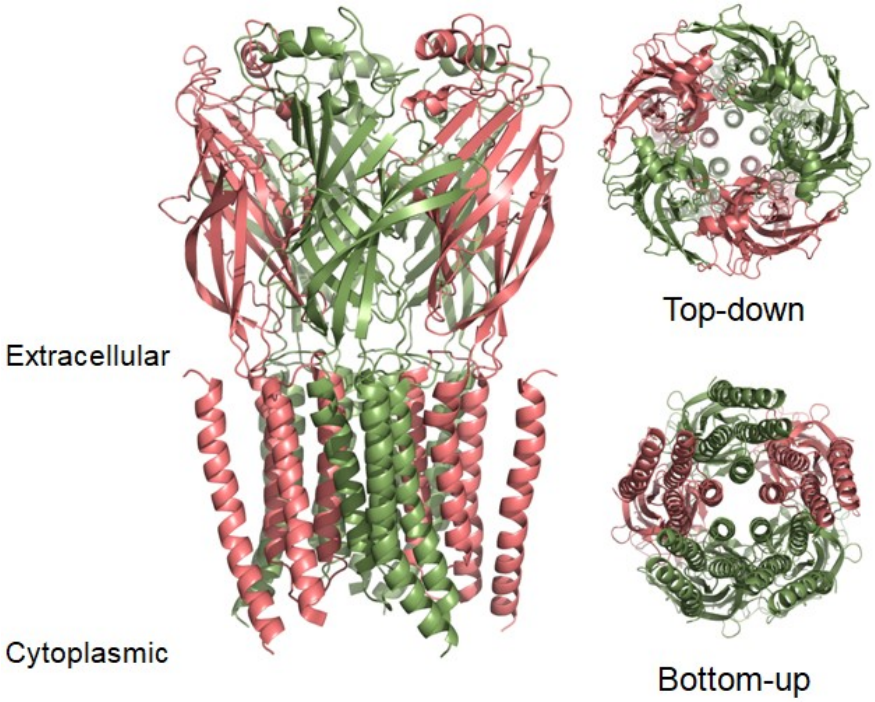

Figure 2. pLGIC GlyR pentamer. Multiple GlyR topology views of cryo-electron microscopy zebrafish GlyR structure (PDB #3JAD) adapted from Du et al. (2015).[100] The large globular ECD includes Cys-loop and ligand binding domain (see side view and top-down).TMD helices form the central pore (see bottom-up view). The M3-M4 loop and the C-terminal tail are removed.

Most eukaryotic pLGICs are heteromeric assemblies, with multiple homologous subunit species within a single pLGIC labeled α, β, γ, etc, which are further divided into subtypes: α1, α2, etc.[93] Recent structures of both prokaryotic (*Erwinia chrysanthemi* ligand-gated ion channel (ELIC),[97] GLIC[98] and eukaryotic (GluCl,[99] GlyR[100]) channels show high conservation of the structures of both the ECD and TMD comprising of the majority of the channel (Figure 2). The minimally characterized intracellular M3-M4 loop region is least conserved among pLGICs having a wide range of sequence length and divergence.[101] Therefore, it is typically removed or truncated in most pLGIC models due to the increased heterogeneity and lack of structural stability making it difficult to generate sufficient resolution.[96]

1.3.2 pLGIC Superfamily Function and Significance

Electrochemical gradients consist of two driving forces of ion movement across a membrane: an electrical driving force and a chemical (concentration) driving force.[102] The electrical drive force contributing to the membrane potential arises when the electrical charge on two sides of a membrane differ due to unequal amounts of charged ions.[18] The chemical or concentration driving forces arises due to asymmetric concentrations of each ion on both sides of a membrane. Together these forces create an electrochemical gradient, with the reversal potential (also known as the Nernst potential) occurring when no net flow of a particular ion occurs.[18,102]

The pLGIC superfamily contributes to all central nervous system functions that include sensory and motor processing, central autonomous control, memory, attention, sleep, wakefulness, reward, pain, anxiety, emotions, and cognition.[103] Channel activation involves long range allosteric conformational rearrangements initiated by ligand binding that propagates movements ultimately disrupting the permeation gate, producing a transient open, ion-conducting channel (Figure 3).[104] Passive movement of ions down their electrochemical gradient alters the membrane potential affecting the resting potential across the membrane allowing rapid movement of ions across an otherwise impermeable hydrophobic membrane, endowing millisecond cellular communication.[105,106] Influx of cations (Na^+, K^+, Ca^{2+}) typically depolarize membrane potential while anion (Cl^-) influx induces membrane hyperpolarization.[107] Continued presence of bound ligand causes further structural rearrangements to a long-lived non-conducting desensitized state refractory to further activation.[104,108] Channels recover from desensitization relatively slowly, transitioning to apo-structures that can be ligand-activated and continue the thermodynamic cycle.[109]

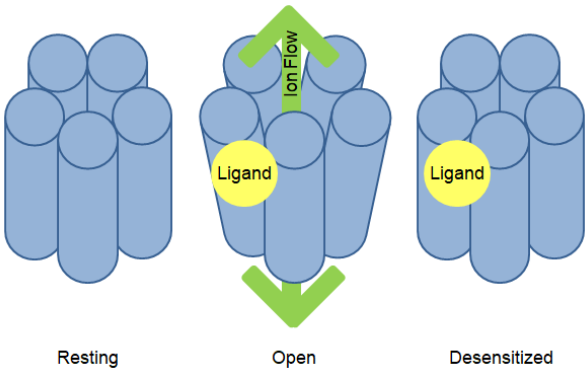

Figure 3. Major ion channel states. Simplified cartoon depiction of allosteric transitions from the apo-state (Resting/Closed) to the ligand-bound ion conducting state (Open) to the ligand-bound non-conducting state (Desensitized).[257]

The pLGIC superfamily's ability to modulate neuronal and muscular activity coupled with their sensitivity to a variety of drugs has made this superfamily of ion channels attractive and significant pharmaceutical targets.[110] pLGICs are targeted by drugs such as nicotine, alcohol, cannabinoids, and benzodiazepines.[93,111] Both nAChRs and 5-HT_3Rs are major targets in drug discovery for several psychiatric, neurological, and peripheral disorders, leading beyond clinical trials to marketed drugs.[112,113] Additionally, pLGICs malfunction are implicated in serious conditions such as Alzheimer's disease,[114] Parkinson's disease,[115] epilepsy,[116] smoking addiction,[117] and alcohol dependence.[118] Defects in GlyR activity underlie pathological mechanisms of various neurological diseases such as startle disease (hyperekplexia) where missense mutations in genes encoding GlyR subunits cause glycinergic dysfunction leading to the neurological disorder.[119] Inadequate clinical efficacy and adverse side effects occurring in gastrointestinal and the central nervous system (CNS) are the major current barriers in therapeutic strategies, emphasizing the necessity for discovery and refinement of therapeutic small molecule modulators.[112] Further refinement of allosteric ion channel structure at drug interaction is essential for the understanding of the nature of specific drug action onto the pLGIC therapeutic targets.[95]

1.3.3 GlyR Allostery

The inhibitory GlyR is comprised of α (α1-4, ~48 kDa) and β (β1, ~58 kDa) subunits that typically assemble pentamerically at a 2α:3β ratio.[120] Functional homopentameric α subunit channels can be overexpressed for biochemical and biophysical characterization,[121] however β subunits are required for physiological postsynaptic clustering due to high affinity binding of its M3-M4 loop regions with gephyrin scaffolding.[122] Each subunit ECD contains the characteristic Cys-loop within a ten strand β-barrel-like (β1-10) structure with two short α-helices connecting β3

and β4.[123] Glycine ligand binds at the interface of two adjacent subunits in the ECD, and this neurotransmitter binding site is located between three loops "A-C" of the principal subunit and three β strands (β1,β2, and β5) of the complementary subunit.[100,123] Upon glycine binding, GlyR allosterically transitions to a transient open conformation, where channels become permeable to small anions such as chloride, resulting typically in Cl^--influx and hyperpolarization.[124] The TMD of GlyR (M1-M4) is connected by extracellular (M2-M3) and cytoplasmic (M1-M2, M3-M4) loops where M2s forming the central ion pore flanked by M1/M3, and M4 associated with M1/M3 most distant from the pore (Figure 4).[125] The channel gate(s) corresponds with the narrow channel pore region(s) at residues near the TMD:ICD interface critical for charge selectivity whereby residue side chains help control the electrostatic environment and create selectivity filters.[106,126] The TMD connecting loops, specifically the M1-M2 and M2-M3 loops flanking M2, interact with proximal regions of the ECD/ICD including the ligand binding domain and are also involved in channel gating.[127,128] The eighteen length amino acid binding site of gephyrin,[129] as well as endocannabinoid interactions[130] with GlyR, are mapped to the M3-M4 loop. Immediately downstream of transmembrane helix M3 within the loop resides a cluster of basic residues containing topological information imperative for localization.[131]

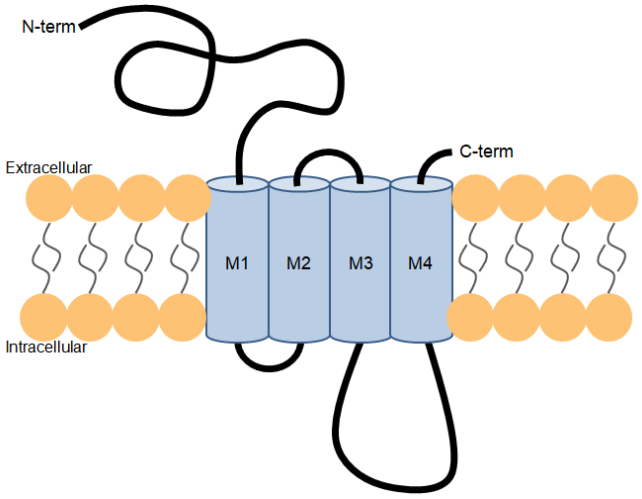

Figure 4. GlyR single subunit structure. Simplified diagram of GlyR single subunit, illustrating domains of the subunit.[258] The extracellular domain features both N- and C- termini, a large pre-M1 globular region, and the M2-M3 loop. The transmembrane is comprised of M1-M4 α helices. The intracellular domain consists of the M1-M2 loop and M3-M4 loop.

1.4 pLGIC Pharmacology

1.4.1 Pharmaceutical Agents and Bioactive Lipids

An array of pharmaceutical agents (anesthetics, barbiturates, benzodiazepines, cannabinoids, and alcohol) and bioactive lipids (progesterone, sphingomyelin, and ceramide) specifically targets the pLGIC superfamily of ion channels.[111,132–134] Anesthetics generally potentiate inhibitory anion-permeable channels while inhibiting excitatory cation-permeable channels, observed in the general anesthetic propofol enhancement of GABA and GlyR agonist-induced activation with inhibition of 5-HT_3R and nAChR channels, however the molecular mechanism of channel modulation remains unresolved.[135,136] In a similar manner, barbiturates modulate a variety of neuronal receptors both cationic (including α-amino-3-hydroxy-5-methyl-4-isoxazolepropionic acid receptor, kainite receptor, nAChR, and 5-HT_3R) and anionic (including

GABA, and GlyR) through inhibition and enhancement, respectively.[137] Endocannabinoids are direct GlyR allosteric modulators with both positive and negative modulation based upon endocannabinoid subtypes with Δ^9-tetrahydrocannabinol exhibiting positive modulation, highlighting relevant cannabinoid-induced analgesia strategies in pain therapeutics.[130] At least GlyRs and GABARs of the pLGIC superfamily demonstrate sensitivity to allosteric modulation by n-alcohols (ethanol and butanol) that bind/interact in generally hydrophobic pockets/regions of which are closely associated or within the lipid membrane.[138,139]

Bioactive lipids also play a diverse role in modulating pLGIC activity. Amongst their effects are regulation of cell-surface nAChR levels,[134] the inhibition of GABAR,[133] and the modulation of nAChR desensitization.[140] Lipoprotein(a) is linked to the generation and maintenance of pain by modulating ion channel/receptors signaling pathways and gating properties through specific direct interactions.[141] Cannabinoid-like GlyR potentiator screening providing an effective tool to discover novel interactions,[111] highlighting the necessity to develop methodologies that accurately probe and refine protein-lipid interactions. Collectively, there are at least 170 compounds (psychiatric medications, anesthetics, anticonvulsants, natural extracts, amino acids, ions, endogenous substances, drugs of abuse, and miscellaneous medications) of electrophysiological studies that can promiscuously modulate a subpopulation of LGICs (GABA, nAChR, GlyR, and $5HT_3$) suggesting extensive interactions that require characterization to not only increase efficacy but to also provide templates to guide drug development.[142] Intriguingly, both anesthetics and bioactive lipids partition with the cellular membrane specifically at the lipid-protein interface,[143,144] with anesthetics observed in crystal structures of pLGIC structural homologues,[145,146] providing tremendous opportunity to discern molecular mechanisms of pLGIC allostery.[135]

1.5 Photocrosslinking Coupled with Tandem Mass Spectrometry

1.5.1 Crosslinking Studies

Hundreds of thousands of protein interactions stemming from approximately twenty thousand protein-encoding genes create a dynamic protein-protein interactome network underlying all biological processes.[147] The elucidation of these vast diverse networks provides insight into protein regulation and function.[148] The majority of proteins function through complex assemblies including dynamic non-covalent associations of individual proteins, highlighting the potential to link interactions at a longer time scale.[149] A novel method of elucidating protein interactions within networks is through protein crosslinking comprised of chemical, enzymatic, or chemoenzymatic formation of covalent bonds between polypeptides.[150] By introducing a stable chemical linkage, transiently associated species establish a permanent interaction that previously would be difficult to detect and define.[151]

Crosslinking occurs naturally through enzymatic-catalyzed linkages seen by transglutaminases, sortases, and lysyl oxidases in various protein matrices.[150] General crosslinking to immobilize protein environments within cells is commonly completed using formaldehyde, an efficient cell-permeable small compound creating DNA-protein, RNA-protein, and protein-protein crosslinks. Glutaraldehyde is one of the most effective and commonly used crosslinking reagents due to the variety of different forms of the compound yielding a vast range of suitable conditions like pH, temperature, and concentration, making it one of the most efficient crosslinkers for protein and enzyme immobilization.[152] The amine-reactive N-hydroxysuccinimide esters are sensitive to primary amines, namely lysine residues, making it an effective crosslinker to proteins in living

cells allowing the probing of three-dimensional structures.[153] Maleimide-based crosslinkers react rapidly to sulfyhydryl groups with minor reactivity with amino groups, allowing for intramolecular crosslinking of protein subunits.[154] Given the variety of approaches for *in vitro* and *in vivo* crosslinking utilizing multifunctional crosslinkers (including homobifunctional and heterobifunctional) with varying length and reactive groups generates enormous diversity of available crosslinking reagent-based methodologies.[150]

Photoaffinity labels offer reproducible labeling in time- and location-specific manner in the presence of ultraviolet light to the target protein.[155] Photoaffinity labeling features a light-sensitive reactive motif for covalent linkage and commonly employed in drug discovery, drug target binding, and protein-ligand interactions having the advantage as useful tools in live cells and physiologically relevant systems to convert transient short-lived interaction into permanent covalent bonds amenable to a variety of analysis techniques.[156,157] Azide photocrosslinking (Figure 5, Right) chemistry is commonly used to obtain structural constraints in biological systems through

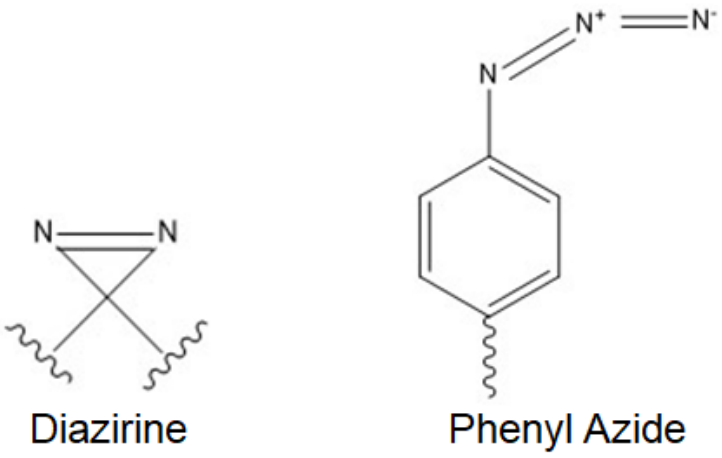

Figure 5. Photoreactive crosslinkers. Two examples of many photocrosslinkers available. The diazirine motif (Left) creates carbene intermediates for concerted addition reactions. The azide motif (Right) creates nitrene intermediates for addition reactions.[259]

formation of reactive nitrene intermediates targeting primarily C-H and C=C bonds for addition reactions, characterizing the higher order structure of RNA and RNA-protein complexes.[158,159] Benzophenone crosslinkers typically react with unreactive C-H bonds having mapped nucleotide-binding sites in ATPases and confirmation flexibility in solution, micelles, and membranes.[160] In particular, diazirines (Figure 5, Left) are commonly utilized photoreactive probes to study ligand-receptor, ligand-enyzme, and protein-protein interactions.[161]

1.5.2 Mass Spectrometry

In modern proteomics, mass spectrometry is increasingly utilized and rapidly advancing the variety of approaches and instrument resolution to elucidate cell protein compositions, complex formation, stoichiometry, architecture, and dynamics.[162] The application of mass spectrometry to proteomics is the use of one or more techniques from a collection of methodologies (sample preparation, chromatography systems, mass analyzers) where each can have particular strengths suited to specific investigations, all based upon the measurement of mass-to-charge ratios of gas-phase ions.[163,164] In general, analyte enters the ionization source where molecules are converted to the gas phase and ionized, directed into a variety of mass analyzers separating ions based upon mass-to-charge ratios through modulation of electric and magnetic fields, ultimately reaching the detector to be measured (Figure 6).[164,165] Advances in modern mass spectrometry have lead to the development of methodologies achieving extraordinary mass accuracy (>2ppm), resolving power (>100,000), and limit of detection (sub-nanogram).[166,167]

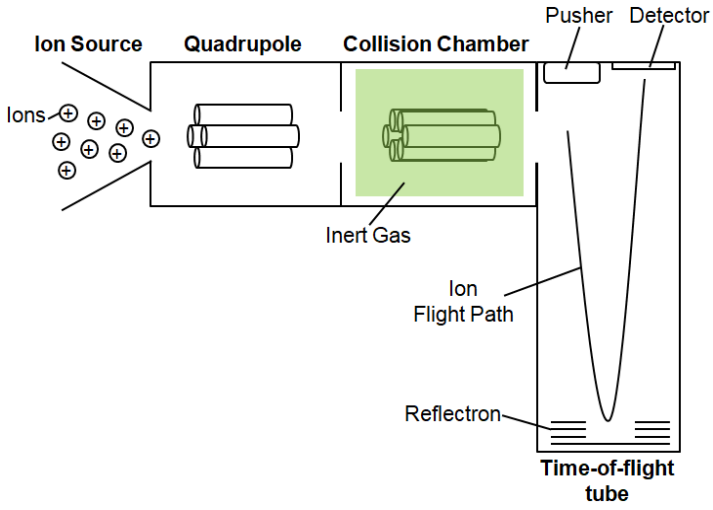

Figure 6. Quadrupole time-of-flight schematic. For tandem MS experiments, ions from the source enter and are filtered through the quadrupole, enter the collision chamber for fragmentation, and finally enter the time-of-flight tube for ion separation before reaching the detector.[260]

The implementation of tandem mass spectrometry (MS-MS) analysis has become an essential tool in the analysis of protein identification, complex structures, and protein modifications, where precursor ions are selected, activated through energetic collisions with neutral gas causing dissociation into product ions that reveal additional information about the protein, complex, or analyte assayed.[168–170] For protein and peptide based MS analysis, the most commonly employed ionization sources for mass spectrometers are soft ionization methods including matrix assisted laser desorption ionization and electrospray ionization (ESI) that can preserve native structure and complexes entering the mass spectrometer which are then discriminated typically by quadrupole, time-of-flight, or ion trap analyzers with the inclusion of collision cells for fragmentation.[171]

Given the sample's potential complexity, the implementation of high performance liquid chromatography (HPLC) preceding mass spectrometry increases the dynamic range and

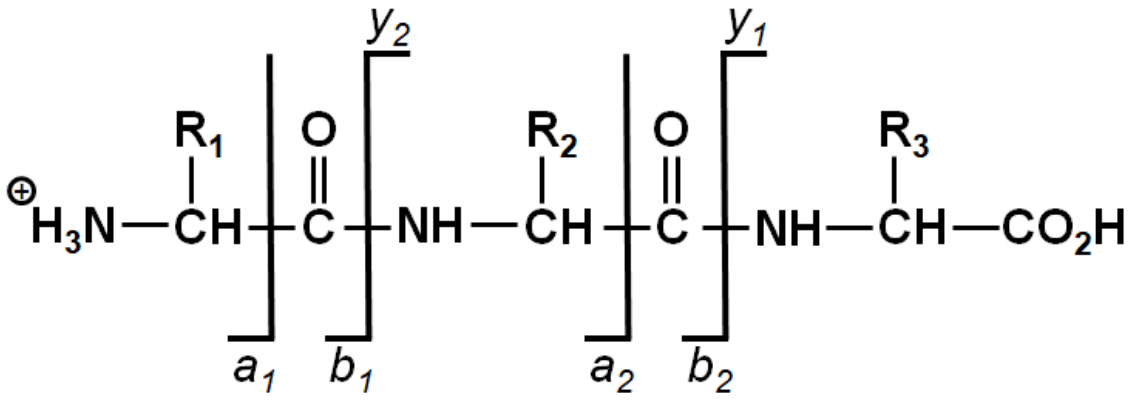

Figure 7. Collision-induced fragmentation pattern. Diagram of CID product ions produces after precursor ion fragmentation. CID typically produces "b" and "y" ions with less occurring "a" ion production.[261]

identification coverage of analyte through separation based upon analyte interactions with chromatographic stationary and mobile phases.[172] In determining protein complex composition, the dissociation of subunits follows a predominant fragmentation pathway with the expulsion of mono/multimeric protein subunits sequentially from the now stripped complex, allowing for the elucidation of subunit organization and stoichiometry.[169] Varying dissociation pathways in response to increased collision-induced dissociation (CID) energy are observed in peroxiredoxin ring assembly MS studies where dimers preferentially associate as intermediate pentamers, 6-mers, and 8-mers, with subunit dissociation as dimers opposed to monomer dissociation.[173] The MS-MS peptide dissociation pathway using CID provides reproducible fragmentations typically through cleavage of an amide bond (denoted as "b" ions if charge retained on N-terminus fragment and "y" if retained on C-terminus fragment) in the peptide providing information regarding the specific order of amino acids in smaller fragments stemming from the original peptide (Figure 7).[174,175] This is commonly employed in protein sequencing or modification assays where MS-MS fragmentation produces unique product ions that are compared with potential sequence masses in secession and/or refines the targeted modification location from a peptide to potentially single

amino acid resolution.[176] Advances in MS instrumentation have allowed for the analysis and identification of low abundant crosslinked peptides from complex biological samples providing more comprehensive and complete information for studies.[177]

1.5.3 CX-MS as a Biochemical Tool

Current CX-MS strategies capture both the identity and connectivity of protein-protein interactions from their native cellular environment.[177] The incorporation of sensitive MS-based approaches to photocrosslinking workflows allows for the potential to not only map protein-protein interactions but also identify allosteric dynamics of protein structure and interactions with its environment.[178,179] The transient nature of protein dynamics, exemplified in neuronal receptor allostery, typically poses a challenge for characterization, however the approach of using photocrosslinking provides a dynamic representation of protein alterations including receptor gating and desensitization.[179,180] Crosslinking reagents are of a defined length resulting in distance constraints (shortest distance between linked amino acids given protein volume) essential for structural validation, modeling, and *de novo* prediction.[177]

Photoaffinity labeling coupled with modern MS instrumentation can provide additional structural and mechanistic information compared to other photolabeling techniques regarding protein complexes, ligand-receptor stoichiometry, binding pocket maps, and single amino acid binding resolution.[181] CX-MS is rapidly advancing becoming a promising approach to gain structural information on large, potentially transient protein assemblies, intrinsically disordered proteins, and protein interaction networks both *in vivo* and *in vitro*.[182] Current tandem MS instruments have the mass accuracy and sensitivity to unambiguously identify and refine

crosslinked species to amino acid residue(s) within a given peptide.[178,183,184] CX-MS has be used to guide complementing structural techniques like crystallography in protein complex crystallization and conversely employed to verify and refine pre-determined crystal structures.[185] Interaction networks of mitochondrial proteins analyzed *in vivo* generating mitochondrial interactomes highlight capabilities where native molecular environments need to be maintained.[186]

CX-MS in conjunction with computational modeling elucidated a comprehensive protein-protein interaction network of proteasome complexes generating nearly 500 linkages of both inter- and intra-protein interaction highlighting structural dynamics and conformation heterogeneity.[177,187] The ability of coupling additional quantification techniques to CX-MS studies to not only identify specific interactions but report the frequency of interactions, observed in calmodulin quantification of substrate interactions which determined the abundance of complex formations, demonstrating the ability of crosslinking to be quantified by traditional calibration curve or isotope dilution methods.[188,189] Photoaffinity labeling coupled with MS has the capability to map lipid accessibility of proteins and protein:lipid interactions elucidating the propofol binding site of GLIC[190] and GABAR[191] as well as cholesterol interactions with the peripheral-type benzodiazepine receptor (PBR),[192] voltage-dependent anion channel-1,[193] nAChR,[194,195] and GlyR.[178] The coupling of these techniques highlights the advantages of providing more comprehensive information of greater detail, sensitivity, and less analysis times than traditional biophysical labeling techniques.[181]

1.5.4 Advantages and Limitations

The most basic and essential advantage of CX-MS is the generation of covalent bonds between target protein/lipids that can by highly specific and of high capacity, stabilizing a long-

lived association amenable for analysis.[196] An essential benefit of *in vivo* CX-MS is to characterize structural information (cellular compartmentalization, concentrations, interacting partners) within native environments at or near physiological conditions.[197] CX-MS assays can be a quick and convenient approach that does not require a large amount of protein or at high purity and is applicable to a variety of proteins and protein complexes after minor affinity purification.[198] In most cases, the performance of CX-MS does not depend on the length, size, or tertiary structure of proteins being beneficial in analysis of large proteins and disordered regions of proteins.[198]

Taking advantage of MS exquisite accuracy and resolution, CX-MS studies have the ability to unambiguously identify crosslinks within proteins upon fragmentation to refine the modification site.[199] For substrate binding studies compared to computational methods, CX-MS does not require prior structural knowledge or information of the protein or binding site of interest.[198] Multifunctional crosslinkers offer users the ability to select the initial attachment allowing for precise positioning of the crosslinker within the protein for improved crosslinker functionality.[200] Comprehensive structural data can be additional acquired through the combination of varying lengths crosslinkers within single experiments.[201] Targeted quantitative CX-MS of crosslinked peptides accurately quantifies dynamic changes in protein structure, complexes, and interactions or varying experimental conditions and biological states, allowing for state-dependent mapping of protein-protein or protein-lipid interactions.[202]

One of the most prominent limitations of CX-MS studies is the requirement of high-resolution mass spectrometry instrumentation coupled with an efficient enrichment process of desired crosslinks given the low population of crosslinks within complex samples.[203] CX-MS can generate uneven distribution of crosslinking within a protein structure influenced by enzymatic digestion site distribution.[201]A limitation of CX is that crosslinkers generate artificial crosslinks

more prominent with longer crosslinker spacers, requiring greater effort of independent validation of identified crosslinks.[196] Crosslinker:protein ratios are kept low to avoid structural perturbations including crosslinker-induced polymerization.[203]

When targeting specific regions of protein/complexes, the crosslinker must be accessible to the desired site(s) of interest to interact and provide information.[150] Distance constraints crested through current crosslinkers may not have the resolution to resolve structural arrangements such as β-sheets.[201] A restriction or bottleneck of CX-MS studies arises during MS data analysis due to the lack of automated algorithms and programs to process both MS and MS-MS spectra limiting throughput stemming from the large diversity and uniqueness of individual assays as well as highly complex spectra with low signal intensity.[204]

1.6 Cholesterol-GlyR Interactions

1.6.1 Rationale

Lipid interaction studies with nAChR[83,86] demonstrate the requirement of cholesterol in bilayers for ion channel activity and asymmetric interactions based upon concentration. Cholesterol concentrations (>25 mol% and 40 mol%) were selected given cholesterol's activity threshold of ~33 mol%[40] coupled nAChR activity studies showing enhanced cholesterol-mediated ion flux up to ~35 mol % cholesterol membrane content,[86] correlating both lead to the hypothesis that if cholesterol crosslinking was used to analyze cholesterol accessibility to GlyR under both concentrations (<25 mol% and >40 mol%), the cholesterol accessibility/crosslinking pattern of <25 mol% would be entirely contained within the pattern of cholesterol accessibility/crosslinking of >40 mol% with additional crosslinking solely observed in the >40 mol% studies. Conversely to

traditional binding site studies, the <25 mol% crosslinking is hypothesized to be non-specific random interactions due to cholesterol's negligible activity while the >40 mol% crosslinking is hypothesized to be a collection of both non-specific interactions (observed in <25 mol% studies) and specific interactions unique to the elevated cholesterol condition.

It is hypothesized that azi-cholesterol-GlyR CX-MS studies can provide state-dependent differential crosslinking patterns that capture dynamic structural information about individual and distinct GlyR conformations. pLGICs including GlyR display distinct allosteric state conformations and when coupled with the ability to stabilize GlyR in the resting, open, and desensitized states allow the interrogation of state-dependent cholesterol interactions. This CX-MS study can not only elucidate concentration- and state-dependent effects on the GlyR-cholesterol interaction profile, but also reveal structural information (lipid accessibility through bilayer proximity and/or hydrophobic pockets) about unresolved portions of GlyR (M3-M4 loop and C-terminal tail). It is hypothesized that crosslinking identified in open state studies is a combination of crosslinking from channels sampling both resting- and open-like conformations and that crosslinking uniquely identified in open-state datasets are representative of the open state confirmation. Similarly, it is speculated that crosslinking identified under desensitizing conditions is a collection of crosslinking from channels sampling the resting, open, and desensitized conformations. Comparative studies can similarly be used to find unique crosslinks not observed in resting and open-state studies, such that crosslinking can be attributed to the desensitized receptor.

1.6.2 Experimental Overview

Given the essential, yet undefined role of cholesterol's modulation of pLGICs as well as other membrane proteins, we examined cholesterol accessibility of homomeric α1 GlyR in a concentration- and state-dependent manner using CX-MS. CX-MS concentration-dependent studies were conducted on apo-state GlyR at <25 mol% and >40 mol% cholesterol content within the lipid membrane. Resting state studies, performed previously[178] using WT apo-GlyR stabilize channels in a unbound, non-conducting manner. Azi-cholesterol, a photoactivatable cholesterol analog non-specific probe, was used to covalently capture cholesterol-GlyR interactions with equal incorporation into both concentration studies (<25 mol% and >40 mol%). To further define cholesterol's role in pLGIC modulation and expand on the apo-state GlyR studies, state-dependent cholesterol crosslinking was conducted on GlyR in conditions stabilizing the open and desensitized states at >40 mol% cholesterol in the lipid membrane. Open state studies were completed on a doubly mutant (F207A/A288G) GlyR in the presence of ivermectin (30 nM) yielding an ivermectin-sensitive non-desensitizing channel.[205] Desensitized state studies were conducted in the presence of saturating concentrations of glycine, stabilizing WT GlyR in a higher-affinity ligand-bound desensitized conformation. This study shows that photocrosslinking coupled with tandem MS can map a lipid-protein interface in several allosteric states/conformations, depicting lipid accessibility during transient structural changes. Direct cholesterol-GlyR interactions have been identified in different allosteric conformations that can help refine GlyR crystallographic/cryo-electron microscopic models, principally in unresolved regions, provide insight into ion channel dynamics of gating and desensitization.

CHAPTER 2: APO-STATE CHOLESTEROL-GLYR INTERACTIONS

2.1 Abstract

GlyR belongs to a superfamily of pLGICs that mediate fast neurotransmission. GlyR typically modulates inhibitory transmission by antagonizing membrane depolarization through anion influx. Allosteric interactions between the receptor and its lipid surroundings affect receptor function, and cholesterol is essential for pLGIC activity. Cholesterol at compositions below ~33 mol percent has been shown to have negligible chemical activity, suggesting that specific interactions between membrane proteins and cholesterol become significant only at concentrations above this stoichiometric threshold. Human α1 GlyR was purified from baculovirus infected insect cells and reconstituted in unilamellar vesicles at cholesterol:lipid ratios above and below the cholesterol activity threshold with equivalent aliquots of azi-cholesterol, a photoactivatable non-specific crosslinker. After photoactivation, crosslinked cholesterol-GlyR was trypsinized and mass fingerprinted. Mass shifted peptides containing cholesterol were identified by ESI-Q-TOF MS, and sites of direct covalent attachment to peptides were refined by targeted MS-MS. Differential patterns of dozens of cholesterol-GlyR crosslinks were identified in these comparative studies, with sites of crosslinking found primarily in the fourth transmembrane helix and extramembranous connecting loops and mapping the lipid-accessible surface of the receptor. Unique crosslinking observed in both reduced and elevated cholesterol composition suggests different apo-state structural conformations of GlyR as a function of cholesterol concentration and, in the latter studies, identified potential specific binding sites for cholesterol in the receptor.

2.2 Introduction

The current model of the biological membrane suggests lipids and proteins are not homogeneously distributed and form microdomains, with cellular processes at membranes modulated as a function of its composition.[52] Lipid composition alters the physicochemical properties of the bilayer, and this local environment may modulate the structure and function of membrane proteins.[53,54] Striking examples of these effects include the different topologies exhibited by lactose permease as a function of phospholipid composition,[206] the abrogation of dimer formation of the leucine transporter from cardiolipin delipidation,[63] the lipid dependence of glucose transporter activity,[207] and the effects of cholesterol on ion channels and other membrane proteins.[80,208,209] Crystallographic studies have further highlighted the importance of these interactions as structures often contain specific bound lipids.[65] For example, cholesterol has been co-crystallized with G-protein coupled receptors,[65] Na^+,K^+ ATPase,[69] and the dopamine transporter.[71]

Sterols preferentially associate with increasing acyl chain saturation of phospholipids and with sphingolipids, forming complexes and microdomains that target the transmembrane regions of some proteins.[210,211] Cholesterol in molar excess of the capacity of these complexes has high accessibility and fugacity, and will be referred to as "active cholesterol".[36] Above this stoichiometric threshold there is a sharp increase in sterol availability to cholesterol oxidase, perfringolysin, and methyl-β-cyclodextrin.[37–39] Sterol availability typically emerges at concentrations above 25-35 mol percent and at lower concentrations it has negligible chemical activity.[40,41] Membrane–intercalating amphihiles can activate cholesterol by displacing cholesterol from its lipid complexes.[212] Consistent with these observations, cholesterol activity increases in

the presence of sphingomyelinase.[213] Taken together, significant specific cholesterol-protein binding is expected to emerge only at higher cholesterol concentrations.

The interactions between pLGICs, the superfamily of ion channels that are essential for fast neuronal signaling between cells, and the surrounding lipids influence their function.[72,73] Lipids are proposed to allosterically modulate GluCl by inducing an expanded open-like conformation and by potentiating agonist binding.[75] Both depletion and enrichment of membrane cholesterol reduced efficacy of GABAR channel activation.[79] Cholesterol and anionic phospholipids have been shown to be a key modulator of nAChR function and critical for conformational transitions between allosteric states.[82–84] In reconstituted lipid vesicles lacking cholesterol or phosphatidic acid, agonist fails to stimulate nAChR ion flux.[85,86] Increasing cholesterol/phosphatidic acid concentration within the lipid environment enhances nAChR-mediated ion flux and was found to saturate at ~35 mol percent cholesterol and ~12 mol percent phosphatidic acid.[86] Below this concentration, nAChR favors a desensitized-like uncoupled state, while approaching and exceeding this threshold favors the resting state, which has the ability to undergo agonist-induced conformational transitions.[214]

A novel way of gaining structural information to further understand protein-lipid interaction is through the use of chemical crosslinking.[215] Photoaffinity labeling studies directly identified the propofol-binding site of GLIC[190] and GABAR.[191] Cholesterol homologs were similarly used to map sites of cholesterol interactions with the PBR and putative cholesterol recognition amino acid consensus (CRAC) motifs were identified.[192] Cholesterol photoaffinity probes have also characterized lipid-protein interactions of cholesterol and nAChR.[194,195] In these studies, azi-cholesterol bound extensively to the M4 region within nAChR (~75%), as compared to the M1 and M3 segments (~25%), with binding regions congregated toward charged amino

acids located at the ends of the M4 segment, leading researchers to question whether peptide labeling is driven by proximity of the azi-cholesterol or by diffusional encounters with accessible side chains.[194] The advent of MS methodologies offers the opportunity to more sensitively and specifically detect and map covalent crosslinks with lipids.

Given the essential, yet not completely defined role of cholesterol's influence of membrane protein structure and function, we propose to examine the cholesterol accessibility of a paradigmatic pLGIC as a function of cholesterol concentration in comparative studies above and below its "activity" threshold. In this study we have focused on identifying non-specific (cholesterol at low mol percent) and specific (additional unique interactions with active cholesterol present only at high mol percent in comparative studies) interactions of cholesterol with the GlyR using CX-MS. The pentameric GlyR is typically comprised of two transmembrane subunit homologs (α and β) surrounding a central anion-selective pore arranged with a 2α:3β subunit stoichiometry.[120] Each subunit consists of a large ECD followed by four transmembrane segments (denoted M1-M4) and an extracellular tail.[125] The ligand-binding site is located at the interface between neighboring subunits in its ECD, with aromatic residues lining the binding pocket.[216] Upon binding of the neurotransmitter glycine, GlyR transitions to a metastable open state conformation, characteristically hyperpolarizing the post-synaptic neuron through chloride influx, and then a long-lived non-conducting desensitized state that more tightly binds glycine.[217] The intracellular domain consisting of loop-like structures (M1-M2 and large M3-M4 loops) has roles in receptor trafficking and localization, and the M3-M4 loop contains a site of phosphorylation. However the structure of this large M3-M4 loop is poorly refined in studies of pLGICs, as it is typically excised in structural studies due to its expected flexibility. This region contains the greatest sequence diversity among pLGICs and has not been resolved in any pLGIC

structure,[96,218,219] highlighting the importance of the development of methods that can provide information regarding the structure of the M3-M4 loop. The C-terminal tail after M4 is also poorly resolved in current structures. In addition, given that the structure and function of pLGICs is modulated by lipid composition (as described above), it is imperative to develop new complementary techniques that provide investigators with the tools to examine membrane protein structures in native-like reconstituted membranes in the absence of detergents. CX-MS studies can provide some of this complementary information.

Elucidating the lipid accessible regions of pLGICs are essential as modulatory anesthetics and bioactive lipids partition within the bilayer and their effects may be mediated through the lipid-protein interface.[143,144] Here, we analyzed cholesterol-human α1 GlyR interactions in the resting state of the receptor using photocrosslinking coupled with multidimensional MS. Advancements in MS technologies have improved the sensitivity and accuracy of detection in CX-MS experiments, increasing the number of low-intensity crosslinked peptides identified and subjected to tandem MS analysis.[185] Current tandem mass spectrometers have the sensitivity and mass accuracy for the unambiguous identification of crosslinked species and through peptide fragmentation, allowing the identification of specific amino acid residue(s) involved in crosslinking.[183,184]

Given the differential activities of cholesterol at low and high mol percent, azi-cholesterol, a photoactivatable cholesterol analog, was crosslinked to wild-type human homomeric α1 GlyR at conditions that probe interactions when cholesterol has negligible chemical activity (<25 mol percent natural cholesterol in membrane) and when cholesterol is more chemically active (>40 mol percent natural cholesterol in membrane).[42,220] Only at concentrations above this approximate threshold does one observe the emergence of free "liquid" cholesterol that is chemically active.[220]

This threshold correlates with the approximate concentration of cholesterol (~35 mol percent) required for functional nAChR.[86] Therefore, it is speculated that in conditions where cholesterol has negligible chemical activity (<<33 mol percent), cholesterol would not specifically interact with potential cholesterol-binding sites in GlyR, as chemically inactive cholesterol is postulated to be sequestered among phospholipids and microdomains. Rather, identified crosslinks are hypothesized to result from random diffusional encounters of cholesterol and protein. Conversely, in chemically active cholesterol conditions (>>33 mol percent), the free "liquid" cholesterol is chemically active (it is postulated that at elevated concentrations, cholesterol's affinity for lipid is exceeded) and is available to additionally interact specifically with GlyR, such that identified crosslinks are a result of specific and non-specific interactions with cholesterol. This study shows that MS can sensitively identify covalent sites of lipid-protein interactions, as picomoles of purified protein are sufficient to allow identification of dozens of sites of crosslinking in each experiment. These studies directly identify lipid-protein interactions and can aid in the refinement of GlyR structural models derived from crystallographic and cryo-electron microscopic studies, particularly in identifying cholesterol interactions with GlyR in reconstituted vesicles.

2.3 Materials and Methods

2.3.1 Purification of GlyR from *Sf*9 insect cells into mixed detergent micelles

Purified GlyR in mixed detergent/lipid micelles were isolated as previously described.[121] Briefly, WT human α1 GlyR was overexpressed in a baculovirus infected *Sf*9 insect cells. Three days post-infection *Sf*9 insect cells were gently pelleted, washed with 1X phosphate buffered saline (PBS) pH 7.4, and resuspended in a hypotonic solution (5 mM Tris pH 8.0, 5 mM

ethylenediaminetetraacetic acid (EDTA), 5 mM ethylene glycol tetraacetic acid (EGTA), 10 mM dithiothreitol (DTT)). An anti-proteolytic cocktail (1.6 μunits/mL aprotinin, 100 μM phenylmethanesulfonyl fluoride (PMSF), 1 mM benzamidine, 100 μM benzethonium chloride) was added to reduce protein degradation immediately preceding lysis. Cells were lysed by sonication followed by centrifugation (387,000 x g for 30 min) to isolate cell membranes containing GlyR. Cell membranes were washed with a resuspension buffer (hypotonic solution, 300 μM NaCl) followed by centrifugation again to remove peripheral membrane proteins. The protein pellet was solubilized in 10:1 digitonin:deoxycholate buffer (12 mM mixed lipids (9:1 plant extract (95% phosphatidycholine purity, Avanti): egg extract (60% phosphatidycholine purity, Avanti) at 15 mg/mL, stored as suspended vesicles), 0.10 % deoxycholate, 1.0 % digitonin, 25 mM potassium phosphate monobasic, 79 mM potassium phosphate dibasic, 1 M KCl, 5 mM EDTA, 5 mM EGTA, 10 mM DTT, anti-proteolytic cocktail) overnight, and solubilized micelles were isolated after centrifugation (387,000 x g for 1 hr). GlyR/lipid/detergent micelles were affinity purified on 2-aminostrychnine agarose and eluted competitively with the addition of excess glycine (2 M) to the solubilization buffer.

2.3.2 Reconstitution of GlyR into lipid vesicles at defined concentrations of cholesterol, incorporating azi-cholesterol

GlyR vesicle reconstitution was completed as previously described[124] with the following modifications to the lipid composition. All steps were conducted in the dark and at 5˚C unless noted. Mixed lipids (9:1 plant extract (95% phosphatidycholine purity): egg extract (60% phosphatidycholine purity) at 15 mg/mL, stored as suspended vesicles) were added to purified GlyR/lipid/detergent micelles to yield a final concentration of 1.5 mg/mL. Cholesterol (15.07 mM

in methanol) was included to yield >40 mol percent and <25 mol percent for defined conditions. Azi-cholesterol was kept at constant concentrations in both conditions at 6 μM. As previously described, samples were added to dialysis cassette (3500 MW cutoff, Thermo) for dialysis against excess potassium phosphate buffer (6.25 mM, pH 7.4). The final reconstituted protein pellet was dissolved in potassium phosphate buffer (25 mM, pH 7.4). GlyR concentrations were quantitated using a modified Lowry assay.[221]

2.3.3 Photo-crosslinking of Azi-cholesterol to GlyR and separation of crosslinked GlyR

Reconstituted GlyR vesicles were placed into quartz cuvettes on ice to maintain temperature. Cuvettes were exposed to a 420 W Hg Arc lamp (Newport, Model 97435-1000-1, 260-320 nm) for 4 sessions of 5 minutes at 7 cm, with 5 minute periods of no exposure in between each UV exposure session to prevent sample warming. SDS-PAGE (11 % resolving, 5 % stacking) separated the crosslinked oligomeric and monomeric GlyR from lipids, with gel plugs excised between migration distances of 250 kDa and 37 kDa, encompassing the mass of oligomeric and monomeric forms of GlyR.

2.3.4 In-gel Trypsin digestion of crosslinked GlyR

Gel plugs were washed with 50:50 absolute methanol: 50 mM ammonium bicarbonate twice for 40 min with gentle agitation (VWR Thermal Shake Touch, 900 rpm). Gel plugs were dehydrated by adding 500 μL acetonitrile. Once gel plugs turned whitish, acetonitrile was removed and gel plugs were dried in an Eppendorf 5301 Vacufuge Concentrator for approximately 15 minutes. Trypsin solution (10 μL at 20 μg/mL in 50 mM ammonium bicarbonate) was added to gel plugs and incubated on ice for 15 minutes, then incubated overnight at 37˚C with gentle

agitation (VWR Thermal Shake Touch, 900 rpm). Digested peptides extracted into supernatant and transferred to VWR non-stick microcentrifuge tubes. Tryptic fragments were further extracted by incubating gel plugs twice for 30 minutes in 300 µL of 0.1 % formic acid in 50:50 acetonitrile:H_2O. The supernatant was collected and combined with initial supernatant. Tryptic extract solution was dried in an Eppendorf 5301 Vacufuge Concentrator.

2.3.5 Mass fingerprinting of crosslinked cholesterol to GlyR

50:50 Acetonitrile: H_2O with 0.1 % Formic Acid (50 µL) was added to tubes containing dried tryptic extracts. ESI-Q-TOF-MS measurements were taken using an Agilent 6530 Q-TOF-MS with an Agilent HPLC-Chip II G4240-62006 ProtID-Chip-150, comprised of a 40 nL enrichment column and a 75 µm x 150 mm separation column packed with Zorbax 300SB-C18 5 µm material. The mass spectrometer was run on positive ion mode using internal standards (1221.9906 and 299.2944) for calibration, supplied by Agilent. Mobile phase compositions used were Solvent A (95 % H_2O, 5 % ACN, 0.1 % Formic acid) and Solvent B (95 % ACN, 5 % H_2O, 0.1 % Formic acid) The nanoflow elution gradient was developed as follows at 0.50 µl/min of Solvent A (minute: percent A): 0.00: 95 %, 4.00: 10 %, 6.00: 70 %, 9.00: 50 %, 11.50: 95 %, 13.00: 95 %. Data were processed using Agilent Qualitative Analysis Software 6.0. Cholesterol crosslinked peptides within a 10 ppm accuracy window were identified, accounting for possible peptide modifications (oxidation, acrylamidation).

For MS-MS studies, crosslinked samples were run again on the Agilent 6530 Q-TOF-MS, targeting the specific m/z ratio, charge, and retention time of the crosslinked peptides identified in MS analysis. CID was used for MS-MS fragmentation following a linear increase in collision energy by m/z using the equation: $y=3.7x+2.5$. CID was performed at $\pm$ 0.2 min from initial MS

scan retention time of each crosslinked precursor ion identified. Data were processed using Agilent Qualitative Analysis Software 6.0 in conjunction with ProteinProspector v5.14.3 available through the University of California, San Francisco.

2.4 Results and Discussion

2.4.1 Cholesterol crosslinking to resting state GlyR at reduced cholesterol composition

As noted previously, cholesterol is expected to exhibit very different chemical activity as a function of its concentration in reconstituted membranes, so comparative crosslinking studies conducted at low and high cholesterol composition can be used to potentially map non-specific and specific sites of protein-cholesterol interactions, respectively. Functional GlyRs were purified from baculovirus infected *Sf*9 insect cells[121] and reconstituted into vesicles under conditions that have been shown to retain complete GlyR activity in outside-out orientations[124] at selected lipid composition containing constant levels of mixed plant/egg phosphatidylcholine (12 mM) and photoactivatable azi-cholesterol (6 μM, Figure 8).

For comparative studies, the only variable was the cholesterol content in the vesicles, which was <25 or >40 mol percent, well below or well above the published typical threshold limits

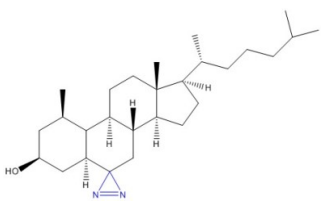

Figure 8. Chemical structure of photoactivatable azi-cholesterol. Chemical structure of cholesterol crosslinker analog, with the reactive site highlighted in blue.

for cholesterol activity,[42,220] respectively. The lipid composition in reconstituted vesicles was chosen to reflect the generic lipid compositions (i.e., saturated and unsaturated acyl chains with various headgroups) found in the cell lines used in activity assays (HEK and insect cells), dynamic neuronal membranes[56] and the studies examining cholesterol activity (described previously).[86,40] At <25 mol percent, cholesterol is expected to exhibit negligible chemical activity (sequestered in microdomains) and identified crosslinks to GlyR are ascribed to random diffusional encounters, and are expected to map the lipid accessible surface of the receptor. At >40 mol percent, cholesterol is expected to have much greater chemical activity and identified crosslinking will be due to specific interactions of the active cholesterol as well as non-specific random diffusional encounters. In comparing the two studies (low and high cholesterol), crosslinking unique to the >40 mol percent conditions are expected to be the specific cholesterol binding sites in GlyR, or changes in lipid accessibility of GlyR due to structural changes as a function of increased cholesterol concentration.

Table 1. Cholesterol crosslinking at reduced cholesterol composition. Identified mass-shifted precursor ions crosslinked with cholesterol (within 10 ppm error, identified in at least 2 of 3 trials) at <25 mol percent cholesterol conditions shown in left column. Sites of covalent modification identified upon analyses of product ions upon CID fragmentation are bolded and underlined; spaces separating amino acids represent single point amino acid crosslinking sites in succession. *Modifications of the precursor ion, including crosslinked cholesterol. Precursor ions identified with different combinations of modifications are shown for each precursor ion. Parenthesized numbers following "Azi" represent the number of crosslinked cholesterol(s) within the mass-shifted peptide.

Amino Acid Sequence	Structural Location	Modifications*
^{60}VNIF**<u>LR</u>**^{65}	Pre-M1 ECD	Azi
^{60}**<u>VNI</u>**FLRQQWNDP**<u>R</u>**^{72}		Azi (3) Azi (4)
^{191}**<u>E</u>**EK**<u>DL</u> <u>R</u>**YC**<u>T</u> <u>K</u>**^{200}		Azi, Acryl (2) Azi (2), Acryl Azi (2) Azi (3)
^{194}**<u>DL</u>**RY**<u>CT</u>**K^{200}		Azi Azi, Acryl
^{310}QH**<u>K</u>**ELL**<u>R</u>**^{316}	M3-M4 Loop	Azi (4)
^{313}**<u>EL</u>**L**<u>R</u>**FR**<u>R</u>**^{319}		Azi
^{321}R**<u>RH</u> <u>H</u> <u>K</u>**^{325}		Azi Azi, Ox (2) Azi (2), Acryl
^{323}**<u>HH</u>**KEDEAGEG**<u>R</u>**^{333}		Azi, Acryl, Ox
^{326}**<u>ED</u>**EAGE**<u>GR</u>**FNFSAYGMG PACLQAKD**<u>GI</u>**SV**<u>K</u>**^{355}		Azi (3), Acryl
^{334}FNFSAYGMPACLQA**<u>K</u>**^{349}		Azi
^{372}**<u>S</u>**PE**<u>E</u>**M**<u>R</u>**K^{378}	M3-M4 Loop/M4	Azi, Acryl Azi, Ox Azi (2), Ox
^{378}KLF**<u>IQ</u> <u>R</u>**^{383}	M4	Azi Azi, Acryl Azi (3)
^{384}**<u>AK</u>**KID**<u>K</u>**^{389}		Azi (2), Acryl
^{386}K**<u>ID</u> <u>KI</u>**SR^{392}		Azi (4)

To identify lipid accessible surface of GlyR in its resting state that interacts with cholesterol in a non-specific manner, the total cholesterol was limited to <25 mol percent where it

is expected to exhibit negligible chemical activity.[42,220] After photoactivation, GlyR containing vesicles were subjected to SDS-PAGE and GlyR containing bands were excised, trypsinized, and subsequently extracted peptides were analyzed by tandem MS (allowing up to 2 missed tryptic cleavages, as photocrosslinking at Arg or Lys sites might result in reduced trypsinolysis). For all studies, duplicate MS runs were conducted on samples from purified GlyR from 3 independent infections/preparations, and mass shifted peptides are reported with an n of $\geq$ 2. Initial MS analysis identified precursor mass ions consistent with lipid crosslinking (cholesterol m/z shift, +386.3549 amu) using a 10 ppm cutoff (Table 1, left column).

Crosslinking analysis was conducted on data sets of each of the 3 trials with peptide identified sequence coverage of GlyR up to 60 percent. Crosslinking analysis was not limited to a single cholesterol crosslinking event, but allowed up to 4 cholesterol crosslinks per tryptic peptide, as cholesterol is distributed in both leaflets of the lipid bilayer having the potential to interact at multiple sites within a single tryptic peptide (Table 1, right column, number following "Azi" modification), as well as "piggybacking" (cholesterol crosslinking to a GlyR bound cholesterol).

The identified precursor ions assigned to mass-shifted peptides containing cholesterol were subjected to targeted CID, and product ions were analyzed to refine the site of crosslinking within the mass-shifted peptide and confirm initial assignments (Table 1, bolded and underlined amino acid(s) within each peptide). CID fragmentation typically produces *b* and *y* product ions of the precursor mass ion. Through comparison of product ions (*b*, *y*, and occasionally *a* ions) containing mass shifts due to attached cholesterol to those that do not, the site of attachment can be refined, typically to a single amino acid site. Given that tryptic peptides could be modified at

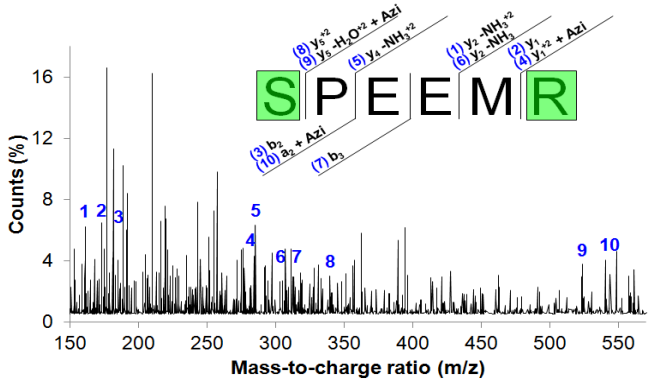

Figure 9. Representative CID-induced fragmentation of crosslinked precursor ion. The identified product ion fragments (1-10), including those mass shifted (+ Azi), are highlighted.

more than a single site (for example, if two different amino acids on a given peptide are modified, these isobaric precursor ions would provide product ions after CID that obscure assignment), MS-MS spectra are strictly matched by retention time to their precursor ion. Given that in-line liquid chromatography can potentially separate isobaric peptides via differential chemical properties, each correlated (with respect to retention time) precursor/product pair is capable of yielding a refined crosslinking site(s) even when present at multiple sites (sites of crosslinking within isobaric tryptic fragments are bolded and underlined in Table 1). By individually analyzing each product ion fragmentation spectrum at a given retention time, isobars may be unequivocally resolved in MS-MS studies. Only precursor ions assigned to cholesterol crosslinked peptides ($\geq$ tetrapeptides) identified having overlapping sequence coverage in $\geq$ 2 of 3 trials were mapped. CID fragmentation within the retention time window (+/- 0.2 minutes) produces product ion fragmentation spectra (2-12 spectra) of each cholesterol crosslinked peptide assigned precursor ion were individually analyzed to identify the site of covalent attachment in its respective precursor ion. Only product ion spectra with $\geq$ 2 assigned product ions and $\geq$ 2 cholesterol mass shifted product ions were considered, with product ion spectra typically assigning up 12 cholesterol mass

shifted ions. A representative product ion fragmentation pattern detailing the identification of site(s) of covalent modification is shown in Figure 9.

Sites of cholesterol crosslinking following targeted MS-MS refinement were mapped to onto a model of α1 GlyR for visualization (Figure 10A and C), however many sites of crosslinking occur in the M3-M4 intracellular loop and the C-terminal tail of the receptor, regions that are not resolved in any pLGIC homologs and are thus missing from the homology-based model (these regions are discussed at greater length below and highlight the utility of CX-MS based approach as a complement to other biophysical methods). Refinement identified single amino acid crosslinking sites in succession as well as individual sites, with nearly all cholesterol crosslinks refined to single amino acids, and the largest identified refined site to be a tripeptide. The refined crosslinking sites at reduced cholesterol composition were identified in the large ECD preceding M1 (preceding residue 220), the M3-M4 loop (residues 309-378), and transmembrane helix M4 (residues 379-410) of the GlyR resting state and are shown in Table 1 and Figure 10A and C. Within the pre-M1 ECD, crosslinking was found in regions nearing the lipid bilayer either in beta sheets or loops. Within the M3-M4 loop, crosslinking was identified mainly in regions nearing either M3 or M4 transmembrane helices. Crosslinking within M4 was identified near the cytoplasmic M3-M4 loop.

Cholesterol crosslinking sites unique to reduced cholesterol composition were observed (Figure 10A, light green) when compared to elevated cholesterol composition. Overall, the findings suggest the non-specific cholesterol:GlyR interactions to be mainly within extra/intracellular domains nearing or buried within the lipid bilayer and the M4 transmembrane helix, with these areas of GlyR expecting to have the most accessibility with the lipid interface

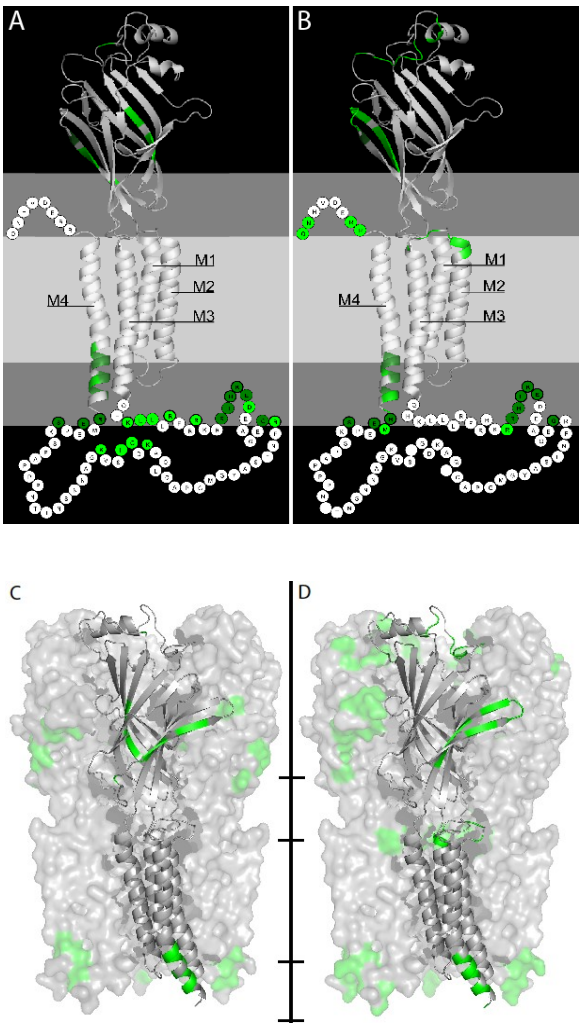

Figure 10. GlyR-cholesterol interactions as a function of cholesterol concentration. Azi-cholesterol crosslinking at (A) reduced and (B) elevated cholesterol conditions mapped to a single α1 subunit of zebrafish GlyR (PDB #3JAD) using PyMOL v1.8.[100] Areas corresponding to the bilayer are shown in gray (~15Å interfacial regions) and light gray (~30 Å hydrophobic acyl chain region). (A). Sites of crosslinking (bolded and underlined amino acids in Table 1 and 2, respectively) uniquely identified at either low or high cholesterol levels are light green and those observed under both conditions are dark green. Beads represent regions not resolved in the zebrafish structure (M3-M4 loop and C-terminal tail) with crosslinks arbitrarily placed in close proximity to the lipid bilayer. Bolded beads represent refined sites of attachment. Space-filling GlyR pentamer (with one single subunit shown as ribbon diagram) with sites of crosslinking highlighted in green for <25 mol percent cholesterol (C) and >40 mol percent cholesterol (D). Unresolved regions of the receptor are not shown in panels C and D.

given the pentameric structure, highlighting the lipid accessible regions of GlyR in its resting state when cholesterol exhibits negligible activity.

2.4.2 Cholesterol crosslinking to resting state GlyR at elevated cholesterol composition

Comparative studies and analysis analogous to those conducted with reconstituted GlyR in its resting state at reduced cholesterol composition were similarly conducted at elevated cholesterol composition of >40 mol percent. As before, GlyRs were purified from baculovirus infected insect cells (duplicate MS studies of 3 independent infections) and reconstituted into vesicles with total cholesterol enriched to >40 mol percent, but invariant levels of photoactivatable azi-cholesterol (6 μM). At >40 mol percent, cholesterol is expected to exhibit significantly greater

Table 2. Cholesterol crosslinking at elevated cholesterol composition. Identified precursor ion crosslinked peptides at >40 percent cholesterol with conditions as described in Table 1.

Amino Acid Sequence	Structural Location	Modifications
^{17}L**MG R**TSGY**DAR**^{27}	Pre-M1 ECD	Azi
^{28}**IR P N**F**K**^{33}		Azi, Acryl Azi (2), Acryl
^{197}Y**CTK**HYNTG**K**^{206}		Azi, Ox
^{197}YCTKH**YNTGKF** T**CIEAR**^{213}		Azi (2), Acryl (3), Ox
^{272}**ASL**PK**VS**Y**V**K^{281}	M2-M3 Loop	Azi Azi, Acryl Azi (2), Acryl (2)
^{321}**RR**H**H K**^{325}	M3-M4 Loop	Azi Azi, Ox Azi (2)
^{323}**HH**K**E**DEAGE**G**R^{333}		Azi, Acryl, Ox
^{372}**S**PE**E M R**^{377}		Azi, Ox
^{372}SPEE**M**R**K**^{378}	M3-M4 Loop/M4	Azi, Acryl
^{372}SPEEMR**KL**IFQR^{383}		Azi (3), Ox
^{378}**K**L**FIQ**RA**K**^{385}	M4	Azi, Acryl Azi (4), Acryl
^{384}**AK K I**D**K**^{389}		Azi Azi, Acryl (3)
^{387}**IDK**ISRIGFPMAFLIFNMFYWIIYK^{411}		Azi (4), Acryl, Ox
^{415}**RE**DVH**NQ**^{421}	C-terminal tail	Azi Azi (2), Ox

chemical activity,[42,220] and specific interactions, as well as non-specific interactions (observed in trials conducted at <25 mol percent), are expected to be observed. Alternatively, different crosslinking sites might also be identified if higher levels of cholesterol stabilize the apo-GlyR in a different conformation (discussed below), thus altering the lipid accessibility profile of apo-GlyR. After photoactivation, GlyR was similarly subjected to SDS-PAGE and the excised GlyR bands were trypsinized and extracted peptides were analyzed by MS-MS.

As before, MS analyses identified precursor ions corresponding to trypsinized peptides mass shifted consistent with covalent modification with cholesterol using a 10 ppm cutoff (Table 2, an expanded Table is provided in Supplemental Material). Mass shifted precursor ions were targeted for CID and product ions analyzed to further refine the site(s) of crosslinking. Targeted MS-MS analysis identified product ion fragments including those containing cholesterol crosslinks, allowing for the identification of crosslinking to single amino acids (Table 2) and these were mapped onto a model of α1 GlyR (Figure 10B and D). The refined cholesterol crosslinking sites were found in the large ECD preceding M1, the M2-M3 loop, the M3-M4 loop, transmembrane helix M4, and the extracellular C-terminal tail (Table 2 and Figure 10B and D). Within the pre-M1 ECD, crosslinking was identified in regions of beta sheets and loops. Within the M3-M4 loop, crosslinking was identified in regions near both M3 and M4 transmembrane helices, primarily M3. At elevated cholesterol concentrations of >40 mol percent, crosslinking emerged in the M2-M3 loop and post M4 C-terminal tail compared to cholesterol crosslinking in reduced cholesterol conditions (<25 mol percent). Cholesterol crosslinking sites unique to elevated cholesterol lipid composition were observed (Figure 10B, light green) when compared to reduced cholesterol lipid composition. Unique crosslinking sites may be due to specific cholesterol:GlyR interaction sites in active cholesterol conditions, and these regions were identified in the pre-M1

ECD in beta sheets and unstructured loops, the M2-M3 loop, regions of the M3-M4 loop, M4, and the post M4 C-terminal tail. Taken together, elevated cholesterol studies revealed not only redundant crosslinking observed in low cholesterol studies, but additional unique crosslinking unique to studies conducted at elevated cholesterol content. Emergence of unique crosslinking to elevated cholesterol conditions, but only partial redundancy as compared to reduced cholesterol conditions suggests that subtle structural conformational changes occur as a function of cholesterol concentration (discussed at more length below).

This CX-MS study highlights the power of MS to sensitively and directly identify the cholesterol:GlyR sites of interaction in reconstituted bilayers with minute quantities of protein. These photocrosslinking studies directly identify covalent linkages between cholesterol and GlyR

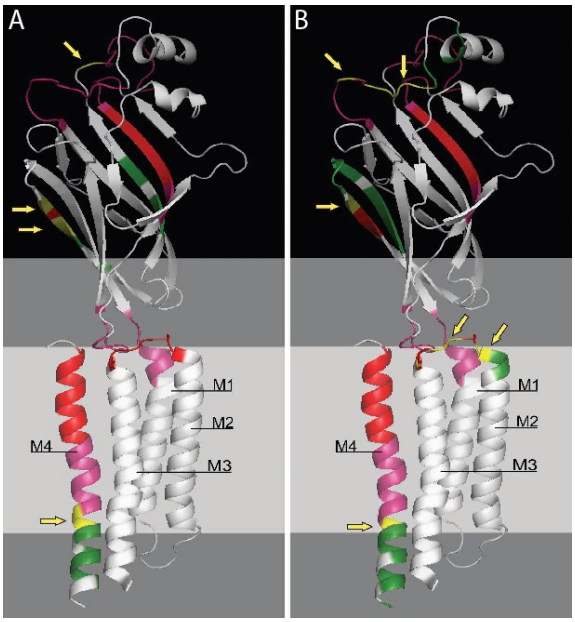

Figure 11. Comparison of predicted and experimentally determined sites of GlyR-cholesterol interaction. CRAC (red) and CARC (dark pink) motifs and experimentally determined crosslink sites (green) under reduced (A) or elevated (B) cholesterol composition are mapped to a single α1 subunit of zebrafish GlyR.[100] Overlap between predicted and experimental sites are shown in yellow (see arrows). No CARC or CRAC motifs are found in the M3-M4 loop and C-terminal tail (not shown).

as a function of cholesterol concentration. An assumption in the study is the functional and chemical equivalence of azi-cholesterol and cholesterol, as validated in other published studies using this crosslinker.[86,222–224] Given their nearly equivalent structure, it is reasonable that azi-cholesterol and cholesterol interact with surrounding lipid and protein in a similar manner, and that these two lipids share identical chemical activities that vary as a function of their aggregate concentration. All studies were conducted at room temperature, consistent with conditions used in determining cholesterol activity as a function of its concentration,[40] as well as the temperature typically used in whole cell patch clamping conditions used to correlate structure and function. However, it should be noted that these studies were conducted at non-physiological temperatures, and this may affect some of the observed interactions.

Elucidating the lipid-protein interface of ion channels is essential as it is a major site for interactions of general anesthetics with pLGICs,[225,226] synthetic neurosteroids of homomeric α1 GlyR,[227] and tetrahydrocannabinol with GlyR.[111] All of these lipophilic compounds partition within the bilayer and bind and modulate pLGIC activity,[85,86] but high resolution structural determination of membrane proteins typically require the presence of detergents and disruption of the bilayer. Herein we show the capability of CX-MS to directly interrogate protein-lipid interactions and define dozens of sites of cholesterol's interactions with apo-GlyR in reconstituted vesicles of defined lipid composition. Thus, this complementary analytical tool is shown to sensitively map the lipid-protein interface as a function of lipid composition, allowing us to better map the lipid interactome with membrane proteins. In addition, some of the sites of these interactions are located in other poorly resolved regions of current models of pLGICs.

Amino acid consensus motifs predictive of cholesterol binding have been identified where CRAC motifs have the sequence (L/V)-(X_{1-5})-(Y)-(X_{1-5})-(R/K) and inverted CRAC (CARC)

motifs have the sequence (R/K)-(X_{1-5})-(Y/F)-(X_{1-5})-(L/V) where X is any amino acid.[17] CRAC and CARC motifs were mapped to a single subunit cryo-EM zebrafish α1 GlyR[100] and compared with the crosslinking data (Figure 11). Cholesterol crosslinked regions of GlyR coincided to CARC motifs at locations within the ECD preceding and at the beginning of M1 and within M4. However, many of the binding sites observed at reduced and elevated cholesterol composition were not in the predicted regions. Conversely, some of the predicted binding sites were not observed experimentally. Taken together, this suggests that although the predictive CRAC/CARC motifs have utility, more data is necessary to ensure the motifs are more selective to accurately identify sites of cholesterol interactions. Investigators continue to computationally model specific sites of interaction of cholesterol with membrane proteins given the physiological significance of these interactions.[224,228]

Of note, many of the regions observed in our crosslinking data are in the large intracellular M3-M4 loop and the post-M4 C-terminal tail, regions of the receptor that are not resolved in any crystal or cryo-EM structures of pLGICs.[75,218] In particular, crosslinking within the M3-M4 loop was often observed to charged residues of this large intracellular loop, predominately arginine, lysine, histidine, and glutamate. Significantly, arginine and lysine are identified in CARC and CRAC recognition sites for cholesterol binding. Evidence of lipid-accessible residues within regions whose structure is unresolved by other biophysical methods highlights the potential of CX-MS to complement other high-resolution biophysical studies and provide a wealth of unique data. Cholesterol crosslinks in both the M3-M4 loop and post-M4 C-terminal tail suggest that these regions are in close proximity with the membrane surface. Additionally, these events may be due to the fluidity of the bilayer and/or protein dynamics allowing GlyR to sample different depths within the bilayer, bringing parts of the ECD in close proximity to the membrane surface. A striking

example of conformational flexibility of ion channels is evidenced in recent cryo-EM studies of NMDA receptors,[229] where dramatic movements of the large ECD of these receptors were observed in a single, antagonist bound state. This large allosteric complex exhibited multiple conformations within a single allosteric state, with regions in the ECD appearing to be intimately associated with the bilayer. Site-directed spin-labeling studies have also large conformational exchanges to be present in regions of membrane proteins in native bilayers that are not observed in well-ordered crystallographic studies.[230] The sensitivity of CX-MS to capture conformational heterogeneity via covalent crosslinking is yet another tool that may assist in identifying dynamic intimate associations between regions of membrane proteins. One potential limitation to CX-MS is the inability to easily determine the relative frequency of these events, as quantification of the relative abundance of crosslinks is difficult, and will be further discussed below.

The M4 region of pLGICs face the periphery of the receptor and have been shown to be lipid accessible,[195] so it was anticipated that CX-MS studies would identify amino acids within this region under low and high cholesterol conditions. Multiple crosslinking sites at the intracellular end of M4 were reproducibly identified in both cholesterol conditions, with unique crosslinking of R^{383} at low conditions and K^{386} at high conditions, suggesting a subtle rotation of M4 as a function of cholesterol content. Thus, our results are consistent with nAChR studies[231] that posits conformationally distinct resting states under low and elevated cholesterol content. As expected, M4 sites were identified in CX-MS studies, however, cholesterol crosslinking in both reduced and elevated cholesterol composition were also identified in other regions of the receptor, including the ECD preceding M1 and the M3-M4 loop (Figure 10). Given the high solubility of cholesterol in DOPC bilayers (67 mol%),[232] its strong partition coefficient for octanol over water ($\log P_{oct/wat}$ is 7.39) and its essential insolubility in water (~2.6×10^{-5} mg/ml),[233] it is assumed that

all cholesterol is sequestered within the bilayer. In addition to crosslinks within M4, covalently modified sites were reproducibly identified in regions expected to be far from the bilayer (e.g., ^{60}VNIFLRQQWNDP***R***^{72} and ^{17}L***MGR***TSGY***DARIRPN***F***K***^{33} (residues in bold identify sites of covalent modifications within the mass-shifted tryptic peptide) in reduced and elevated cholesterol composition, respectively). While it is difficult to accommodate bilayer cholesterol interacting directly with some of the regions that appear to be far away from the membrane in the ECD (Figure 9), the reproducibility of distinct binding sites as a function of cholesterol concentration is observed in our studies and this reproducibility is considered evidence that these are not random events due to misfolded protein and/or cholesterol in the aqueous phase. Rather, these sites, that also contain CARC and CRAC motifs, are postulated as being a hydrophobic cavity that may sequester cholesterol introduced in the mixed micelles during purification. Isoflurane and ketamine, general anesthetics, bind to homologous regions of the ECD of nAChR[234] and GLIC,[146] consistent with the presence of conserved hydrophobic binding pockets in the ECD of pLGICs located distantly from the bilayer.

Under elevated cholesterol conditions (>40 mol percent), cholesterol crosslinking locations were refined to many of the same regions as observed in comparative studies at reduced cholesterol levels, but additionally included unique sites in the ECD, the M2-M3 loop, and the post-M4 C-terminal tail of the receptor. As described previously, at membrane concentrations below ~33 mol percent, cholesterol exhibits negligible chemical activity due to its affinity to form complexes with phospholipids).[42,220] We propose that cholesterol crosslinks identified uniquely at high cholesterol levels may be due to specific cholesterol binding sites in the receptor or changes in lipid accessibility if the receptor adopts a different conformation at elevated cholesterol levels. Within the ECD preceding M1, extensive labeling of specific cholesterol crosslinked residues were

refined to ^{25}***DARIRPN***F***K***^{33} and ^{202}***YNTGKF***T***CIEAR***^{213}, the latter of which precedes the M1 transmembrane helix and might be expected to be located near the interfacial region of the lipid headgroups. Residues ^{272}***ASL***PK***VS***Y***V***^{280} of the M2-M3 loop were specifically crosslinked only at elevated cholesterol conditions, a region of the protein that is flanked by a neighboring subunit, suggesting non-annular interactions. This region is believed to be critical in allosterically linking ligand binding events with channel gating. With the post-M4 C-terminal tail, a region not resolved in any pLGICs,[218] extensive labeling was only observed at elevated [cholesterol] at residues ^{415}***RE***DVH***NQ***^{421}, suggesting an intimate association with the bilayer surface at these levels.

Cholesterol crosslinks identified under conditions where cholesterol is expected to have low chemical activity are assumed to identify non-specific sites of lipid-accessibility to GlyR. As described in the previous paragraph, some subtle differences were observed in the labeling of M4 as a function of cholesterol concentration. Unique crosslinking sites at lower cholesterol composition were also refined to the large ECD preceding M1 and the M3-M4 loop. Within the ECD preceding M1, exclusive labeling was refined to ^{60}***VNI***F***LR***QQWNDP***R***^{72} and ^{191}***E***EK***DLR***Y***CTK***^{200}, the former being a region flanked by a neighboring subunit with some lipid accessibility while the later is directly exposed at the protein:lipid interface of GlyR. Within the intracellular M3-M4 loop, a poorly resolved region in structural determinations of all pLGICs to date, cholesterol crosslinking is uniquely observed to ^{349}***K***D***GI***SV***K***^{355}, suggesting this region is intimately associated with the membrane surface only at lower cholesterol concentrations. For visualization, unique crosslinking sites observed in both reduced and elevated cholesterol compositions were mapped to a single subunit of a single subunit cryo-EM zebrafish α1 GlyR[100] (Figure 10A and B, light green regions). Given that unique crosslinking locations were also observed in the reduced cholesterol composition (<25 mol percent) not observed in the elevated

cholesterol composition (>40 mol percent), this suggests that GlyR adopts subtly different conformations at low and high cholesterol levels. This is consistent with observations that nAChR adopts an uncoupled conformation in the absence of cholesterol and anionic lipids that is distinct from the resting and desensitized states.[231]

A limitation of the current studies is that the relative abundance of the crosslinking events could not be determined as peak intensities in MS studies reflect the abundance of the mass ion, reporting on the relative ionization of the species, not its concentration. Accurate quantification would allow discrimination of high probability events from low probability events, further refining the specific interactions of cholesterol with GlyR. This is a common problem in MS-based discovery studies that confound the use of isotopically enriched standards. Future studies plan to incorporate a laser-induced fluorescence microfluidic platform under development to sensitively quantify derivatized peptides concurrent with MS-MS studies. Regardless, the methods described have reproducibly identified dozens of cholesterol crosslinks as a function of cholesterol concentration. Of note, these CX-MS studies do not require large amounts of purified receptor, as picomoles of protein in a single SDS-PAGE gel is sufficient to identify dozens of crosslinks. In addition, these studies are conducted in reconstituted lipid vesicles, in the absence of detergents, and can be conducted in a state-dependent manner in the presence or absence of agonists, antagonists, allosteric ligands with any desired lipid composition to identify changes in lipid accessibility upon channel gating and desensitization.

CHAPTER 3: STATE-DEPENDENT CHOLESTEROL-GLYR INTERACTIONS

3.1 Abstract

PLGIC allostery is dependent on dynamic associations with its diverse environment. The cellular membrane's lipid composition influences channel function with cholesterol being a key regulator of channel activity. Human **α**1 GlyR was purified from baculovirus infected insect cells and reconstituted in unilamellar vesicles at physiological cholesterol:lipid ratios with aliquots of azi-cholesterol, a photoactivatable non-specific crosslinker. The receptor in vesicles was then enriched in either a resting, open, or desensitized state prior to photocrosslinking. Following photoactivation, crosslinked cholesterol-GlyR was trypsinized and sites of direct covalent attachment to peptides were identified by targeted MS-MS. Dozens of state-dependent crosslinks were identified and differential patterns of cholesterol-GlyR crosslinks were observed in the extracellular region nearing the lipid bilayer, in the M4 transmembrane helix, and in the large intracellular M3-M4 loop. Unique crosslinks in comparative studies identify changes in lipid accessibility or modulation of hydrophobic cavities in GlyR as a function of receptor allostery. Most notably, the outward twisting of M4 and differential crosslinking within the M3-M4 loop provide new insight into allosteric repositioning of GlyR. More generally, this study provides an accurate and sensitive approach to mapping the protein-lipid interactions to discern state-dependent structural movements of membrane proteins.

3.2 Introduction

Protein function is modulated by dynamic interactions with other biomolecules such as metabolites, proteins and lipids, and the cellular membrane's lipid composition has been

increasingly recognized as a major contributor in membrane protein function.[235,236] The current model of the lipid membrane suggests a non-homogenous distribution of lipids and proteins that form microdomains, with the lipid composition modulating cellular processes at the protein-lipid interface either directly (i.e., binding) or indirectly (altering the physiochemical properties of the bilayer).[52–54] Examples of these effects are the influence of lipid composition on the structure/stability of the transmembrane domain of amyloid precursor protein,[58] the modulation of β2-adrenergic receptor dimer interface stabilization through cholesterol occupancy,[62] the abrogation of dimer formation of the leucine transporter from cardiolipin delipidation,[63] and the effects of cholesterol on ion channels.[80,208,209] Lipids modulate agonist binding of GluCl through occupancy of membrane-spanning intersubunit crevices, promoting an expanded, open-like conformation that potentiates the receptor.[75] The potency of GABAR is diminished by cholesterol depletion and restored through cholesterol enrichment of neurons.[79] Lipids are frequently observed co-crystallized with membrane proteins, underlining the importance of specific protein-lipid interactions.[65] For example, cholesterol co-crystallizes with G-protein coupled receptors,[68] Na^+,K^+ ATPase,[69] and the dopamine transporter,[71] and phospholipid co-crystallizes with GluCl[75] and GLIC.[77]

Many pharmaceuticals (anesthetics, barbiturates, benzodiazepines, cannabinoids, and alcohol) and bioactive lipids (progesterone, sphingomyelin, and ceramide) specifically target the pLGIC superfamily of ion channels.[111,132–134] Anesthetics alter the permeability of both anion-selective and cation-selective channels. However the molecular mechanism of channel modulation remains poorly understood.[135] Bioactive lipids play a more diverse role, including the regulation of cell-surface nAChR levels,[134] the inhibition of GABAR,[133] and the modulation of nAChR desensitization.[140] Intriguingly, both anesthetics and bioactive lipids partition at the lipid-protein

interface in cellular membranes,[143,144] with the former being observed in crystal structures of pLGIC structural homologues.[145,146] Cannabinoids such as Δ^9-tetrahydrocannabinol potentiate GlyR activity via interactions at the protein-lipid interface.[237] Screening of GlyR for cannabinoid-like potentiating agents is an effective tool to discover novel therapeutics[111] highlighting the importance in developing methodologies to sensitively probe protein-lipid interactions. Direct effect of anesthetic agents and alcohol of pLGICs provide valuable models for general allosteric modulation and to further develop anesthetic agents.[238]

Cholesterol and saturated lipids enrich lipid rafts forming highly ordered microdomain complexes distinct from the surrounding disordered lipid environment, with this highly ordered domain providing a mechanism for protein interactions and the regulation of cellular processes.[239] Cholesterol in molar excess of the capacity of these complexes has high fugacity, and is regarded as "active cholesterol",[36] as seen by an abrupt increase in sterol availability to cholesterol oxidase,[37] perfringolysin,[38] and methyl-β-cyclodextrin[39] emerging at concentrations above 25-35 mol percent.[40,41] Excess cholesterol exhibits high chemical activity in a chemical phase distinct from that observed under negligible chemical activity[42] that may potentially drive regulatory processes within or on the plasma membrane surface,[43] either indirectly by modulating plasma membrane physical properties or directly as a protein regulator.[20] Cholesterol and anionic phospholipids modulate nAChR allosteric transitions whereby cholesterol enrichment of cholesterol-depleted membranes up to a given threshold (~35 mol%) enhanced receptor-mediated ion flux from inactive channels to being able to undergo agonist-induced state transitions.[82–86] This profound regulatory effect of cholesterol also causes nAChR to adopt distinct conformations as a function of cholesterol concentration, where in the absence of cholesterol or anionic phospholipids adopting a conformation that has properties distinct of the resting or desensitized state in which

the allosteric coupling between neurotransmitter binding sites and the transmembrane pore is lost.[87,88] Similarly, CX-MS studies identified differential GlyR-cholesterol crosslinking patterns at low and high cholesterol concentrations, suggesting that GlyR adopted distinct conformations as a function of cholesterol concentration.[178]

The transient nature of neuronal receptor allostery typically poses a challenge for experimental characterization, however the approach of using photocrosslinking provides an opportunity to probe the dynamics of receptor gating and desensitization.[179,180] Photoaffinity labeling studies identified the propofol-binding site of GLIC[190] and GABAR[191] as well as cholesterol interactions with the PBR,[192] nAChR,[194,195] and GlyR.[178] The incorporation of sensitive MS-based approaches to sensitively identify sites of photocrosslinking has the potential to identify allosteric dynamics of protein structure in membranes and to examine the role of lipids in receptor allostery.[178,179] Current tandem MS instruments have the mass accuracy and sensitivity to unambiguously identify and refine crosslinked species to amino acid residue(s) within a given peptide.[178,183,184] CX-MS studies provide a valuable adjunct to crystallography and cryo-EM studies particularly in less resolved regions of images by providing amino acid proximity and distance constraint information useful in homology or *de novo* modeling.[240] Data provided by state-dependent CX-MS can supplement assays elucidating channel mechanisms of activation/desensitization[241] and allosteric coupling of domains[242] by providing dynamic localized information regarding structural changes often in unresolved regions of proteins.

Given the essential, yet poorly characterized structural effects of cholesterol modulation of pLGICs, we examined cholesterol accessibility of GlyR at physiological levels, >40 mol% (above its activity threshold), in a state-dependent manner. This study focuses on comparative cholesterol-GlyR interactions, i.e. comparing differential azi-cholesterol crosslinking under

elevated “active” cholesterol conditions of the resting, open (F207A/A288G, 30 nM ivermectin),[205] and desensitized state (10 mM glycine) using photocrosslinking coupled with multidimensional MS. The F207A/A288G double mutant GlyR produces an ivermectin-sensitive channel unable to desensitize.[205] These studies expand upon a previous study[178] that contrasted azi-cholesterol crosslinking to the resting state of α1 GlyR under low and high cholesterol levels. GlyR in the presence of saturating concentrations of glycine activate and stabilize channels predominantly in a higher-affinity ligand-bound conformation, with potential sampling of other states. F207A/A288G GlyR in the presence of nanomolar concentrations of ivermectin has been shown to stabilize channels in a conducting conformation that does not desensitize.[205] Azi-cholesterol, a photoactivatable cholesterol analog, was crosslinked to human homomeric α1 GlyR (wild-type and F207A/A288G) at conditions that probe interactions when cholesterol is chemically active (>40 mol percent natural cholesterol in membrane) in a state-dependent manner.[42,220] This study shows that photocrosslinking coupled with tandem MS can map a lipid-protein interface in several allosteric states/conformations, depicting lipid accessibility during transient structural changes. Direct cholesterol-GlyR interactions have been identified in different allosteric conformations that can help refine GlyR crystallographic/cryo-electron microscopic models, principally in unresolved regions, provide insight into ion channel dynamics of gating and desensitization.

3.3 Materials and Methods

3.3.1 Purification of GlyR from Sf9 insect cells into mixed detergent micelles

Purified GlyR in mixed detergent/lipid micelles were isolated as previously described.[121] Briefly, WT human α1 GlyR was overexpressed in a baculovirus infected *Sf*9 insect cells. Three days post-infection *Sf*9 insect cells were gently pelleted, washed with phosphate buffered saline (137 mM NaCl, 2.7 mM KCl, 10 mM Na2HPO4, 1.8 mM KH2PO4, pH 7.4), and resuspended in a hypotonic solution (5 mM Tris pH 8.0, 5 mM EDTA, 5 mM EGTA, 10 mM DTT). An anti-proteolytic cocktail (1.6 μunits/mL aprotinin, 100 μM phenylmethanesulfonyl fluoride, 1 mM benzamidine, 100 μM benzethonium chloride) was added to reduce protein degradation immediately preceding lysis. Cells were lysed by sonication followed by centrifugation (387,000 x g for 30 min) to isolate cell membranes containing GlyR. Cell membranes were washed with a resuspension buffer (hypotonic solution above with 300 μM NaCl) followed by centrifugation again to remove peripheral membrane proteins. The protein pellet was solubilized in 10:1 digitonin:deoxycholate buffer (12 mM mixed lipids (9:1 plant extract (~95% phosphatidycholine purity, Avanti): egg extract (~60% phosphatidycholine purity, Avanti) at 1.5 mg/mL, stored as suspended vesicles), 0.10 % deoxycholate, 1.0 % digitonin, 25 mM potassium phosphate (KP_i, pH 7.4), 1 M KCl, 5 mM EDTA, 5 mM EGTA, 10 mM DTT, anti-proteolytic cocktail) overnight, and solubilized micelles were isolated after centrifugation (387,000 x g for 1 hr). GlyR/lipid/detergent micelles were affinity purified on 2-aminostrychnine agarose and eluted competitively with the addition of excess glycine (2M for WT preps) or strychnine-sulfate pentahydrate (1.5 mM for F207A/A288G preps) to the solubilization buffer.

3.3.2 Reconstitution of GlyR into lipid vesicles incorporating azi-cholesterol

GlyR vesicle reconstitution was completed as previously described[124] with the following modifications to the lipid composition. All steps were conducted in the dark and at 5˚C unless noted. Mixed lipids (9:1 plant extract (95% phosphatidycholine purity): egg extract (60% phosphatidycholine purity) at 15 mg/mL, stored as suspended vesicles) were added to purified GlyR/lipid/detergent micelles to yield a final concentration of 1.5 mg/mL. Cholesterol (15.07 mM in methanol) with 6 μM azi-cholesterol was included to yield >40 mol percent. As previously described, samples were added to dialysis cassette (3500 MW cutoff, Thermo) for dialysis against excess 6.25 mM KP_i buffer at pH 7.4. The final reconstituted protein pellet was dissolved in 25 mM KP_i buffer at pH 7.4. GlyR concentrations were quantitated using a modified Lowry assay.[221]

3.3.3 Photo-crosslinking of azi-cholesterol to GlyR and separation of crosslinked GlyR

Reconstituted GlyR vesicles were placed into quartz cuvettes on ice to maintain temperature. Photocrosslinking of azi-cholesterol to GlyR was completed as previously described[178] with the following modifications. To enrich for GlyR in the open state, 30 nM ivermectin was added to reconstituted GlyR vesicles (F207A/A288G) immediately before UV light exposure. To enrich for GlyR in the desensitized state, 10 mM glycine was added to reconstituted GlyR (WT) vesicles immediately before UV light exposure. Cuvettes were exposed to a 420 W Hg Arc lamp (Newport, Model 97435-1000-1, 260-320 nm) for 4 sessions of 5 minutes at 7 cm, with 5 minute periods of no exposure in between each UV exposure session to prevent sample warming. SDS-PAGE (11 % resolving, 5 % stacking) separated the crosslinked oligomeric and monomeric GlyR from lipids, with gel plugs excised between migration distances of 250 kDa and 37 kDa, encompassing the mass of oligomeric and monomeric forms of GlyR.

3.3.4 In-gel Trypsin digestion of crosslinked GlyR

Gel plugs were washed with 50:50 methanol: 50 mM ammonium bicarbonate twice for 40 min with gentle agitation (VWR Thermal Shake Touch, 900 rpm). Gel plugs were dehydrated by adding 500 µL acetonitrile. Once gel plugs turned whitish, acetonitrile was removed and gel plugs were dried in an Eppendorf 5301 Vacufuge Concentrator for approximately 15 minutes. Trypsin solution (10 µL at 20 µg/mL in 50 mM ammonium bicarbonate) was added to gel plugs and incubated on ice for 15 minutes, then incubated overnight at 37˚C with gentle agitation (VWR Thermal Shake Touch, 900 rpm). Digested peptides extracted into supernatant and transferred to VWR non-stick microcentrifuge tubes. Tryptic fragments were further extracted by incubating gel plugs twice for 30 minutes in 300 µL of 0.1 % formic acid in 50:50 acetonitrile:H_2O. The supernatant was collected and combined with initial supernatant. Tryptic extract solution was dried in an Eppendorf 5301 Vacufuge Concentrator.

3.3.5 Mass fingerprinting of crosslinked cholesterol to GlyR

50:50 Acetonitrile: H_2O with 0.1 % Formic Acid (50 µL) was added to tubes containing dried tryptic extracts. ESI-Q-TOF-MS measurements were taken using an Agilent 6530 Q-TOF-MS with an Agilent HPLC-Chip II G4240-62006 ProtID-Chip-150, comprised of a 40 nL enrichment column and a 75 µm x 150 mm separation column packed with Zorbax 300SB-C18 5 µm material. The mass spectrometer was run on positive ion mode using internal standards (1221.9906 and 299.2944) for calibration, supplied by Agilent. Mobile phase compositions used were solvent A (95 % H_2O, 5 % ACN, 0.1 % formic acid) and solvent B (95 % ACN, 5 % H_2O, 0.1 % formic acid) The nanoflow elution gradient was developed as follows at 0.50 µl/min of

solvent A (minute: percent A): 0.00: 95 %, 4.00: 10 %, 6.00: 70 %, 9.00: 50 %, 11.50: 95 %, 13.00: 95 %. Data were processed using Agilent Qualitative Analysis Software 6.0. Cholesterol crosslinked peptides within a 10 ppm accuracy window were identified, accounting for possible peptide modifications (oxidation, acrylamidation).

For MS-MS studies, crosslinked samples were run again on the Agilent 6530 Q-TOF-MS, targeting the specific m/z ratio, charge, and retention time (RT) of the crosslinked peptides identified in MS analysis. CID was used for MS-MS fragmentation following a linear increase in collision energy by m/z using the equation: $y=3.7x+2.5$ (y= m/z, x= collision energy). CID was performed at $\pm$ 0.2 min from initial MS scan RT of each crosslinked precursor ion identified. Data were processed using Agilent Qualitative Analysis Software 6.0 in conjunction with ProteinProspector v5.14.3 available through the University of California, San Francisco.

3.4 Results

Our previous study[178] identified *apo* state azi-cholesterol-α1 GlyR crosslinking as a function of cholesterol concentration where differential crosslinking patterns were observed between cholesterol conditions of negligible chemical activity and chemically active, suggesting two distinct structural conformations of apo-state GlyR as a function of cholesterol concentration. The dependence of pLGIC activity on cholesterol has been long established and these studies were consistent with FTIR studies demonstrating the uncoupling of ligand binding from pore opening as a consequence of decreased cholesterol content.[231] Given the requirement for GlyR activity on more elevated cholesterol concentrations, all of our comparative studies of homopentameric human α1 GlyR examining cholesterol crosslinking as a function of receptor allostery were conducted at the higher cholesterol concentrations consistent with physiological conditions.

In our previous studies,[178] azi-cholesterol crosslinking was observed in pre-M1 extracellular domain on the outer lipid-exposed surface, the extracellular M2-M3 loop, regions of the large intracellular M3-M4 loop, the M4 transmembrane helix, and the post-M4 c-terminal tail (Table 2). In this study we extend these studies to examine cholesterol photocrosslinking in a state-dependent manner, conducting comparative crosslinking studies on purified and reconstituted human α1 GlyR enriched in either its resting, open or desensitized states. Ivermectin promotes predominant stabilization of channels in a conducting conformation (open state) in F207A/A288G a1 GlyR.[205] In our hands, F207A/A288G GlyR expressed in insect cells were gated by ivermectin in whole cell patch clamp studies and showed no evidence of desensitization (Tomcho et al.,

Table 3. Identified open state precursor/product ion crosslinked peptides at >40 percent cholesterol with conditions as described in Table 2.

Amino Acid Sequence	Structural Location	Modifications
^{17}L**MG R**TSGY**DAR**^{27}	Pre-M1 ECD	Azi
^{28}**IR P N**F**K**^{33}		Azi, Acryl Azi (2), Acryl
^{197}Y**CTK**HYNTG**K**^{206}		Azi, Ox
^{197}YCTKH**YNTGKF** T**CIEAR**^{213}		Azi (2), Acryl (3), Ox
^{272}**ASL**PK**VS**Y**V**K^{281}	M2-M3 Loop	Azi Azi, Acryl Azi (2), Acryl (2)
^{321}**RR**H**H K**^{325}	M3-M4 Loop	Azi Azi, Ox Azi (2)
^{323}**HH**K**E**DEAGE**G**R^{333}		Azi, Acryl, Ox
^{372}**S**PE**E M R**^{377}		Azi, Ox
^{372}SPEE**M**R**K**^{378}	M3-M4 Loop/M4	Azi, Acryl
^{372}SPEEMR**KL**IFQR^{383}		Azi (3), Ox
^{378}**K**L**FIQ**RA**K**^{385}	M4	Azi, Acryl Azi (4), Acryl
^{384}**AK K** I**D K**^{389}		Azi Azi, Acryl (3)
^{387}**IDK**ISRIGFPMAFLIFNMFYWIIYK^{411}		Azi (4), Acryl, Ox
^{415}**RE**DVH**NQ**^{421}	C-terminal tail	Azi Azi (2), Ox

manuscript in preparation), consistent with published observations.[205] Under excess ivermectin conditions (1.5 mM) these non-desensitizing channels are expected transition between open or resting states, and comparative CX-MS studies with apo studies should identify mass-shifted ions unique to each study, thus allowing identification of unique cholesterol binding sites restricted to each of these states (or exposed during structural transitions between the resting and open state). Similarly, in order to examine cholesterol accessibility in the desensitized state of the receptor, cholesterol interactions were examined in conditions of excess glycine enriching GlyR in a higher-affinity ligand-bound desensitized conformation. Given that the receptor is expected to exist in resting, open, and (primarily) desensitized states, comparative studies are conducted to identify crosslinking sites uniquely observed in the presence of excess glycine and not in our resting or open state studies.

In this section we present evidence of crosslinks identified by LC-MS-MS in each of the three comparative studies, but defer more detailed interpretation of these data until the following Discussion section. In all cases, crosslinks presented were identified in at least 2 of 3 independent sample preparations/MS analysis pairings. Identified crosslinks from independent preparations were obtained from a single LC-MS and LC-MS-MS paired experiment. For LC-MS-MS analysis, mass errors in precursor/product ion identification were restricted to < 10 ppm/0.1 Dalton, respectively. Due to the presence of isobaric species (i.e., cholesterol binding at more than one location, such as adjacent amino acids, within a given proteolytic fragment), strict pairing of the retention times of product ions and their respective precursors allows multiple crosslinks to be

identified from isobaric precursor ions in single trials due to their respective differential retention times on the LC-MS-MS platform.

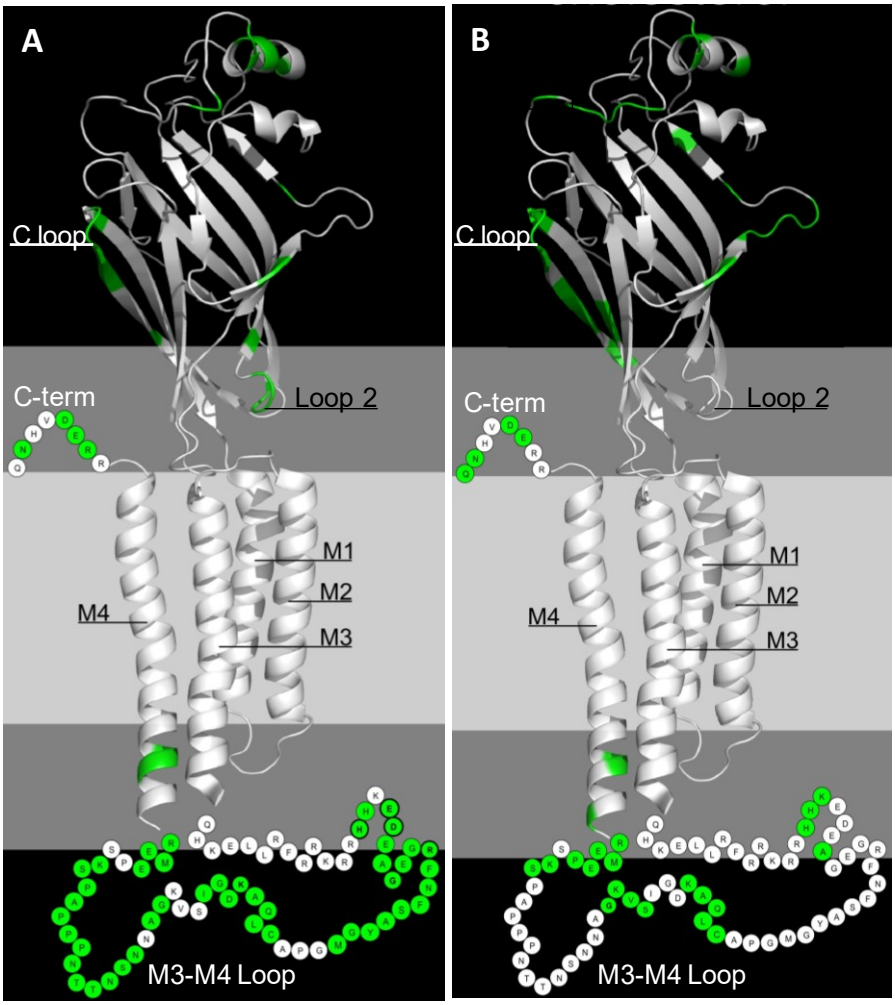

Figure 12. State-dependent GlyR-cholesterol interactions at active cholesterol conditions. Azi-cholesterol crosslinking at (A) open state and (B) desensitized state mapped to a single α1 subunit of zebrafish GlyR (PDB #3JAD) using PyMOL v1.8.[100] Areas corresponding to the bilayer are shown in gray (~15Å interfacial regions) and light gray (~30 Å hydrophobic acyl chain region). Sites of crosslinking in the open and desensitized (bolded and underlined amino acids in Table 2-3, respectively) identified are shown in green. Beads represent regions not

In studies conducted on non-desensitizing F207A/A288G GlyR, cholesterol crosslinking was identified in the pre-M1 extracellular domain in regions distant of the membrane and closer proximity with the ECD-TMD interface, the entire span of the large intracellular M3-M4 loop, the lower portion of the M4 transmembrane helix, and the post-M4 C-terminal tail (Table 3), and these sites were visualized on a single α1 subunit of zebrafish GlyR (PDB #3JAD)(Figure 12A).[100]

Many crosslinks were found in unresolved regions of the α1 GlyR model (the M3-M4 loop and C-terminal tail), and are depicted as colored beads. These crosslinking events suggest that these sites are in close proximity hydrophobic core of the lipid bilayer, suggesting an intimate association of large swaths of the heretofore unresolved M3-M4 linker with the periphery of the hydrophobic core of the bilayer (the expected depth of the diazirine moiety on azi-cholesterol

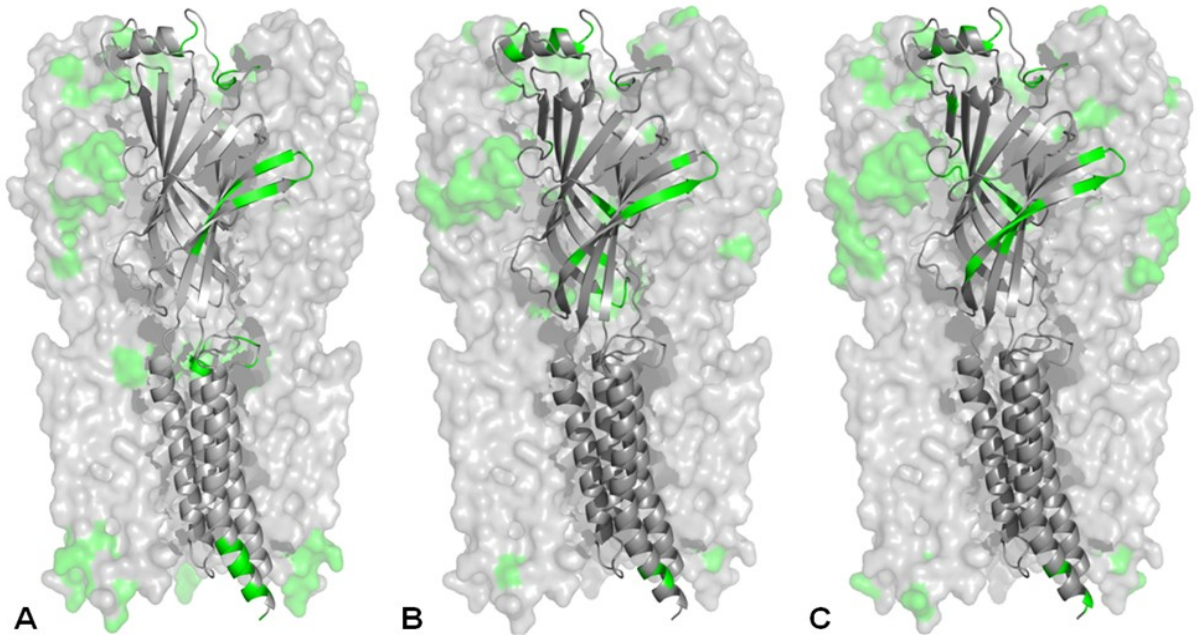

Figure 13. Allosteric GlyR-cholesterol interactions at active cholesterol conditions. Side view of the space-filling GlyR pentamer (with one single subunit shown as ribbon diagram, PDB #3JAD[100]) with sites of crosslinking highlighted in green for the (A) resting state[178], (B) open state, and (C) desensitized at >40 mol percent cholesterol. Unresolved regions of the receptor are not shown in panels A-C.

(Figure 12). A profile side view of crosslinked regions (Figure 13B) displays these annular associations, yet also exposes more buried non-annular cholesterol interactions in hydrophobic pockets between subunits consistent with nAChR[222] and $GABA_AR$[79] studies.

In bottom-up views of the receptor (Figure 14B) crosslinking locations are localized on outer surface of GlyR, highlighting the expected predominant annular lipid surface accessibility. Cholesterol crosslinking only identified in open state studies, not in the apo-state is suggested to be unique cholesterol-GlyR interactions of the open state. Cholesterol crosslinking unique to the open state GlyR was observed in the pre-M1 extracellular domain in regions distant to (residue numbers 3, 10, 15-16, 52-55, 58) and nearing (residue numbers 105-106, 116, 193, 197, 201) the membrane, the large intracellular M3-M4 loop (residue numbers 227-231, 233, 237-241, 245-247, 249, 334-337, 345-348, 350-352, 356-357, 359-371, 374), the M4 transmembrane helix (residue number 383), and the post-M4 c-terminal tail (residue number 417).

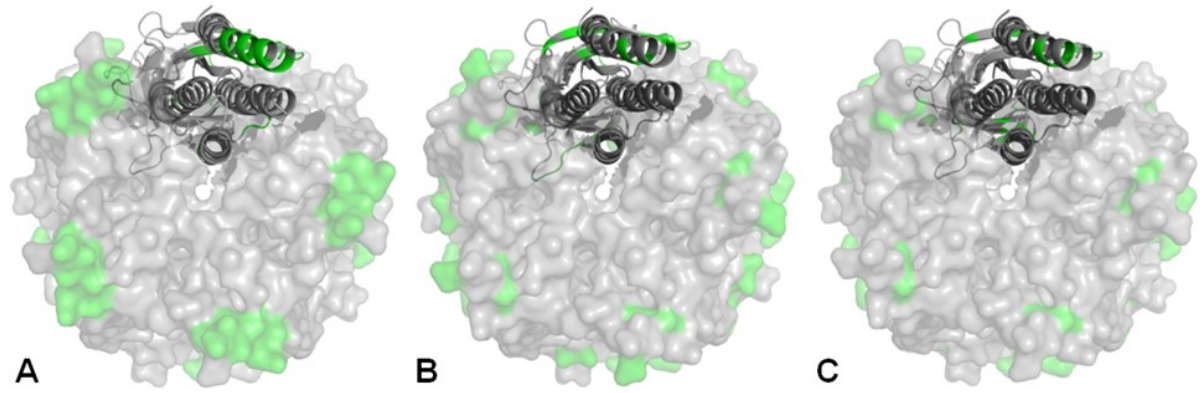

Figure 14. Allosteric GlyR-cholesterol interactions at active cholesterol conditions. Bottom-up view of the space-filling GlyR pentamer (with one single subunit shown as ribbon diagram, PDB #3JAD[100]) with sites of crosslinking highlighted in green for the (A) resting state[178], (B) open state, and (C) desensitized at >40 mol percent cholesterol. Unresolved regions of the receptor are not shown in panels A-C.

In studies conducted on WT receptor in the presence of excess glycine, cholesterol crosslinking was identified in the pre-M1 extracellular domain in regions distant of the membrane and closer proximity with the ECD-TMD interface, three distinct regions of the large intracellular M3-M4 loop, the lower region of the M4 transmembrane helix, and the post-M4 C-terminal tail, mapped to a single α1 subunit of zebrafish GlyR (PDB #3JAD) (Table 4, Figure 12B).[100]

Table 4. Identified desensitized state precursor ion crosslinked peptides at >40 percent cholesterol with conditions as described in Table 2.

Amino Acid Sequence	Structural Location	Modifications
^{1}AR**S**ATKPMSP**S**DFLD**K**^{16}	Pre-M1 ECD	Azi, Acryl, Ox Azi, Ox
^{3}**SA TK**PMSPSDFLDKLM**GR**TSGYDA**R**^{27}		Azi, Acryl (2), Ox Azi, Ox Azi, Acryl (2), Ox (2)
^{28}**IR PN**F**K**^{33}		Azi (2), Acryl
^{105}**GA**HFHEITTDN**K**^{116}		Azi, Ox (2) Azi Azi, Acryl, Ox
^{105}**G**AH**F HEIT**TDNKLL**R**^{119}		Azi, Acryl, Ox (2)
^{191}**EE**K**DL R**YCT**K**^{200}		Azi, Acryl Azi, Acryl (2)
^{194}**DL**R**Y**CT**K HY**NTG**K**^{206}		Azi, Acryl (2), Ox Azi, Acryl (3), Ox Azi, Acryl (3) Azi, Acryl Azi, Ox
^{197}YCTK**H YNTG**KFTCIE**A R**^{213}		Azi, Acryl Azi (2), Acryl
^{323}**HHK**EDEAGEGRFNFSAYGMGPA**CLQAK**^{349}	M3-M4 Loop	Azi, Ox
^{326}EDE**A**GEGRFNFSAYGMGPA**C**LQAKDGI**SVK**^{355}		Azi
^{356}**G**ANNSNTTNPPPAP**SK**S**PEE MR**^{377}		Azi Azi, Acryl Azi, Ox
^{379}**L**FIQR**AK**^{385}	M4	Azi (4) Azi
^{415}R**ED**VH**NQ**^{421}	C-terminal Tail	Azi (2) Azi, Ox Azi

Crosslinking was observed in unresolved M3-M4 loop and C-terminal tail of the α1 GlyR model (Figure 12B, M3-M4 loop and C-terminal tail, depicted as colored beads) and suggested to be intimately associated with the lipid membrane. Examination of the accessible surface of the pentamer, either by profile side view (Figure 13C) or viewed intracellularly facing outward (Figure 14C), show sites of crosslinking on both the outer surface, annular lipid-accessible regions of GlyR as well as more buried non-annular regions consistent with crosslinking observed in the resting and open state trials. Cholesterol crosslinking uniquely observed in studies in excess glycine are proposed to be unique cholesterol-GlyR interactions of the desensitized state, and was identified in the pre-M1 extracellular domain in regions distant to (residue numbers 4-6, 11) and nearing (residue numbers 108-112, 119, 191-192, 194-196) the membrane, and intracellular M3-M4 loop (residue numbers 353-355, 373).

3.5 Discussion

The differential cholesterol crosslinking patterns discerned in this study between conditions stabilizing the resting, open, and desensitized states of GlyR shows that CX-MS can identify unique cholesterol interactions in a state-dependent manner. This change in the pattern of cholesterol crosslinking between functional states details structural movements between allosteric conformations and define lipid-accessible hydrophobic regions of GlyR, as well as hydrophobic pockets in the receptor. Currently there are structures of GlyR bound to agonist/antagonist,[100] ivermectin,[100,218] and analgesic potentiators,[243] as well as forthcoming cryo-EM structures.[241] However, many of these structures have deletions and mutations for thermostability, are bound to ligand, and often lack the presence of a bilayer, providing limitations in modeling function of pLGICs. This discontinuity emphasizes the need for continued and improved methodologies to be

able to provide additional information for each allosteric state for full-length receptors in the presence of a lipid bilayer. State-dependent comparative CX-MS studies offer the unique capability of complementing other high resolution methodologies to help refine dynamic changes of membrane proteins under physiological conditions. Under physiological conditions, CX-MS can differentiate subtle structural movements throughout the majority of the protein, including regions absent in current structures. The synergistic utility of CX-MS with common structural techniques (x-ray crystallography and cryo electron microscopy) can drastically enhance the allosteric understanding of membrane proteins.

In the absence of quantification, this comparative state-dependent cholesterol-GlyR study is unable to distinguish high frequency from low frequency crosslinks identified. Therefore, it is assumed that crosslinking studies conducted in the presence of ivermectin (labeled as open state crosslinking) will capture crosslinks of both resting and open state channels as well as accessibility during state transitions as we are unable to distinguish crosslinking specific to the resting, open, or intermediate structures. Similarly, crosslinking studies conducted in the presence of glycine (labeled as desensitized state crosslinking) will capture crosslinks of the resting, open, and desensitized channels as well as accessibility during state transitions as we are unable to distinguish crosslinking specific to the resting, open, desensitized, or intermediate structures. Unique crosslinks identified within each three conditions tested are suggested to be distinctive cholesterol-GlyR interaction profiles and consist of up to ~58% of crosslinks identifies within each condition.

Sites of cholesterol crosslinking determined in CX-MS studies were visualized through mapping on the α1 GlyR strychnine-bound model.[100] This model was selected to most closely resemble the apo-state conditions tested in the previous study given the three available α1 GlyR

models (strychnine, glycine, and glycine/ivermectin bound).[100] To maintain consistency, all crosslinks of this CX-MS study are mapped on this single static model to enhance identification of regions exhibiting changes in lipid accessibility, thereby identifying movements of the receptor underlying gating and desensitization. Consequently the mapping shown for each allosteric state (open and desensitized) may not accurately represent structural-based crosslink localization identified for each state, however gives an approximate depiction of the crosslinked regions. Exact structural changes based upon state-dependent cholesterol crosslinking patterns mapped on the model are suggested to be a result of either cholesterol or protein relocation. Changes in cholesterol's interaction location based upon lipid relocation are suggested to be from repositioning within hydrophobic pockets or regions of lipid accessibility. Changes in cholesterol's interaction location based upon GlyR repositioning causes mapped crosslinked site(s) to differ from state to state, where the directional movement of cholesterol location is the opposite of GlyR actual repositioning.

Shifts of crosslinking patterns within M4 (Figure 15A-C) are proposed to be a result of M4 helix repositioning during gating and desensitization. Comparative CX-MS studies suggest the M4 helix undergoes a twisting during channel activation followed by an outward bending during desensitization. This proposed mechanism reflects the loss of crosslinking from the outer-most lipid accessible side of the M4 helix (resting state residues 378-382, 384-389, Table 2, Figure 15A) to more pronounced and concentrated crosslinking on the inner-most pore-facing side of M4 (open state residues 383-385, Figure 15B) indicating a clockwise twist (top-down view) of the M4 helix. Transition to desensitized state (residues 379, 384-385, Figure 15C) displays an increase in crosslinking lower on M4 at residues closer towards the intracellular domain signifying the

outward tilt or translation of the bottom portion of M4 helix. Taken together, state-dependent crosslinking of M4 suggests a outward twisting motion as the helix allosteric transitions which is consistent with general TMD movements observed between GlyR cryo structures stabilizing for the same allosteric states.[100] Cholesterol crosslinking within the portion of M4 nearing the M3-M4 loop (bilayer lower leaflet region) is consistent with similar studies of nAChR[195] showing N-terminal M4 cholesterol crosslinking. Our state-dependent cholesterol CX-MS study expands upon the lipid-channel studies by being able to not only highlight the specific crosslinking locations throughout the entire receptor, yet also distinguish the differential crosslinks in a state-dependent manner.

Differential crosslinking patterns were also observed in the ECD nearing the transmembrane domain. In initial CX-MS studies examining cholesterol crosslinking as a function of cholesterol content,[178] cholesterol crosslinking in the upper ECD is suggested to arise from azi-cholesterol accessibility to hydrophobic cavities during the detergent-based reconstitution process following purification, and these crosslinked regions corresponded to predicted cholesterol interaction locations. In resting state studies (Table 2, Figure 16A), the M2-M3 loop as well as the

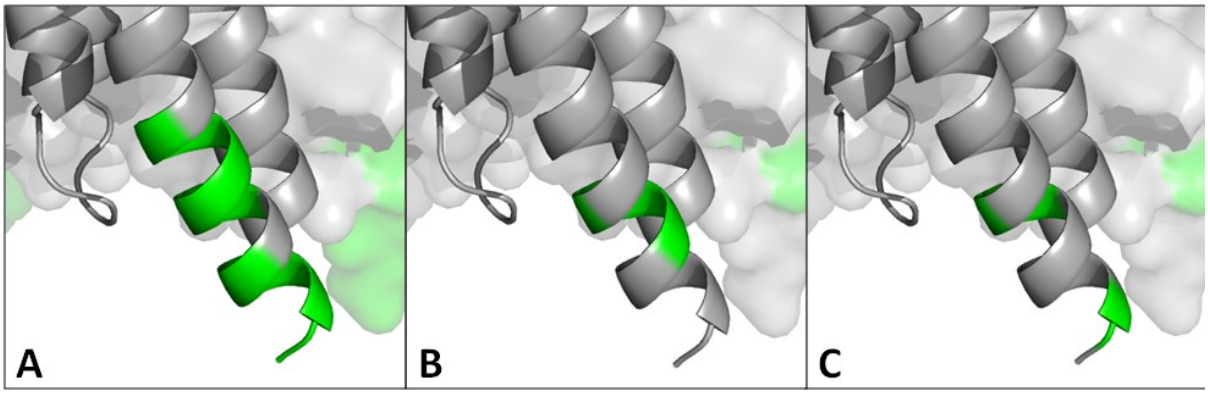

Figure 15. M4 differential cholesterol crosslinking. Comparison of state-dependent cholesterol crosslinking for the resting (A), open (B), and desensitized (C) conditions at > 40 mol percent

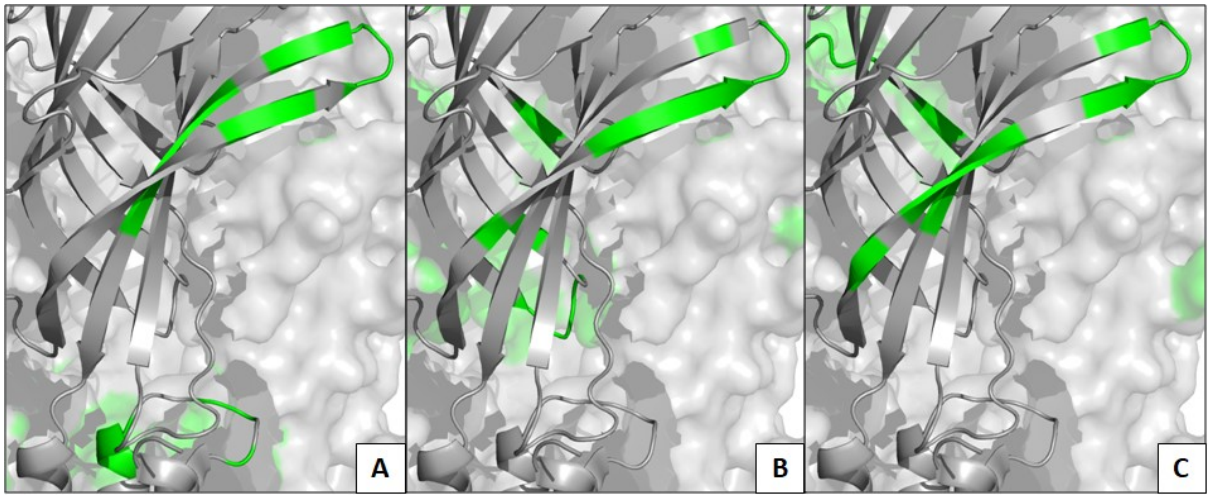

Figure 16. ECD differential cholesterol crosslinking. Comparison of state-dependent cholesterol crosslinking for the resting (A), open (B), and desensitized (C) conditions at > 40 mol percent cholesterol within the pre-M1 ECD region at the transmembrane interface.

"C loop" region of the outer β-sheet[100] flanking above the characteristic Cys-loop were extensively labeled, suggesting the incorporation and presence of cholesterol into the upper leaflet of the bilayer along with a hydrophobic pocket between neighboring subunits. The crosslinked M2-M3 loop residues adjoin a hydrophobic pocket at the ECD-TMD core[244] in a region shown to harbor transmembrane cavities that bind cholesterol,[79] anesthetics,[245] and correspond to predicted cholesterol recognition motifs identified in proteins.[178] Cholesterol crosslinking within and near the C Loop encompass the hydrophobic β-core conserved among pLGICs[246] correlating with determined CRAC/CARC interaction motifs.[178] This is a region of dynamic structural alterations during channel gating and desensitization[247] as well as Zn^{2+} modulation.[248] Comparing apo-state studies with conditions stabilizing the open state (Figure 16B) reveals a loss of M2-M3 loop crosslinking (residues 272-274, 277-278, 280, Table 2) in conjunction with a shift of crosslinking from exclusively outer β-sheet C Loop region to incorporate regions within the inner β-sheet (residues 52-55, 58, 105-106, 116) and lower "Loop 2"[249] that adjoin ECD-TMD interface,

suggesting a reorientation of the ECD during gating that either exposes the lower crosslinked residues identified or alters the hydrophobic cavity around/within the β-sheets. Juxtaposing crosslinking in conditions that stabilized an open channel with desensitization (Figure 16C) exposed nearly identical crosslinking with the exception of the loss of crosslinking in the lower Loop 2 (residues 52-55, 58), suggesting allosteric repositioning of the lower ECD- upper TMD interface during desensitization. Taken together, the ECD structure appears to be more similar between conducting and desensitized GlyRs than apo-state channels and that more dynamic movements are observed during channel activation in the lower ECD region where expansion from the central pore is noted.[75,100]

The large intracellular M3-M4 loop was profoundly crosslinked by cholesterol in all three allosteric states assayed with differential crosslinking patterns observed that clearly demonstrate its intimacy with the lipid membrane as well as structural movements. Given that the M3-M4 loop is often removed or is unresolved in the reported structures of pLGICs[96,100,218,219] it is difficult to speculate detailed structural movements of the M3-M4 loop as GlyR transitions between allosteric states. Cholesterol crosslinking was identified in regions proximal to the M4 transmembrane helix in all allosteric states (Figure 12). Contrasting crosslinking patterns from apo-state to stabilized conducting-state studies (Figure 12A) show nearly identical patterns with the dramatic emergence of crosslinking within central region of the M3-M4 loop (residues 327-341, 345-352, 356-357, 359-371) suggesting a reorientation of the M3-M4 loop during the gating process exposing previously lipid-inaccessible residues. Allosteric shifting from open to desensitized states illustrates the retention of cholesterol crosslinking at the ends (observed ubiquitously) and middle of the M3-M4 loop (Figure 12A-B), suggesting minimal conformational rearrangement that promotes less lipid accessibility. Taken together, the cholesterol crosslinking suggests three distinct

allosteric conformations of the M3-M4 loop most notably through the emergence of profound crosslinking in open and desensitized states exposing novel evidence pertaining to this elusive region of GlyR.

In a similar manner, the unresolved post-M4 C-terminal tail of GlyR absent in structural models[100] was crosslinked by cholesterol in all three allosteric states assayed (Figures 13A-B, previous publication).[178] The smaller size and lack of structural resolution makes it difficult to interpret results, however the crosslinked region of GlyR is assumed to be intimately associated with the lipid membrane. This area of the receptor is highly dynamic upon activation/desensitization and implicated in Zn^{2+} modulation, highlighting the potential relevance of the crosslinking data.[248] Given the propensity GlyR to interact with intracellular proteins and be targeted for post-translational modification[250,251] these effects may be partially due to altered interactions with lipids/accessibility or influenced by the lipid's modulation of structure. Cholesterol crosslinking between allosteric states was nearly identical in the C-terminal tail, with subtle shifts in cholesterol labeling indicating no major differences (residues 415-417, 420-421). This suggests minimal alterations in lipid accessibility of the post-M4 c-terminal tail of GlyR. None the less, the crosslinking data sheds light on this unresolved portion of the receptor and may have relevance to further elucidate this region.

Taken together, cholesterol dramatically associates and intimately interacts with α1 GlyR in all domains, underlying its influence in membrane protein activity. Differential crosslinking patterns of cholesterol were observed as a function of concentration and allosteric state highlighting cholesterol's role in channel allostery. In apo-state studies, cholesterol displayed deferring interactions as a function of cholesterol/channel activity whereby unique patterns where displayed corresponding to cholesterol chemical activity, suggesting two distinct apo-state GlyR

structures. State-dependent cholesterol interactions exhibit differential labeling in regions of GlyR that can suggest allosteric movements. Regions of the ECD, ECD-TMD interface, M3-M4 loop, and M4 suggest more drastic structural movements from apo-state to open-state conducting channels. This methodology can provide specific and accurate structural information in a state dependent manner without potential detrimental structural alterations required for other high resolution structure studies.

CHAPTER 4: OVERVIEW AND FUTURE DIRECTION

4.1 Summary

The incorporation of tandem CX-MS analyses into biochemical workflows can drastically expand the wealth of dynamic information gathered in a single experiment through generation of sensitive yet accurately reproducible distance constraints occurring in physiological relevant systems. Differential azi-cholesterol crosslinking patterns to GlyR were observed as a function of cholesterol concentrations as well as between conditions stabilizing GlyR in its resting, open, or desensitized states. This suggests either a change in lipid contacts with GlyR and/or GlyR structural alterations that change hydrophobic pocket(s). Cholesterol interactions were observed in the ECD, the ECD-TMD interface, the intracellular M3-M4 loop, and the M4 transmembrane helix. Theses studies have identified dozens of cholesterol crosslinks in each trial using picomoles of purified and reconstituted GlyR in varying lipid environments and allosteric conformations. The CX-MS approach pioneered herein can be applied and implemented into a variety of biochemical systems including other channels/transporters using any desired crosslinkers in varying functional states, under native-like conditions, to widen the breadth of understanding of allostery.

Currently there are structures of GlyR bound to agonist/antagonist,[100] ivermectin,[100,218] and analgesic potentiators.[243] However these studies have limitations modeling the highly allosteric function of pLGICs as they require deletions and mutations for thermostability, are bound to ligand, and often lack the presence of a bilayer. These limitations emphasize the need for continued and improved methodologies to be able to offer precise models for each allosteric state for full-length receptors in the presence of a physiologically-appropriate lipid bilayer. In current GlyR models, the large intracellular M3-M4 loop as well as the post-M4 C-terminal tail are absent. State-dependent comparative CX-MS studies offer the unique capability of complementing other

high resolution methodologies to help refine dynamic changes of membrane proteins under physiological conditions including the unresolved regions where other methods provide minimal, if any, information. CX-MS can differentiate subtle structural movements throughout the protein, including regions absent in current structures under physiological conditions and can drastically enhance the allosteric understanding of membrane proteins.

As described in Chapter 2, cholesterol within a bilayer displays differential chemical activity as a function of concentration. Chemically active cholesterol arises around and above ~33 mol% cholesterol within the lipid bilayer. The chemical activity of cholesterol in turn, alters the channel activity of pLGICs, with elevated cholesterol levels increasing chemical activity, and this effect plateaus at ~35 mol% cholesterol. Unique cholesterol crosslinking patterns where displayed corresponding to cholesterol chemical activity, suggesting two distinct apo-state GlyR structures.

Cholesterol interactions, as evidenced by CX-MS, were observed in Chapter 3 to exhibit state-dependent differential labeling in regions of GlyR including the ECD, ECD-TMD interface, M3-M4 loop, and M4. These comparative studies highlight structural movements in this receptor that occur in transitions from apo state to open state to desensitized state. This change in cholesterol crosslinking patterns between allosteric states show structural movements between conformations and define lipid-accessible hydrophobic regions of GlyR. This information complements the limited availability of GlyR models that encompass allostery.[100,243,252] Unresolved regions of current truncated/altered models based on structural studies conducted in non-physiological systems emphasizes the need for continued and improved methodologies to assist in generating precise models for each allosteric state. CX-MS studies can elucidate subtle structural alterations in a lipid-concentration and state-dependent manner throughout the entirety of the receptor reconstituted in native bilayers.

4.2 Future Studies

To further define the lipid accessible regions of the receptor and highlight potential specific binding sites for different classes of lipids, analogous CX-MS investigations can be performed using photoactivatable phospholipid crosslinkers. Anionic phospholipids like PA are required for nAChR resting state stabilization (analogous to cholesterol dependence studies) whereby membrane enrichment enhances receptor-mediated ion flux up to a given threshold (~12 mol%).[86] The potential for specific phospholipid-GlyR interactions necessary for function can be discerned in a state-dependent manner through comparison of PA and PC crosslinking at defined concentrations (>12 mol%). PC can map general phospholipid/lipid accessibility to channels, depicting general lipid bilayer interactions/accessibility which can differentiate hydrophobic pocket interactions potentially observed in the cholesterol crosslinking studies. PA crosslinking can map novel specific interactions or binding sites influencing channel activity through differentiation of PC interactions which are assumed to highlight general bilayer accessibility.

In addition, in order to probe depth in the bilayer, the photoreactive diazirine motif can be moved to either carbons more distant or near to the glycerol backbone, providing an effective way to probe membrane depth and asymmetric depth-dependent lipid-protein interactions using phospholipid crosslinkers. Although less defined, the incorporation of photoactivatable diazirine motifs into sphingomyelin type lipids can map interactions to yet another class of lipids[253] to probe specific concentration-dependent protein studies, such in the dimerization of SERT.[254] This toolbox of crosslinkers can be utilized to map lipid-interaction profiles of other pLGIC members and structural homologs.

Given that the MS methods we describe cannot quantify crosslinking events, additional methodology needs to be developed to quantify crosslinking events. Such quantification will

enrich the information of crosslinking datasets to not only provide the exact crosslinking site location, but additionally determine the relative crosslinking frequency. Differentiating the frequency of each crosslinking event can illuminate regions of prolonged lipid:protein interactions (higher frequency events) contrasted against crosslinking regions representing cholesterol:GlyR interactions that sparsely occur (low frequency events) yet are captured by the exceptional sensitivity of the CX-MS methodology. The Cascio lab is developing a sensitive laser-induced fluorescence microfluidic device that can be used as a parallel quantification tool to quantitate tryptic peptdies (Davic, PhD thesis 2018). Peptides are derivatized on chip in immiscible microdroplets with an amine-reactive fluorophore that only emits strongly when derivatized and fluorescent emission is directly proportional to peptide concentration. Current studies are being conducted to normalize fluorescent emission obtained from varying amino acids and peptides (Apa, senior thesis, 2019).

The lipid-protein CX-MS studies will also be integrated with protein-protein CX-MS studies initiated by Dr. Rathna Veeramachaneni and currently being conducted by Kayce Tomcho. Both lipid-protein and protein-protein CX-MS studies provide complementary information to further elucidate GlyR structure, specifically when crosslinking of both studies are mapped to regions of models that may not be completely resolved in current models. The complementary information can validate our determinations of regions being in closer proximity or intimately associated with the lipid bilayer. The information obtained from both CX-MS studies supports crosslinking data that appears artifactual or spurious when mapped to the current models. By coupling the distance constraints created in the protein-protein CX-MS studies with the lipid/bilayer accessibility of the lipid-protein CX-MS studies, regions of current GlyR models can be more accurately defined, particularly in the regions absent in models. Overall, both lipid-protein

and protein-protein CX-MS studies allow for the probing and elucidation of GlyR in membranes at physiological-relevant different allosteric states which can complement crystallographic and cryo-microscopy studies to provide a better understanding of these allosteric molecular machines that are essential for cellular communication.

REFERENCES

1. van Meer, G. Cellular lipidomics. *EMBO J.* **24,** 3159–3165 (2005).
2. Ayyappan, J. P., Paul, A. & Goo, Y.-H. Lipid droplet-associated proteins in atherosclerosis. *Mol. Med. Rep.* **13,** 4527–4534 (2016).
3. Saliba, A., Vonkova, I. & Gavin, A. The systematic analysis of protein-lipid interactions comes of age. *Nat. Rev. Mol. Cell Biol.* **16,** 753–761 (2015).
4. Morita, M. *et al.* The lipid mediator protectin D1 inhibits influenza virus replication and improved severe influenza. *Cell* **153,** 112–125 (2013).
5. Harayama, T. & Reizman, H. Understanding the diversity of membrane lipid composition. *Nat. Rev. Mol. Cell Biol.* **19,** 281–296 (2018).
6. van Meer, G. Membrane lipids: Where they are and how they behave. *Voelker, Dennis R Feigenson, Gerald W* **9,** 112–124 (2008).
7. Dowhan, W. Molecular basis for membrane phospholipid diversity: Why are there so many lipids? *Annu. Rev. Biochem.* **66,** 199–232 (1997).
8. Spector, A. & Yorek, M. Membrane lipid composition and cellular function. *J. Lipid Res.* **26,** 1015–1035 (1985).
9. McMahon, H. & Boucrot, E. Membrane curvature at a glance. *J. Cell Sci.* **128,** 1065–1070 (2015).
10. Zimmerberg, J. & Kozlov, M. How proteins produce cellular membrane curvature. *Nat. Rev. Mol. Cell Biol.* **7,** 9–19 (2006).
11. Di Paolo, G. & De Camilli, P. Phosphoinositides in cell regulation and membrane dynamics. *Nature* **443,** 651–657 (2006).
12. Chernomordik, L. & Kozlov, M. Protein-lipid interplay in fusion and fission of biological membranes. *Annu. Rev. Biochem.* **72,** 175–207 (2003).
13. Siliakus, M. F., van der Oost, J. & Kengen, S. W. Adaptations of archaeal and bacterial membranes to variations in temperature, pH and pressure. *Extremophiles* **21,** 651–670 (2017).
14. Jansen, M. & Blume, A. A comparative study of diffusive and osmotic water permeation across bilayers composed of phospholipids with different head groups and fatty acyl chains. *Biophys. J.* **68,** 997–1008 (1995).
15. Cantor, R. Lipid composition and the lateral pressure profile in bilayers. *Biophys. J.* **76,** 2625–2639 (1999).
16. Raffy, S. & Teissié, J. Control of lipid membrane stability by cholesterol content. *Biophys. J.* **76,** 2072–2080 (1999).
17. Fantini, J. & Barrantes, F. J. How cholesterol interacts with membrane proteins: An exploration of cholesterol-binding sites including CRAC, CARC, and tilted domains. *Front. Physiol.* **4,** 1–9 (2013).
18. Alberts, B. *et al. Molecular Biology of the Cell*. (Garland Science, 2002).
19. Fantini, J. & Barrantes, F. J. Sphingolipid/cholesterol regulation of neurotransmitter receptor conformation and function. *Biochim. Biophys. Acta - Mol. Cell Biol. Lipids* **1788,** 2345–2361 (2009).
20. Ohvo-Rekilä, H., Ramstedt, B., Leppimäki, P. & Peter Slotte, J. Cholesterol interactions with phospholipids in membranes. *Prog. Lipid Res.* **41,** 66–97 (2002).
21. Yeagle, P. L. Cholesterol and the cell membrane. *Biochim. Biophys. Acta - Biomembr.* **822,** 267–287 (1985).

22. Lund-Katz, S., Laboda, H. M., McLean, L. R. & Phillips, M. C. Influence of molecular packing and phospholipid type on rates of cholesterol exchange. *Biochemistry* **27,** 3416–3423 (1988).
23. Subczynski, W., Pasenkiewicz-Gierula, M., Widomska, J., Mainali, L. & Raguz, M. High cholesterol/low cholesterol: Effects in biological membranes: A review. *Cell Biochem. Biophys.* **75,** 369–385 (2017).
24. Sezgin, E., Levental, I., Mayor, S. & Eggeling, C. The mystery of membrane organization: Composition, regulation and physiological relevance of lipid rafts. *Nat. Rev. Mol. Cell Biol.* **18,** 361–374 (2017).
25. Pike, L. J. Lipid rafts: Bringing order to chaos. *J. Lipid Res.* **44,** 655–667 (2003).
26. Simons, K. & Ehehalt, R. Cholesterol, lipid rafts, and disease. *J. Clin. Invest.* **110,** 597–603 (2002).
27. Javanainen, M., Martinez-Seara, H. & Vattulainen, I. Nanoscale membrane domain formation driven by cholesterol. *Sci. Rep.* **7,** 1143 (2017).
28. Simons, K. & Toomre, D. Lipid rafts and signal transduction. *Nat. Rev. Mol. Cell Biol.* **1,** 31–39 (2000).
29. Hong, W. & Amara, S. Membrane cholesterol modulates the outward facing conformation of the dopamine transporter and alters cocaine binding. *J. Biol. Chem.* **285,** 32616–32626 (2010).
30. Magnani, F., Tate, C., Wynne, S., Williams, C. & Haase, J. Partitioning of the serotonin transporter into lipid microdomains modulates transport of serotonin. *J. Biol. Chem.* **279,** 38770–38778 (2004).
31. Bjork, K. & Svenningsson, P. Modulation of monoamine receptors by adaptor proteins and lipid rafts: Role in some effects of centrally acting drugs and therapeutic agents. *Annu. Rev. Pharmacol. Toxicol.* **51,** 211–242 (2011).
32. Baenziger, J. E., Henault, C., Therien, J. P. D. & Sun, J. Nicotinic acetylcholine receptor–lipid interactions: Mechanistic insight and biological function. *Biochim. Biophys. Acta - Biomembr.* **1848,** 1806–1817 (2015).
33. Dart, C. Lipid microdomains and the regulation of ion channel function. *J. Physiol.* **588,** 3169–3178 (2010).
34. Lange, Y. & Steck, T. L. Cholesterol homeostasis and the escape tendency (activity) of plasma membrane cholesterol. *Prog. Lipid Res.* **47,** 319–332 (2008).
35. Steck, T. L. & Lange, Y. Cell cholesterol homeostasis: Mediation by active cholesterol. *Trends Cell Biol.* **20,** 680–687 (2010).
36. Lange, Y. & Steck, T. L. Active membrane cholesterol as a physiological effector. *Chem. Phys. Lipids* **199,** 74–93 (2016).
37. Lange, Y., Cutler, H. B. & Steck, T. L. The effect of cholesterol and other intercalated amphipaths on the contour and stability of the isolated red cell membrane. *J. Biol. Chem.* **255,** 9331–9337 (1980).
38. Das, A., Goldstein, J. L., Anderson, D. D., Brown, M. S. & Radhakrishnan, A. Use of mutant 125I-perfringolysin o to probe transport and organization of cholesterol in membranes of animal cells. *Proc. Natl. Acad. Sci.* **110,** 10580–10585 (2013).
39. Litz, J. P., Thakkar, N., Portet, T. & Keller, S. L. Depletion with cyclodextrin reveals two populations of cholesterol in model lipid membranes. *Biophys. J.* **110,** 635–645 (2016).
40. Radhakrishnan, A. & McConnell, H. M. Chemical activity of cholesterol in membranes. *Biochemistry* **39,** 8119–8124 (2000).

41. Sokolov, A. & Radhakrishnan, A. Accessibility of cholesterol in endoplasmic reticulum membranes and activation of SREBP-2 switch abruptly at a common cholesterol threshold. *J. Biol. Chem.* **285,** 29480–29490 (2010).
42. McConnell, H. M. & Radhakrishnan, A. Condensed complexes of cholesterol and phospholipids. *Biophys. J.* **77,** 1507–1517 (1999).
43. Lange, Y., Ye, J. & Steck, T. L. How cholesterol homeostasis is regulated by plasma membrane cholesterol in excess of phospholipids. *Proc. Natl. Acad. Sci.* **101,** 11664–11667 (2004).
44. Niu, S.-L., Mitchell, D. & Litman, B. Trans fatty acid derived phospholipids show increased membrane cholesterol and reduced receptor activation as compared to their cis analogs. *Biochemistry* **44,** 4458–4465 (2005).
45. Sarkar, D., Singh, Y. & Kalia, J. Protein–lipid interfaces can drive the functions of membrane-embedded protein–protein complexes. *Chem. Biol.* **13,** 2689–2698 (2018).
46. Singer, S. & Nicolson, G. The fluid mosaic model of the structure of cell membranes. *Science (80-.).* **175,** 720–731 (1972).
47. Liu, Y., Cong, X., Liu, W. & Laganowsky, A. Characterization of membrane protein-lipid interactions by mass spectrometry ion mobility mass spectrometry. *J. Am. Soc. Mass Spectrom.* **28,** 579–586 (2017).
48. Hinderliter, A., Biltonen, R. L. & Almeida, P. F. Lipid modulation of protein-induced membrane domains as a mechanism for controlling signal transduction. *Biochemistry* **43,** 7102–7110 (2004).
49. Brown, M. F. Curvature forces in membrane lipid-protein interactions. *Biochemistry* **51,** 9782–9795 (2012).
50. Lee, A. How lipids affect the activities of integral membrane proteins. *Biochim. Biophys. Acta - Mol. Cell Biol. Lipids* **1666,** 62–87 (2004).
51. Marius, P., de Planque, M. & Williamson, P. Probing the interaction of lipids with the non-annular binding sites of the potassium channel KcsA by magic-angle spinning NMR. *Biochim. Biophys. Acta - Biomembr.* **1818,** 90–96 (2012).
52. Contreras, F., Ernst, A. M. & Wieland, F. Specificity of intramembrane protein − lipid interactions. *Cold Spring Harb. Perspect. Biol.* **3,** 1–19 (2011).
53. Laganowsky, A. *et al.* Membrane proteins bind lipids selectively to modulate their structure and function. *Nature* **510,** 172–175 (2014).
54. Chattopadhyay, A. & Ruysschaert, J. Membrane proteins occupy a central role in cellular physiology. Introduction. *Biochim. Biophys. Acta - Mol. Cell Biol. Lipids* **1848,** 1727–1728 (2015).
55. Marsh, D. Protein modulation of lipids, and vice-versa, in membranes. *Biochim. Biophys. Acta - Biomembr.* **1778,** 1545–1575 (2008).
56. Corradi, V. *et al.* Lipid-protein interactions are unique fingerprints for membrane proteins. *ACS Cent. Sci.* **4,** 709–717 (2018).
57. Moe, P. & Blount, P. Assessment of potential stimuli for mechano-dependent gating of MscL: Effects of pressure, tension, and lipid headgroups. *Biochemistry* **44,** 12239–12244 (2005).
58. Dominguez, L., Foster, L., Straub, J. E. & Thirumalai, D. Impact of membrane lipid composition on the structure and stability of the transmembrane domain of amyloid precursor protein. *Proc. Natl. Acad. Sci.* **113,** E5281–E5287 (2016).
59. Escriba, P. Membrane-lipid therapy: a new approach in molecular medicine. *Trends Mol.*

Med. **12,** 34–43 (2006).
60. Goni, F. & Alonso, A. Structure and functional properties of diacylglycerols in membranes. *Prog. Lipid Res.* **38,** 1–48 (1999).
61. Escriba, P. *et al.* Membrane lipid therapy: Modulation of the cell membrane composition and structure as a molecular base for drug discovery and new disease treatment. *Prog. Lipid Res.* **59,** 38–53 (2015).
62. Prasanna, X., Chattopadhyay, A. & Sengupta, D. Cholesterol modulates the dimer interface of the β2- adrenergic receptor via cholesterol occupancy sites. *Biophys. J.* **106,** 1290–1300 (2014).
63. Gupta, K. *et al.* The role of interfacial lipids in stabilizing membrane protein oligomers. *Nature* **541,** 421–424 (2017).
64. Scanlon, S. M., Williams, D. C. & Schloss, P. Membrane cholesterol modulates serotonin transporter activity. *Biochemistry* **40,** 10507–10513 (2001).
65. Yeagle, P. L. Non-covalent binding of membrane lipids to membrane proteins. *Biochim. Biophys. Acta - Biomembr.* **1838,** 1548–1559 (2014).
66. Belrhali, H. *et al.* Protein, lipid and water organization in bacteriorhodopsin crystals: a molecular view of the purple membrane at 1.9 A resolution. *Structure* **7,** 909–917 (1999).
67. Palsdottir, H. & Hunte, C. Lipids in membrane protein structures. *Biochim. Biophys. Acta - Biomembr.* **1666,** 2–18 (2004).
68. Wu, H. *et al.* Structure of a class C GPCR metabotropic glutamate receptor 1 bound to an allosteric modulator. *Science (80-.).* **344,** 58–64 (2015).
69. Laursen, M., Yatime, L., Nissen, P. & Fedosova, N. U. Crystal structure of the high-affinity Na+,K+-ATPase-ouabain complex with Mg2+ bound in the cation binding site. *Proc. Natl. Acad. Sci.* **110,** 10958–10963 (2013).
70. Hanson, M. *et al.* A specific cholesterol binding site is established by the 2.8 Å structure of the human β2-adrenergic receptor in an alternate crystal form. *Structure* **16,** 897–905 (2008).
71. Penmatsa, A., Wang, K. H. & Gouaux, E. X-ray structure of dopamine transporter elucidates antidepressant mechanism. *Nature* **503,** 85–90 (2013).
72. Bolotina, V., Omelyanenko, V., Heyes, B., Ryan, U. & Bregestovski, P. Variations of membrane cholesterol alter the kinetics of Ca 2+ -dependent K + channels and membrane fluidity in vascular smooth muscle cells. *Pflugers Arch Pflugers Arch. Eur. J. Physiol.* **415,** 262–268 (1989).
73. Criado, M., Eibl, H. & Barrantes, F. J. Effects of lipids on acetylcholine receptor. Essential need of cholesterol for maintenance of agonist-induced state transitions in lipid vesicles. *Biochemistry* **21,** 3622–3629 (1982).
74. Grouleff, J., Irudayam, S. J., Skeby, K. K. & Schiøtt, B. The influence of cholesterol on membrane protein structure, function, and dynamics studied by molecular dynamics simulations. *Biochim. Biophys. Acta - Biomembr.* **1848,** 1783–1795 (2015).
75. Althoff, T., Hibbs, R. E., Banerjee, S. & Gouaux, E. X-ray structures of GluCl in apo states reveal a gating mechanism of cys-loop receptors. *Nature* **512,** 333–337 (2014).
76. Valiyaveetil, F., Zhou, Y. & MacKinnon, R. Lipids in the structure, folding, and function of the KcsA K+ channel. *Biochemistry* **41,** 10771–10777 (2002).
77. Basak, S., Schmandt, N., Gicheru, Y. & Chakrapani, S. Crystal structure and dynamics of a lipid-induced potential desensitized-state of a pentameric ligand-gated channel. *Elife* **6,** e23886 (2017).

78. Poveda, J., Giudici, A., Renart, M., Morales, A. & Gonzalez-Ros, J. Towards understanding the molecular basis of ion channel modulationby lipids: Mechanistic models and current paradigms. *Biochim. Biophys. Acta - Biomembr.* **1859,** 1507–1516 (2017).
79. Hénin, J., Salari, R., Murlidaran, S. & Brannigan, G. A predicted binding site for cholesterol on the GABAA receptor. *Biophys. J.* **106,** 1938–1949 (2014).
80. Levitan, I., Singh, D. K. & Rosenhouse-Dantsker, A. Cholesterol binding to ion channels. *Front. Physiol.* **5,** 1–14 (2014).
81. Rosenhouse-Dantsker, A. Cholesterol-binding sites in GIRK channels: The devil is in the details. *Lipid Insights* **11,** 1–4 (2018).
82. Karlin, A. Emerging structure of the nicotinic acetylcholine receptors. *Nat. Rev. Neurosci.* **3,** 102–114 (2002).
83. Fong, T. M. & McNamee, M. G. Stabilization of acetylcholine receptor secondary structure by cholesterol and negatively charged phospholipids in membranes. *Biochemistry* **26,** 3871–3880 (1987).
84. Jones, O. T. & McNamee, M. G. Annular and nonannular binding sites for cholesterol associated with the nicotinic acetylcholine receptor. *Biochemistry* **27,** 2364–74 (1988).
85. Rankin, S. E., Addona, G. H., Kloczewiak, M. a, Bugge, B. & Miller, K. W. The cholesterol dependence of activation and fast desensitization of the nicotinic acetylcholine receptor. *Biophys. J.* **73,** 2446–2455 (1997).
86. Hamouda, A. K., Sanghvi, M., Sauls, D., Machu, T. K. & Blanton, M. P. Assessing the lipid requirements of the Torpedo californica nicotinic acetylcholine receptor. *Biochemistry* **45,** 4327–4337 (2006).
87. DaCosta, C. J. B., Dey, L., Therien, J. P. D. & Baenziger, J. E. A distinct mechanism for activating uncoupled nicotinic acetylcholine receptors. *Nat. Chem. Biol.* **9,** 701–707 (2013).
88. DaCosta, C. J. B. & Baenziger, J. E. A lipid-dependent uncoupled conformation of the acetylcholine receptor. *J. Biol. Chem.* **284,** 17819–17825 (2009).
89. Corringer, P.-J. *et al.* Structure and pharmacology of pentameric receptor channels: From bacteria to brain. *Structure* **20,** 941–956 (2012).
90. Labriola, J. *et al.* Structural sensitivity of a prokaryotic pentameric ligand-gated ion channel to its membrane environment. *J. Biol. Chem.* **288,** 11294–11303 (2013).
91. Velisetty, P., Chalamalasetti, S. & Chakrapani, S. Structural basis for allosteric coupling at the membrane-protein interface in gloeobacter violaceus ligand-gated ion channel (GLIC). *J. Biol. Chem.* **289,** 3013–3025 (2014).
92. Thompson, A., Lester, H. & Lummis, S. The structural basis of function in Cys-loop receptors. *Q. Rev. Biophys.* **43,** 449–499 (2010).
93. Salari, R., Murlidaran, S. & Brannigan, G. Pentameric ligand-gated ion channels: Insights from computation. *Mol. Simul.* **40,** 821–829 (2014).
94. Alcaino, C. *et al.* Role of the cys loop and transmembrane domain in the allosteric modulation of α4β2 nicotinic acetylcholine receptors. *J. Biol. Chem.* **292,** 551–562 (2017).
95. DaCosta, C. J. B. & Baenziger, J. E. Gating of pentameric ligand-gated ion channels: Structural insights and ambiguities. *Structure* **21,** 1271–1283 (2013).
96. Baptista-Hon, D. T., Deeb, T. Z., Lambert, J. J., Peters, J. A. & Hales, T. G. The minimum M3-M4 loop length of neurotransmitteractivated pentameric receptors is critical for the structural integrity of cytoplasmic portals. *J. Biol. Chem.* **288,** 21558–21568 (2013).

97. Hilf, R. & Dutzler, R. X-ray structure of a prokaryotic pentameric ligand-gated ion channel. *Nature* **452,** 375–379 (2008).
98. Hilf, R. & Dutzler, R. Structure of a potentially open state of a proton-activated pentameric ligand-gated ion channel. *Nature* **457,** 115–118 (2009).
99. Hibbs, R. E. & Gouaux, E. Principles of activation and permeation in an anion-selective Cys-loop receptor. *Nature* **474,** 54–60 (2011).
100. Du, J., Lü, W., Wu, S., Cheng, Y. & Gouaux, E. Glycine receptor mechanism elucidated by electron cryo-microscopy. Nature. *Nature* **526,** 224–229 (2015).
101. O'Toole, K. & Jenkins, A. Discrete M3-M4 intracellular loop subdomains control specific aspects of γ-aminobutyric acid type A receptor function. *J. Biol. Chem.* **286,** 37990–37999 (2011).
102. Cooper, G. M. *The Cell: A Molecular Approach*. (Sinauer Associates, 2000).
103. Nemecz, A., Prevost, M. S., Menny, A. & Corringer, P.-J. Emerging molecular mechanisms of signal transduction in pentameric ligand-gated ion channels. *Neuron* **90,** 452–470 (2016).
104. Keramidas, A. & Lynch, J. An outline of desensitization in pentameric ligand-gated ion channel receptors. *Cell. Mol. Life Sci.* **70,** 1241–1253 (2013).
105. Neverisky, D. L. & Abbott, G. W. Ion channel-transporter interactions. *Crit. Rev. Biochem. Mol. Biol.* **51,** 257–267 (2016).
106. Cascio, M. Structure and function of the glycine receptor and related nicotinicoid receptors. *J. Biol. Chem.* **279,** 19383–6 (2004).
107. Jacob, N. T. Drug targets: Ligand and voltage gated ion channels. *Int. J. Basic Clin. Pharmacol.* **6,** 235–245 (2017).
108. Kinde, M. N. *et al.* Conformational changes underlying desensitization of the pentameric ligand-gated ion channel ELIC. *Structure* **23,** 995–1004 (2015).
109. Auerbach, A. The energy and work of a ligand-gated ion channel. *J. Mol. Biol.* **425,** 1461–1475 (2013).
110. Gicheru, Y. & Chakrapani, S. Direct visualization of ion-channel gating in a native environment. *Proc. Natl. Acad. Sci.* **115,** 10198–10200 (2018).
111. Wells, M. M. *et al.* Ensemble-based virtual screening for cannabinoid-like potentiators of the human glycine receptor α1 for the treatment of pain. *J. Med. Chem.* **58,** 2958–2966 (2015).
112. Wu, Z., Cheng, H., Jiang, Y., Melcher, K. & Xu, H. Ion channels gated by acetylcholine and serotonin: Structures, biology, and drug discovery. *Acta Pharmacol. Sin.* **36,** 895–907 (2015).
113. Jones, S., Sudweeks, S. & Yakel, J. Nicotinic receptors in the brain: Correlating physiology with function. *Trends Neurosci.* **22,** 555–561 (1999).
114. Rissman, R. & Mobley, W. Implications for treatment: GABAA receptors in aging, down syndrome and alzheimer's disease. *J. Neurochem.* **117,** 613–622 (2011).
115. Tanner, C. *et al.* Smoking and parkinson's disease in twins. *Neurology* **58,** 581–588 (2002).
116. Macdonald, R., Gallagher, M., Feng, H. & Kang, J. GABA (A) receptor epilepsy mutations. *Biochem. Pharmacol.* **68,** 1497–1506 (2004).
117. Lippiello, P. *et al.* RJR-2403: A nicotinic agonist with CNS selectivity II. In vivo characterization. *J. Pharmacol. Exp. Ther.* **279,** 1422–1429 (1996).
118. Edenberg, H. *et al.* Variations in GABRA2, encoding the alpha 2 subunit of the GABA(A)

receptor, are associated with alcohol dependence and with brain oscillations. *Am. J. Hum. Genet.* **74,** 705–714 (2004).
119. Schaefer, N., Roemer, V., Janzen, D. & Villmann, C. Impaired glycine receptor trafficking in neurological diseases. *Front. Mol. Neurosci.* **11,** 291 (2018).
120. Grudzinska, J. *et al.* The beta subunit determines the ligand binding properties of synaptic glycine receptors. *Neuron* **45,** 727–39 (2005).
121. Cascio, M., Schoppa, N. E., Grodzicki, R. L., Sigworth, F. J. & Fox, R. O. Functional expression and purification of a homomeric human α1 glycine receptor in baculovirus-infected insect cells. *J. Biol. Chem.* **268,** 22135–22142 (1993).
122. Betz, H. & Laube, B. Glycine receptors: Recent insights into their structural organization and functional diversity. *J. Neurochem.* **97,** 1600–1610 (2006).
123. Burgos, C. F., Yevenes, G. E. & Aguayo, L. G. Structure and pharmacologic modulation of inhibitory glycine receptors. *Mol. Pharmacol.* **90,** 318–325 (2016).
124. Cascio, M., Shenkel, S., Grodzicki, R. L., Sigworth, F. J. & Fox, R. O. Functional reconstitution and characterization of recombinant human alpha 1-glycine receptors. *J. Biol. Chem.* **276,** 20981–8 (2001).
125. Tsetlin, V., Kuzmin, D. & Kasheverov, I. Assembly of nicotinic and other cys-loop receptors. *J. Neurochem.* **116,** 734–741 (2011).
126. Keramidas, A., Moorhouse, A. J., Pierce, K. D., Schofield, P. R. & Barry, P. H. Cation-selective mutations in the M2 domain of the inhibitory glycine receptor channel reveal determinants of ion-charge selectivity. *J. Gen. Physiol.* **119,** 393–410 (2002).
127. Lynch, J. W. *et al.* Identification of intracellular and extracellular domains mediating signal transduction in the inhibitory glycine receptor chloride channel. *EMBO J.* **16,** 110–120 (1997).
128. Lynch, J. W., Han, N.-L. R., Haddrill, J., Pierce, K. D. & Schofield, P. R. The surface accessibility of the glycine receptor M2-M3 loop is increased in the channel open state. *J. Neurosci.* **21,** 2589–2599 (2001).
129. Meyer, G., Kirsch, J., Betz, H. & Langosch, D. Identification of a gephyrin binding motif on the glycine receptor β subunit. *Neuron* **15,** 563–572 (1995).
130. Yevenes, G. E. & Zeilhofer, H. U. Molecular sites for the positive allosteric modulation of glycine receptors by endocannabinoids. *PLoS One* **6,** e23886 (2011).
131. Sadtler, S. *et al.* A basic cluster determines topology of the cytoplasmic M3-M4 loop of the glycine receptor α1 subunit. *J. Biol. Chem.* **278,** 16782–16790 (2003).
132. Krasowski, M. D. & Harrison, N. L. General anaesthetic actions on ligan-gated ion channels. *Cell. Mol. Life Sci.* **55,** 1278–1303 (1999).
133. Kelley, B. G. & Mermelstein, P. G. Progesterone blocks multiple routes of ion flux. *Mol. Cell. Neurosci.* **48,** 137–141 (2011).
134. Gallegos, C. E., Pediconi, M. F. & Barrantes, F. J. Ceramides modulate cell-surface acetylcholine receptor levels. *Biochim. Biophys. Acta - Biomembr.* **1778,** 917–930 (2008).
135. Arcario, M. J., Mayne, C. G. & Tajkhorshid, E. A membrane-embedded pathway delivers general anesthetics to two interacting binding sites in the Gloeobacter violaceus ion channel. *J. Biol. Chem.* **292,** 9480–9492 (2017).
136. Lynagh, T. & Laube, B. Opposing effects of the anesthetic propofol at pentameric ligand-gated ion channels mediated by a common site. *J. Neurosci. Off. J. Soc. Neurosci.* **34,** 2155–2159 (2014).
137. Fourati, Z. *et al.* Barbiturates bind in the GLIC ion channel pore and cause inhibition by

stabilizing a closed state. *J. Biol. Chem.* **292,** 1550–1558 (2017).
138. Ye, Q. *et al.* Enhancement of glycine receptor function by ethanol is inversely correlated with molecular volume at position α267. *J. Biol. Chem.* **273,** 3314–3319 (1998).
139. Sanchez, A. *et al.* Control of ethanol sensitivity of the glycine receptor α3 subunit by transmembrane 2, the intracellular splice cassette and C-terminal domain. *J. Pharmacol. Exp. Ther.* **353,** 80–90 (2015).
140. Colón-Sáez, J. O. & Yakel, J. L. The α7 nicotinic acetylcholine receptor function in hippocampal neurons is regulated by the lipid composition of the plasma membrane. *J. Physiol.* **589,** 3163–3174 (2011).
141. Juarez-Contreras, R., Rosenbaum, T. & Morales-Lazaro, S. Lysophosphatidic acid and ion channels as molecular mediators of pain. *Front. Mol. Neurosci.* **11,** 462 (2018).
142. Bianchi, M. T. & Botzolakis, E. J. Targeting ligand-gated ion channels in neurology and psychiatry: Is pharmacological promiscuity an obstacle or an opportunity? *BMC Pharmacol.* **10,** (2010).
143. Vemparala, S., Saiz, L., Eckenhoff, R. G. & Klein, M. L. Partitioning of anesthetics into a lipid bilayer and their interaction with membrane-bound peptide bundles. *Biophys. J.* **91,** 2815–2825 (2006).
144. Piomelli, D., Hohmann, A. G., Seybold, V. & Hammock, B. D. A lipid gate for the peripheral control of pain. *J. Neurosci.* **34,** 15184–15191 (2014).
145. Gonzalez-Gutierrez, G. *et al.* Mutations that stabilize the open state of the Erwinia chrisanthemi ligand-gated ion channel fail to change the conformation of the pore domain in crystals. *Proc. Natl. Acad. Sci.* **109,** 6331–6336 (2012).
146. Pan, J. *et al.* Structure of the pentameric ligand-gated ion channel GLIC bound with anesthetic ketamine. *Structure* **20,** 1463–1469 (2012).
147. Pham, N., Parker, R. & Kohler, J. Photocrosslinking approaches to interactome mapping. *Curr. Opin. Chem. Biol.* **17,** 90–101 (2013).
148. Kleiner, R., Hang, L., Molloy, K., Chait, B. & Kapoor, T. A chemical proteomics approach to reveal direct protein-protein interactions in living cells. *Cell Chem. Biol.* **25,** 110–120 (2019).
149. Tang, X. & Bruce, J. Chemical cross-linking for protein-protein interaction studies. *Methods Mol. Biol.* **492,** 283–293 (2009).
150. Heck, T., Faccio, G., Richter, M. & Thony-Meyer, L. Enzyme-catalyzed protein crosslinking. *Appl. Microbiol. Biotechnol.* **97,** 461–475 (2013).
151. Kluger, R. & Alagic, A. Chemical cross-linking and protein-protein interactions-a review with illustrative protocols. *Bioorg. Chem.* **32,** 451–472 (2004).
152. Migneault, I., Dartiguenave, C., Bertrand, M. & Waldron, K. Glutaraldehyde: Behavior in aqueous solution, reaction with proteins, and application to enzyme crosslinking. *Biotechniques* **37,** 798–802 (2004).
153. Chen, F. *et al.* On the efficiency of NHS ester cross-linkers for stabilizing integral membrane protein complexes. *J. Am. Soc. Mass Spectrom.* **26,** 493–498 (2015).
154. Partis, M., Griffiths, D., Roberts, G. & Beechey, R. Cross-linking of protein by ω-maleimido alkanoylN-hydroxysuccinimido esters. *J. Protein Chem.* **2,** 263–277 (1983).
155. Sinz, A. Investigation of protein–protein interactions in living cells by chemical crosslinking and mass spectrometry. *Anal. Bioanal. Chem.* **397,** 3433–3440 (2010).
156. Smith, E. & Collins, I. Photoaffinity labeling in target- and binding-site identification. *Future Med. Chem.* **7,** 159–183 (2015).

157. Herner, A. *et al.* 2-Aryl-5-carboxytetrazole as a new photoaffinity label for drug target identification. *J. Am. Chem. Soc.* **138,** 14609–14615 (2016).
158. Buchmueller, K., Hill, B., Platz, M. & Weeks, K. RNA-tethered phenyl azide photocrosslinking via a short-lived indiscriminant electrophile. *J. Am. Chem. Soc.* **125,** 10850–10861 (2003).
159. Albuszis, M., Roth, P., Pauer, W. & Moritz, H. Two in one: Use of azide functionality for controlled photo-crosslinking and click-modification of polymer microspheres. *Polym. Chem.* **7,** 5414–5425 (2016).
160. Chin, J., Martin, A., King, D., Wang, L. & Schultz, P. Addition of a photocrosslinking amino acid to the genetic code of Escherichia coli. *Proc. Natl. Acad. Sci.* **99,** 11020–11024 (2002).
161. Dubinsky, L., Krom, B. P. & Meijler, M. M. Diazirine based photoaffinity labeling. *Bioorg. Med. Chem.* **20,** 554–570 (2012).
162. Walther, T. & Mann, M. Mass spectrometry–based proteomics in cell biology. *J. Cell Biol.* **190,** 491–500 (2010).
163. Han, X., Aslanian, A. & Yates III, J. Mass spectrometry for proteomics. *Curr. Opin. Chem. Biol.* **12,** 483–490 (2008).
164. Yates III, J. Mass spectrometry. From genomics to proteomics. *Trends Genet.* **16,** 5–8 (2000).
165. Siuzdak, G. The emergence of mass spectrometry in biochemical research. *Proc. Natl. Acad. Sci.* **91,** 11290–11297 (1994).
166. Gross, R. The evolution of lipidomics through space and time. *Biochim. Biophys. Acta - Mol. Cell Biol. Lipids* **1862,** 731–739 (2017).
167. Sigman, M., Clark, C., Fidler, R., Geiger, C. & Clausen, C. Analysis of triacetone triperoxide by gas chromatography/mass spectrometry and gas chromatography/tandem mass spectrometry by electron and chemical ionization. *Rapid Commun. Mass Spectrom.* **20,** 2851–2857 (2006).
168. Nesvizhskii, A. Protein identification by tandem mass spectrometry and sequence database searching. *Methods Mol. Biol.* **367,** 87–119 (2007).
169. Hyung, S. & Ruotolo, B. Integrating mass spectrometry of intact protein complexes into structural proteomics. *Proteomics* **12,** 1547–1564 (2012).
170. Larsen, M., Trelle, M., Thingholm, T. & Jensen, O. Analysis of posttranslational modifications of proteins by tandem mass spectrometry. *Biotechniques* **40,** 790–798 (2006).
171. Baldwin, M. Protein identification by mass spectrometry: Issues to be considered. *Mol. Cell. Proteomics* **3,** 1–9 (2004).
172. Qian, W., Jacobs, J., Liu, T., Camp II, D. & Smith, R. Advances and challenges in liquid chromatography-mass spectrometry based proteomic profiling for clinical applications. *Mol. Cell. Proteomics* **5,** 1727–1744 (2006).
173. Yewdall, N., Allison, T., Pearce, F., Robinson, C. V. & Gerrard, J. Self-assembly of toroidal proteins explored using native mass spectrometry. *Chem. Sci.* **9,** 6099–6106 (2018).
174. Harrison, A. Fragmentation of protonated oligoalanines: Amide bond cleavage and beyond. *J. Am. Soc. Mass Spectrom.* **15,** 1810–1819 (2004).
175. Li, S., Arnold, R., Tang, H. & Radivojac, P. On the accuracy and limits of peptide fragmentation spectrum prediction. *Anal. Chem.* **83,** 790–796 (2011).

176. MacCoss, M. *et al.* Shotgun identification of protein modifications from protein complexes and lens tissue. *Proc. Natl. Acad. Sci.* **99,** 7900–7905 (2002).
177. Yu, C. & Huang, L. Cross-linking mass spectrometry (XL-MS): An emerging technology for interactomics and structural biology. *Anal. Chem.* **90,** 144–165 (2018).
178. Ferraro, N. A. & Cascio, M. Cross-linking-mass spectrometry studies of cholesterol interactions with human α1 glycine receptor. *Anal. Chem.* **90,** 2508–2516 (2018).
179. Liu, Z. *et al.* Crosslinking constraints and computational models as complementary tools in modeling the extracellular domain of the glycine receptor. *PLoS One* **9,** e102571 (2014).
180. Tian, M. & Ye, S. Allosteric regulation in NMDA receptors revealed by the genetically encoded photo-cross-linkers. *Sci. Rep.* **6,** 1–12 (2016).
181. Robinette, D., Neamati, N., Tomer, K. B. & Borchers, C. H. Photoaffinity labeling combined with mass spectrometric approaches as a tool for structural proteomics. *Expert Rev. Proteomics* **3,** 399–408 (2006).
182. Sinz, A. Cross-linking/mass spectrometry for studying protein structures and protein-protein interactions: Where are we now and where should we go from here? *Angew. Chemie Int. Ed.* **57,** 6390–6396 (2018).
183. Kaake, R. M. *et al.* A new in vivo cross-linking mass spectrometry platform to define protein–protein interactions in living cells. *Mol. Cell. Proteomics* **13,** 3533–3543 (2014).
184. Chen, Z. A. *et al.* Architecture of the RNA polymerase II–TFIIF complex revealed by cross-linking and mass spectrometry. *EMBO J.* **29,** 717–726 (2010).
185. Rappsilber, J. The beginning of a beautiful friendship: Cross-linking/mass spectrometry and modelling of proteins and multi-protein complexes. *J. Struct. Biol.* **173,** 530–540 (2011).
186. Schweppe, D. *et al.* Mitochondrial protein interactome elucidated by chemical cross-linking mass spectrometry. *Proc. Natl. Acad. Sci.* **114,** 1732–1737 (2017).
187. Huang, X., Luan, B., Wu, J. & Shi, Y. An atomic structure of the human 26S proteasome. *Nat. Sructural Mol. Biol.* **23,** 778–785 (2016).
188. Chavez, J., Liu, N. & Bruce, J. Quantification of protein-protein interactions with chemical cross-linking and mass spectrometry. *J. Proteome Res.* **10,** 1528–1537 (2011).
189. Chan, W. *et al.* Quantification of a novel DNA-protein cross-link product formed by reacting apurinic/apyrimidinic sites in DNA with cysteine residues in protein by liquid chromatography-tandem mass spectrometry coupled with the stable isotope-dilution method. *Anal. Chem.* **91,** 4987–4994 (2019).
190. Chiara, D. C. *et al.* Specificity of intersubunit general anesthetic-binding sites in the transmembrane domain of the human α1β3γ2 γ-aminobutyric acid type A (GABAA) receptor. *J. Biol. Chem.* **288,** 19343–19357 (2013).
191. Yip, G. M. S. *et al.* A propofol binding site on mammalian GABAA receptors identified by photolabeling. *Nat. Chem. Biol.* **9,** 715–720 (2013).
192. Li, H., Yao, Z., Degenhardt, B., Teper, G. & Papadopoulos, V. Cholesterol binding at the cholesterol recognition/ interaction amino acid consensus (CRAC) of the peripheral-type benzodiazepine receptor and inhibition of steroidogenesis by an HIV TAT-CRAC peptide. *Proc. Natl. Acad. Sci. U. S. A.* **98,** 1267–1272 (2001).
193. Budelier, M. M. *et al.* Photoaffinity labeling with cholesterol analogues precisely maps a cholesterol-binding site in voltage-dependent anion channel-1. *J. Biol. Chem.* **292,** 9294–9304 (2017).

194. Middlemas, D. S. & Raftery, M. A. Identification of subunits of acetylcholine receptor that interact with a cholesterol photoaffinity probe. *Biochemistry* **26,** 1219–1223 (1987).
195. Hamouda, A. K., Chiara, D. C., Sauls, D., Cohen, J. B. & Blanton, M. P. Cholesterol interacts with transmembrane alpha-helices M1, M3, and M4 of the Torpedo nicotinic acetylcholine receptor: Photolabeling studies using [3H]Azicholesterol. *Biochemistry* **45,** 976–86 (2006).
196. Miernyk, J. & Thelen, J. Biochemical approaches for discovering protein-protein interactions. *Plant J. cell Mol. Biol.* **53,** 597–609 (2008).
197. Chavez, J. *et al.* Chemical crosslinking mass spectrometry analysis of protein conformations and supercomplexes in heart tissue. *Cell Syst.* **6,** 136–141 (2018).
198. Liu, Q., Remmelzwaal, S., Heck, A., Akhmanova, A. & Liu, F. Facilitating identification of minimal protein binding domains by cross-linking mass spectrometry. *Sci. Rep.* **7,** 13453 (2017).
199. Haupt, C. *et al.* Combining chemical cross-linking and mass spectrometry of intact protein complexes to study the architecture of multi-subunit protein assemblies. *J. Vis. Exp.* 56747 (2017).
200. Walko, M., Hewitt, E., Radford, S. & Wilson, A. Design and synthesis of cysteine-specific labels for photo-crosslinking studies. *RSC Adv.* **9,** 7610–7614 (2019).
201. Schneider, M., Belsom, A. & Rappsilber, J. Protein tertiary structure by crosslinking/mass spectrometry. *Trends Biochem. Sci.* **43,** 157–169 (2018).
202. Chavez, J. *et al.* A general method for targeted quantitative cross-linking mass spectrometry. *PLoS One* **11,** e0167547 (2016).
203. Merkley, E., Cort, J. & Adkins, J. Cross-linking and mass spectrometry methodologies to facilitate structural biology: Finding a path through the maze. *J. Struct. Funct. Genomics* **14,** 77–90 (2013).
204. Leitner, A. *et al.* Probing native protein structures by chemical cross-linking, mass spectrometry, and bioinformatics. *Mol. Cell. Proteomics* **9,** 1634–49 (2010).
205. Lynagh, T. & Lynch, J. W. An improved ivermectin-activated chloride channel receptor for inhibiting electrical activity in defined neuronal populations. *J. Biol. Chem.* **285,** 14890–14897 (2010).
206. Serdiuk, T., Sugihara, J., Mari, S. A., Kaback, H. R. & Müller, D. J. Observing a lipid-dependent alteration in single lactose permeases. *Structure* **23,** 754–761 (2015).
207. Hresko, R. C., Kraft, T. E., Quigley, A., Carpenter, E. P. & Hruz, P. W. Mammalian glucose transporter activity is dependent upon anionic and conical phospholipids. *J. Biol. Chem.* **291,** 17271–17282 (2016).
208. Korinek, M. *et al.* Cholesterol modulates open probability and desensitization of NMDA receptors. *J. Physiol.* **593,** 2279–2293 (2015).
209. Lundbaek, J. A. *et al.* Regulation of sodium channel function by bilayer elasticity: The importance of hydrophobic coupling. Effects of micelle-forming amphiphiles and cholesterol. *J. Gen. Physiol.* **123,** 599–621 (2004).
210. Pike, L. J. The challenge of lipid rafts. *J. Lipid Res.* **50,** S323–S328 (2009).
211. Quinn, P. Lipid-lipid interactions in bilayer membranes: Married couples and casual liaisons. *Prog. Lipid Res.* **51,** 179–198 (2012).
212. Lange, Y., Ye, J. & Steck, T. L. Activation of membrane cholesterol by displacement from phospholipids. *J. Biol. Chem.* **280,** 36126–36131 (2005).
213. Beseničar, M. P., Bavdek, A., Kladnik, A., Maček, P. & Anderluh, G. Kinetics of

cholesterol extraction from lipid membranes by methyl-β-cyclodextrin-A surface plasmon resonance approach. *Biochim. Biophys. Acta - Biomembr.* **1778,** 175–184 (2008).
214. daCosta, C. J. B., Ogrel, A. A., McCardy, E. A., Blanton, M. P. & Baenziger, J. E. Lipid-protein interactions at the nicotinic acetylcholine receptor. A functional coupling between nicotinic receptors and phosphatidic acid-containing lipid bilayers. *J. Biol. Chem.* **277,** 201–8 (2002).
215. Criado, M., Eibl, H. & Barrantes, F. J. Functional properties of the acetylcholine receptor incorporateidn model lipid membranes. *J. Biol. Chem.* **259,** 9188–9198 (1984).
216. Nys, M., Kesters, D. & Ulens, C. Structural insights into cys-loop receptor function and ligand recognition. *Biochem. Pharmacol.* **86,** 1042–53 (2013).
217. Song, Y. & Huang, L. Modulation of glycine receptor chloride channels by cAMP-dependent protein kinase in spinal trigeminal neurons. *Nature* **348,** 242–245 (1990).
218. Huang, X., Chen, H. & Shaffer, P. Crystal structures of human GlyRα3 bound to ivermectin. *Structure* **25,** 1–6 (2017).
219. Unwin, N. Refined structure of the nicotinic acetylcholine receptor at 4 Å resolution. *J. Mol. Biol.* **346,** 967–989 (2005).
220. Radhakrishnan, A., Anderson, T. G. & McConnell, H. M. Condensed complexes, rafts, and the chemical activity of cholesterol in membranes. *Proc. Natl. Acad. Sci. U. S. A.* **97,** 12422–7 (2000).
221. Peterson, G. L. A simplification of the protein assay method of Lowry et al. which is more generally applicable. *Anal. Biochem.* **83,** 346–356 (1977).
222. Brannigan, G., Hénin, J., Law, R., Eckenhoff, R. & Klein, M. L. Embedded cholesterol in the nicotinic acetylcholine receptor. *Proc. Natl. Acad. Sci. U. S. A.* **105,** 14418–23 (2008).
223. Liu, R., Lu, P., Chu, J. & Sharom, F. Characterization of fluorescent sterol binding to purified human NPC1. *J. Biol. Chem.* **284,** 1840–1852 (2009).
224. Fantini, J., Di Scala, C., Evans, L., Williamson, P. & Barrantes, F. A mirror code for protein-cholesterol interactions in the two leaflets of biological membranes. *Sci. Rep.* 21907 (2016).
225. Ziebell, M. R., Nirthanan, S., Husain, S. S., Miller, K. W. & Cohen, J. B. Identification of binding sites in the nicotinic acetylcholine receptor for [3H]azietomidate, a photoactivatable general anesthetic. *J. Biol. Chem.* **279,** 17640–17649 (2004).
226. Hamouda, A. K. *et al.* Identifying barbiturate binding sites in a nicotinic acetylcholine receptor with [3H]allyl m-trifluoromethyldiazirine mephobarbital, a photoreactive barbiturate. *Mol. Pharmacol.* **85,** 735–746 (2014).
227. Ahrens, J. *et al.* The anaesthetic steroid alphaxalone positively modulats alpha 1-glycine receptor function. *Pharmacology* **82,** 228–232 (2008).
228. Rouviere, E., Arnarez, C., Yang, L. & Lyman, E. Identification of two new cholesterol interaction sites on the A2A adenosine receptor. *Biophys. J.* **113,** 2415–2424 (2017).
229. Zhu, S. *et al.* Mechanism of NMDA receptor inhibition and activation. *Cell* **165,** 704–714 (2016).
230. Cafiso, D. S. Identifying and quantitating conformational exchange in membrane proteins using site-directed spin labeling. *Acc. Chem. Res.* **47,** 3102–3109 (2014).
231. Sun, J., Comeau, F. & Baenziger, J. Probing the structure of the uncoupled nicotinic acetylcholine receptor. *Biochim. Biophys. Acta - Mol. Cell Biol. Lipids* **1859,** 146–154 (2017).
232. Parker, A., Miles, K., Cheng, K. H. & Huang, J. Lateral distribution of cholesterol in

dioleoylphosphatidylcholine lipid bilayers: Cholesterol-phospholipid interactions at high cholesterol limit. *Biophys. J.* **86,** 1532–44 (2004).
233. Saad, H. & Higuchi, W. Water solubility of cholesterol. *J. Pharm. Sci.* **54,** 1205–106 (1965).
234. Brannigan, G. & LeBard, D. Multiple binding sites for the general anesthetic isoflurane identified in the nicotinic acetylcholine receptor transmembrane domain. *Proc. Natl. Acad. Sci. U. S. A.* **107,** 14122–14127 (2010).
235. Peng, T., Yuan, X. & Hang, H. C. Turning the spotlight on protein-lipid interactions in cells. *Curr. Opin. Chem. Biol.* **21,** 144–153 (2014).
236. Marino, K. A., Prada-Gracia, D., Provasi, D. & Filizola, M. Impact of lipid composition and receptor conformation on the spatio-temporal organization of μ-opioid receptors in a multi-component plasma membrane model. *PLoS Comput. Biol.* **12,** 1–29 (2016).
237. Xiong, W. *et al.* Cannabinoid potentiation of glycine receptors contributes to cannabis-induced analgesia. *Nat. Chem. Biol.* **7,** 296–303 (2011).
238. Howard, R. J., Trudell, J. R. & Harris, R. Seeking structural specificity: direct modulation of pentameric ligand-gated ion channels by alcohols and general anesthetics. *Pharmacol. Rev.* **66,** 396–412 (2014).
239. Laude, A. J. & Prior, I. A. Plasma membrane microdomains : organisation , function and trafficking. *Mol. Membr. Biol.* **21,** 193–205 (2012).
240. Schmidt, C. & Urlaub, H. Combining cryo-electron microscopy (cryo-EM) and cross-linking mass spectrometry (CX-MS) for structural elucidation of large protein assemblies. *Curr. Opin. Struct. Biol.* **46,** 157–168 (2017).
241. Kumar, A. *et al.* Mechanisms of activation and desensitization of full-length glycine receptor in membranes. *Cold Spring Harb. Press* (2019).
242. Basak, S., Gicheru, Y., Rao, S., Sansom, M. & Chakrapani, S. Cryo-EM reveals two distinct serotonin-bound conformations of full-length 5-HT3A receptor. *Nature* **563,** 270–274 (2018).
243. Huang, X. *et al.* Crystal structures of human glycine receptor α3 bound to a novel class of analgesic potentiators. *Nat. Struct. Mol. Biol.* **24,** 108–113 (2017).
244. Sauguet, L. *et al.* Crystal structures of a pentameric ligand-gated ion channel provide a mechanism for activation. *Proc. Natl. Acad. Sci.* **111,** 966–971 (2014).
245. Heusser, S. A. *et al.* Allosteric potentiation of a ligand-gated ion channel is mediated by access to a deep membrane-facing cavity. *Proc. Natl. Acad. Sci.* **115,** 10672–10677 (2018).
246. Dellisanti, C. D., Hanson, S. M., Chen, L. & Czajkowski, C. Packing of the extracellular domain hydrophobic core has evolved to facilitate pentameric ligand-gated ion channel function. *J. Biol. Chem.* **286,** 3658–3670 (2010).
247. Miller, P. S., Topf, M. & Smart, T. G. Mapping a molecular link between allosteric inhibition and activation of the glycine receptor. *Nat. Sructural Mol. Biol.* **15,** 1084–1093 (2008).
248. Ruthstein, S. *et al.* Pulsed electron spin resonance resolves the coordination site of Cu2+ ions in α1-glycine receptor. *Biophys. J.* **99,** 2497–2506 (2010).
249. Pless, S. A. & Lynch, J. W. Magnitude of a conformational change in the glycine receptor β1-β2 loop is correlated with agonist efficacy. *J. Biol. Chem.* **284,** 27370–27376 (2009).
250. Langlhofer, G. & Villmann, C. The intracellular loop of the glycine receptor: It's not all about the size. *Front. Mol. Neurosci.* **9,** (2016).

251. Vaello, M.-L., Ruiz-Gomez, A., Lerma, J. & Mayor, F. Modulation of inhibitory glycine receptors by phosphorylation by protein kinase c and cAMP-dependent protein kinase. *J. Biol. Chem.* **269,** 2002–2008 (1994).
252. Horani, S. *et al.* Ethanol modulation is quantitatively determined by the transmembrane domain of human α1 glycine receptors. *Alcohol. Clin. Exp. Res.* **39,** 962–968 (2015).
253. Haberkant, P. *et al.* Protein-sphingolipid interactions within cellular membranes. *J. Lipid Res.* **49,** 251–262 (2008).
254. Periole, X., Zeppelin, T. & Schiott, B. Dimer interface of the human serotonin transporter and effect of the membrane composition. *Sci. Rep.* **8,** 5080 (2018).
255. Hansen, K. *et al.* Structure, function, and allosteric modulation of NMDA receptors. *J. Gen. Physiol.* **150,** 1081–1105 (2018).
256. Paoletti, P., Bellone, C. & Zhou, Q. NMDA receptor subunit diversity: Impact on receptor properties, synaptic plasticity and disease. *Nat. Rev. Neurosci.* **14,** 383–400 (2013).
257. Arias, H. Marine toxins targeting ion channels. *Mar. Drugs* **4,** 37–69 (2006).
258. Haverkamp, S., Kolb, H., Fernandez, E. & Nelson, R. Glycine receptor diversity in the mammalian retina. in *The Organization of the Retina and Visual System* (1995).
259. Photoreactive crosslinker chemistry. *ThermoFisher Scientific*
260. Yanofsky, C. A Bayesian approach to peptide identification using accurate mass and time tags from LC-FTIR-MS proteomics experiments. *Conf. Proc. IEEE Eng. Med. Biol. Soc.* 3775–3778 (2008).
261. Ashcroft, A. Protein and peptide identification: the role of mass spectrometry in proteomics. *Nat. Prod. Rep.* **20,** 202–215 (2003).

APPENDIX: NMDA RECEPTOR DIMERIZATION

A.1 Overview

The NMDA receptor is a Ca^{2+}-permeable ligand-gated ion channel component of excitatory neurotransmission within the CNS implicated in synaptic function, plasticity, learning, and memory.[255]NMDA receptors form tetrameric complex assemblies of several homologous subunits.[256] The collaborative study wanted to discern if to regions of neighboring NMDA subunits are in close physical proximity. Specific amino acids from each subunit were mutated to cysteines to probe for intersubunit disulfide linkages.

A.2 Methodology

Gel bands were washed with 50:50 absolute methanol: 50 mM ammonium bicarbonate twice for 40 min with gentle agitation (VWR Thermal Shake Touch, 900 rpm). Gel bands were dehydrated by adding 500 μL acetonitrile for 20 minutes. Acetonitrile was removed and gel bands were dried in an Eppendorf 5301 Vacufuge Concentrator for approximately 15 minutes. Trypsin solution (10 μL at 20 μg/mL in 50 mM ammonium bicarbonate) was added to gel bands and incubated on ice for 15 minutes, then incubated overnight at 37˚C with gentle agitation (VWR Thermal Shake Touch, 900 rpm); trypsin solution (10 μL at 20 μg/mL in 50 mM ammonium bicarbonate) was added to gel bands an hour into incubation. The pH was adjusted to ~2 (5M HCl) and pepsin solution (10 μL at 1 mg/mL in H_2O (pH~3) was added. Tubes were overnight at 37˚C with gentle agitation. Digested peptides extracted into supernatant and transferred to VWR non-stick microcentrifuge tubes. Digested fragments were further extracted by incubating gel bands twice for 30 minutes in 500 μL of 0.1 % formic acid in 50:50 acetonitrile:H_2O. The supernatant

was collected and combined with initial supernatant. Digest extract solution was dried in an Eppendorf 5301 Vacufuge Concentrator. Dried extract was reconstituted in 50 µL of 0.1 % formic acid in H_2O for 30 minutes with gentle agitation. The reconstituted peptides were run through liquid chromatography-mass spectrometry (LCMS). Electrospray ionization quadrupole time-of-flight mass spectrometry was done on the extracted peptides and measurements were taken using an Agilent 6530 Q-TOF-MS with an Agilent HPLC-Chip II G4240-62006 ProtID-Chip-150. Mobile phase compositions used were Solvent A (95 % H_2O, 5 % ACN, 0.1 % Formic acid) and Solvent B (95 % ACN, 5 % H_2O, 0.1 % Formic acid) The nanoflow elution gradient was developed as follows at 0.50 µl/min of Solvent A (minute: percent A): 0.00: 95 %, 4.00: 10 %, 6.00: 70 %, 9.00: 50 %, 11.50: 95 %, 13.00: 95 %. The m/z range was 200-1700 m/z for MS analysis and 100-2000 m/z for MSMS analysis. Data were processed using Agilent Qualitative Analysis Software 6.0 using the following parameters: 2 missed enzymatic cleavages, 20 ppm precursor ion/ 0.1 Da product ion cutoff, and peptide modifications (oxidation and acrylamidation). For MS-MS analysis, the extracted peptide samples were run again on the Agilent 6530 Q-TOF-MS, targeting the specific mass-to-charge (m/z) ratio, charge, and retention time of the cross-linked peptides identified in MS analysis. CID was used for MS-MS fragmentation following a linear increase in collision energy by m/z using the equation: $y=3.7x+2.5$. CID was performed at $\pm$ 0.2 min from initial MS scan retention time of each crosslinked precursor ion identified. Measurements were taken in triplicate from distinctive gel bands at molecular weights of crosslinked dimers. Precursor/product ion pairing identified in >2 of 3 trials of mass ions unique to crosslinked diheteromer gel band and not identified in controls (single subunit and enzymatic solution gel band) were considered.

A.3 Results

Following double enzymatic digestion of gel bands at molecular weights of the dimerized subunits, MS analysis identified up to seven precursor ions from both trials indicative of disulfide-linked peptides and targeted for CID. MS-MS analysis identified product ions corresponding to both individual subunit peptides and the diheteromer linkage (Figure 17, representative figure of dataset).

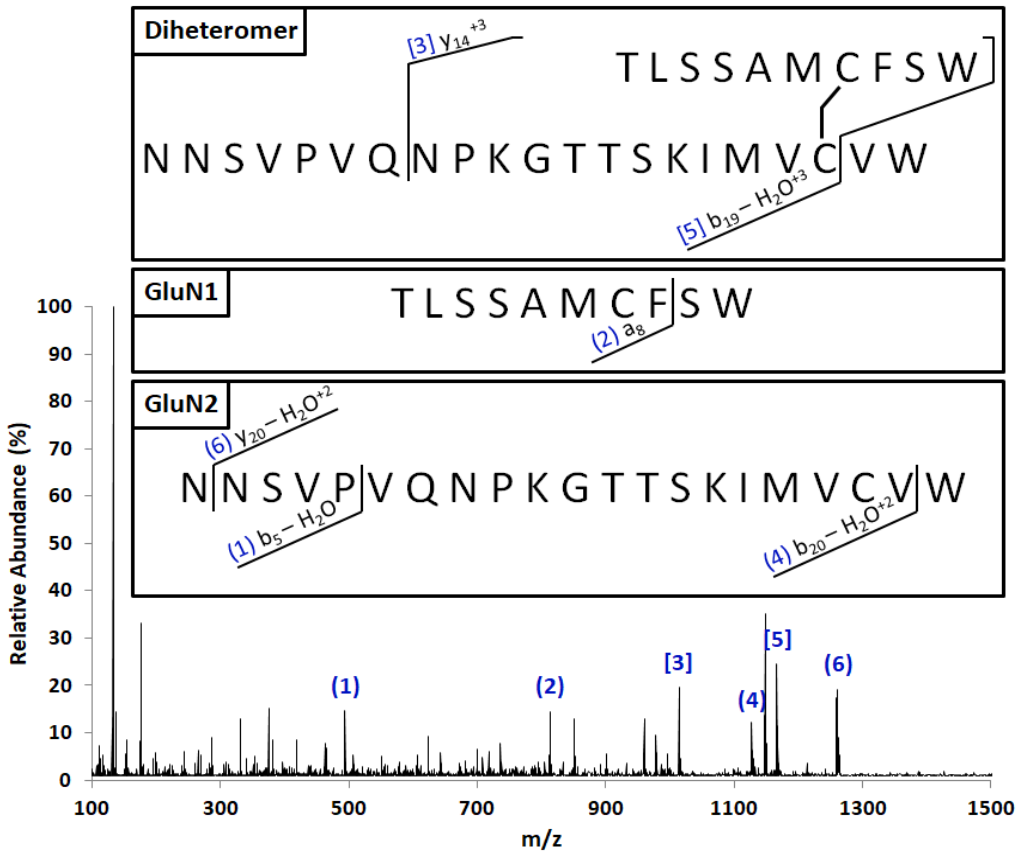

Figure 17. MS analysis of crosslinked diheteromer. Representative tandem MS-MS fragmentation scan of precursor m/z corresponding to crosslinked peptide pair produced from enzymatic double digestion. Fragmented *a*, *b* and *y* product ions (labeled 1-6) stemming from the crosslinked peptide pair precursor ion were assigned to product ions containing the disulfide crosslink between GluN1 and GluN2 (Diheteromer) as well as product ions assigned to individual GluN1 and GluN2 peptides due to CID of the disulfide linkage.